Two-Photon Resonance Fluorescence in a Ladder System

Jacob Peter Kia Ngaha

A thesis submitted in fulfilment of the requirements for the degree of Master of Science (MSc) in Physics, the University of Auckland, 2019.

Abstract

In this thesis we consider a three-level ladder-type atom driven by a coherent laser. When driven on two-photon resonance, the atom is excited into its highest state by absorbing two photons simultaneously, followed by a cascaded decay.

Employing techniques derived from the Lindblad master equation, we solve for the first-order correlation function, from which we can calculate the fluorescence spectrum. We find that under a strong drive field, the fluorescence spectrum contains up to seven different peaks. We aim to explain the emergence of these peaks by looking at transitions amongst the atom's dressed states.

We then aim to characterise the nature of the emitted light by investigating the second-order correlation function. In order to obtain a more precise picture of the photon correlations, we introduce a frequency filtering technique that allows us to isolate individual transitions. Measuring the photon correlations of these transitions provides a more complete picture of the role of specific dressed states of the system. We provide mostly numerical surveys of the fluorescence spectrum and correlations, with some analytic expressions to verify results.

Acknowledgements

First and foremost I would like to thank my supervisor Howard Carmichael for the huge amount of support, guidance, and patience throughout the year. Regardless of how busy he was he would always find time to add his famous "yellow boxes" which were always extremely helpful.

I would also like to thank Victor Canela for his tremendous help with almost everything. Whether it was problems with a derivation of with the programming, we would eventually sort through them.

To my fellow masters students – Abdullah, Alex, Jonathan, Neelesh, Nick, Stan, Toby – thank you for all the entertaining times together.

I would also like to thank my parents, Noel and Debbie, and all my friends for being so patient with me, especially in these last few months. I cannot forget my partner Maisie, who has been extremely supportive of me throughout this year. Also to our dog Attenborough who was always very eager to hear all about how the fluorescence spectrum changed.

A special thanks goes to Alex and Chris from the NeSI platform for their help with the Fortran project Victor and I worked on. Hopefully the new implementations can help future students as much as it helped us.

And last but definitely not least I would like to thank the Dodd Walls Centre for funding this project and for all the opportunities that have arisen through the year.

Contents

List of Figures

1 Introduction

In 1956, Robert Hanbury Brown and Richard Q. Twiss aimed two photo-multipliers at Sirius and found there was a strong correlation of the intensity fluctuations of the amplified anode currents [1–4]; apparently, photons from the star were tending to arrive in groups or "bunches", rather than at random as was expected of chaotic light.

While the theory of the time worked in a classical optics setting, there remained the question of whether or not this bunching effect could be described quantum mechanically. It remained open until 1963, the year in which Roy J. Glauber developed his "quantum theory for optical coherence", bridging the gap between the well-studied coherence of classical optics and quantum mechanics [5, 6].

While photon bunching could be explained classically, its converse, *photon antibunching* [7, 8], was recognized as a purely quantum effect, which could only be understood from the quantum description of light. Photon antibunching was first experimentally observed in 1977 [9]. Since then many more experiments have followed, employing a variety of methods, further confirming the quantum nature of these effects. Recent growth in the field of quantum networks, for example, has shown the importance of single-photon sources as a means of transferring quantum information [10], where photon antibunching provides the standard method used to verify the single-photon character of a source. Antibunched photon correlations have even been observed in *circuit* quantum electrodynamics (QED) [11], where Josephson junctions are configured in a superconducting circuit to provide a microwave analogue of cavity QED.

This thesis is largely motivated by the experimental work of Gasparinetti et al. on a three-level ladder-type artificial atom – fabricated as a superconducting circuit – driven on *two-photon resonance* [12, 13]. The "atom" absorbs two photons simultaneously and, given the three-level ladder structure, each absorption of a photon pair is followed by a cascaded decay accompanied by two-photon emission. We propose to explain this two-photon resonance fluorescence by adopting a *dressed state picture* based on the eigenstates of the interaction Hamiltonian. In particular, we aim to investigate the recently observed dressed states of an artificial three-level atom [14].

It is well known for a two-level atom that, upon strong coherent driving, the fluorescence spectrum splits into a Mollow triplet [15] due to transitions amongst its dressed states. While there has been previous work on two- and three-level systems, showing related behaviour [16–20], we take a slightly different approach such as that used in recent works (see Refs. [21, 22]). In order to completely characterise the photon correlations of the three-level atom, we employ a filtering technique that allows us to isolate individual transitions between the dressed states. In this way we aim to build a complete picture of the dressed state transitions that connects the photon correlations to our understanding of the two-photon resonance fluorescence spectrum.

We begin in chapter 2 by quantising the electromagnetic field, where we find its mathematical analogue in a collection of harmonic oscillators. We are then able to use our result to derive a Hamiltonian of a three-level ladder-type atom interacting with the quantised electromagnetic field. We make use of two important approximations to do so: the *rotating wave approximation* and the *dipole approximation*. Finally, coherent driving is introduced, modelling an atom in an experimental setting where it is driven by a laser.

In chapter 3 we make the description more physically realistic by accounting for spontaneous emission, a dissipative process. Using the *Born and Markov* approximations, we derive an equation of motion for the atom viewed as a quantum *open system*, known as the *Lindblad master equation*. Using master equation techniques we can solve for two important quantities: the first-order and second-order correlation functions. These are two-time correlation functions, which are not inherently simple to compute. We therefore derive an expression for these correlation functions using *quantum regression formulas*. Finally, we introduce a different method of treating the dissipative system, *quantum trajectory theory*, which involves integrating a differential equation for a pure state vector with stochastic quantum "jumps".

In chapter 4 we give a brief review of circuit QED and how the motivating work of this thesis was carried out. We then derive a time-independent Hamiltonian for the driven-three level atom in terms of four important variables: the detuning of the drive frequency from two-photon resonance; the anharmonicity of the three energy levels; the drive field strength; and the dipole moment ratio. With the time-independent Hamiltonian we perform a numerical survey of the steady state populations of the atoms under different parameter regimes. We then derive a Hamiltonian where we have adiabatically eliminated the intermediate state and, using this Hamiltonian, we derive analytic expressions for the steady state density operator.

Chapter 5 begins with a discussion on the eigenstates of the full Hamiltonian, including interactions, also known as the *dressed states*. We derive expressions for the dressed states and their respective eigenfrequencies for the case of two-photon resonance. We wish to study the fluorescence spectrum of the atom, so we start by giving an overview of first-order coherence from a classical and quantum perspective. We then derive an expression for the field radiated from the atom in terms of the atomic dipole operator. Following the pattern of chapter 4, we then provide a numerical survey of the incoherent fluorescence spectrum for different drive strengths and dipole moment ratios. We find that when the atom is driven at single-photon resonance, the fluorescence spectrum resembles that of a driven two-level atom. We then explain the change in the fluorescence spectrum when driven on two-photon resonance by referring to the dressed states and the various transitions that are made possible as the drive strength is increased.

Finally, in chapter 6, we investigate the second-order coherence of the atom. We start by introducing the second-order correlation function and the three main classes of second-order coherence – *bunched* light, *coherent* light, and *anti-bunched* light, where antibunched light is an inherently quantum phenomenon. We start by investigating the *unfiltered* photon correlations. We then implement a filter into the system by coupling the fluorescence into a ring cavity, allowing us to

investigate the auto-correlation of individual transitions. The transitions we are most interested in are the dressed state transitions, which give rise to the multi-peak fluorescence spectrum. Finally, we take the filtering one step further by coupling the fluorescence into a second filter cavity. This allows us to cross-correlate photons from different transitions, with the goal of verifying intuitions drawn from the dressed state picture.

The thesis concludes in chapter 7 where we present a short summary of the topics covered with some concluding remarks. We also discuss possible avenues for extending this work.

2 Three Level Atom Interacting with the Quantised Radiation Field

In this chapter we aim to set the foundations of knowledge for this thesis by introducing key principles that the following chapters will build upon. We start by representing the electromagnetic field in a way that will capture the uniquely quantum mechanical properties. As we are interested in a three-level ladder type atom, we will then develop a model of a three-level atom interacting with the quantised radiation field by making use of two main approximations: the dipole approximation and the rotating wave approximation.

2.1 Free Electromagnetic Field

Starting by considering the field classically we aim to represent the electromagnetic field in terms of quantum mechanical operators. We follow the steps of Walls and Milburn (Ref. [23], ch. 2) by quantising the field in terms of a vector potential and equating it to a set of orthogonal independent harmonic oscillators.

2.1.1 Plane wave expansion of the field

We start with Maxwell's equations for the electric and magnetic fields in free space, $\boldsymbol{E}$ and $\boldsymbol{B}$, respectively;

$$\boldsymbol{\nabla} \cdot \boldsymbol{E}(\boldsymbol{r}, t) = 0, \tag{2.1a}$$

$$\boldsymbol{\nabla} \times \boldsymbol{E}(\boldsymbol{r}, t) = -\frac{\partial \boldsymbol{B}(\boldsymbol{r}, t)}{\partial t}, \tag{2.1b}$$

$$\boldsymbol{\nabla} \cdot \boldsymbol{B}(\boldsymbol{r}, t) = 0, \tag{2.1c}$$

$$\boldsymbol{\nabla} \times \boldsymbol{B}(\boldsymbol{r}, t) = \frac{1}{c^2}\frac{\partial \boldsymbol{E}(\boldsymbol{r}, t)}{\partial t}, \tag{2.1d}$$

where $c = (\mu_0 \epsilon_0)^{-1/2}$ is the speed of light in a vacuum, and μ_0 and ϵ_0 are the free space magnetic permeability and electric permittivity, respectively. Introducing the vector potential $\boldsymbol{A}(\boldsymbol{r}, t)$ and using the *Coulomb gauge*

$$\boldsymbol{\nabla} \cdot \boldsymbol{A}(\boldsymbol{r}, t) = 0, \tag{2.2}$$

we write the magnetic and electric fields as

$$\boldsymbol{E}(\boldsymbol{r}, t) = -\frac{\partial \boldsymbol{A}(\boldsymbol{r}, t)}{\partial t}, \tag{2.3a}$$

$$\boldsymbol{B}(\boldsymbol{r},t) = \boldsymbol{\nabla} \times \boldsymbol{A}(\boldsymbol{r},t). \tag{2.3b}$$

Substituting these expressions into Eq. (2.1d), we then find that $\boldsymbol{A}(\boldsymbol{r},t)$ is a solution to the wave equation

$$\boldsymbol{\nabla}^2 \boldsymbol{A}(\boldsymbol{r},t) - \frac{1}{c^2}\frac{\partial^2 \boldsymbol{A}(\boldsymbol{r},t)}{\partial^2 t} = 0. \tag{2.4}$$

We now consider the field to be contained inside a cubic volume $V = L^3$, such that we may extend any solution to neighbouring volumes with periodic boundary conditions and expand the general solution in terms of a discrete set of orthogonal mode functions;

$$\boldsymbol{A}(\boldsymbol{r},t) = \sum_{\boldsymbol{k}} \boldsymbol{A}_{\boldsymbol{k}}(t) e^{i\boldsymbol{k}\cdot\boldsymbol{r}} + \text{c.c.}, \tag{2.5}$$

with the sum ranging over all wavevectors $\boldsymbol{k} = k_x\hat{\boldsymbol{x}} + k_y\hat{\boldsymbol{y}} + k_z\hat{\boldsymbol{z}}$, where

$$k_x = \frac{2\pi n_x}{L}, \quad k_y = \frac{2\pi n_y}{L}, \quad k_z = \frac{2\pi n_z}{L}, \tag{2.6}$$

with $n_x, n_y, n_z \in \mathbb{Z}$. The mode functions satisfy the transversality condition, Eq. (2.2), if

$$\boldsymbol{k} \cdot \boldsymbol{A} = 0. \tag{2.7}$$

Thus there exist two polarisation vectors, $\hat{\boldsymbol{e}}_{\boldsymbol{k},\lambda=1,2}$, orthogonal to $\boldsymbol{k}$ that satisfy the condition. The vector potential is then expanded as

$$\boldsymbol{A}(\boldsymbol{r},t) = \sum_{\boldsymbol{k},\lambda} A_{\boldsymbol{k},\lambda}(t)\hat{\boldsymbol{e}}_{\boldsymbol{k},\lambda} e^{i\boldsymbol{k}\cdot\boldsymbol{r}} + \text{c.c}, \tag{2.8}$$

where a scale factor has been introduced so that the amplitudes $A_{\boldsymbol{k},\lambda}(t)$ and $A^*_{\boldsymbol{k},\lambda}(t)$ are dimensionless. Substituting this vector potential into the wave equation, Eq. (2.4), yields

$$\boldsymbol{k}^2 A_{\boldsymbol{k}}(t) + \frac{1}{c^2}\frac{\mathrm{d}^2}{\mathrm{d}t^2} A_{\boldsymbol{k},\lambda}(t) = 0, \tag{2.9}$$

which has the solution

$$A_{\boldsymbol{k},\lambda}(t) = A_{\boldsymbol{k},\lambda} e^{-i\omega_{\boldsymbol{k}} t}, \tag{2.10}$$

where we use the dispersion relation $\omega_{\boldsymbol{k}} = kc$. Using this vector potential, the electric and magnetic fields may be written in the form

$$\boldsymbol{E}(\boldsymbol{r},t) = \sum_{\boldsymbol{k},\lambda} i\omega_{\boldsymbol{k}} A_{\boldsymbol{k},\lambda}\hat{\boldsymbol{e}}_{\boldsymbol{k},\lambda} e^{i(\boldsymbol{k}\cdot\boldsymbol{r}-\omega_{\boldsymbol{k}}t)} + \text{c.c.}, \tag{2.11a}$$

$$\boldsymbol{B}(\boldsymbol{r},t) = \sum_{\boldsymbol{k},\lambda} i\left(\boldsymbol{k}\times\hat{\boldsymbol{e}}_{\boldsymbol{k},\lambda}\right) A_{\boldsymbol{k},\lambda} e^{i(\boldsymbol{k}\cdot\boldsymbol{r}-\omega_{\boldsymbol{k}}t)} + \text{c.c.}. \tag{2.11b}$$

2.1.2 Quantisation of the field: a collection of harmonic oscillators

The energy of the field in the cubic volume $V = L^3$ is given by the Hamiltonian

$$H = \int_V \mathrm{d}^3\mathrm{r} \left[\frac{\epsilon_0}{2} \left| \boldsymbol{E}(\boldsymbol{r}, t) \right|^2 + \frac{1}{2\mu_0} \left| \boldsymbol{B}(\boldsymbol{r}, t) \right|^2 \right]. \tag{2.12}$$

As the energy is a conserved quantity we may set $t = 0$ and consider

$$\begin{aligned} H = \int_V \mathrm{d}^3\boldsymbol{r} \Bigg[& \frac{\epsilon_0}{2} \left(\sum_{\boldsymbol{k},\lambda} i\omega_{\boldsymbol{k}} A_{\boldsymbol{k},\lambda} \hat{e}_{\boldsymbol{k},\lambda} e^{i\boldsymbol{k}\cdot\boldsymbol{r}} + \text{c.c.} \right)^2 \\ & + \frac{1}{2\mu_0} \left(\sum_{\boldsymbol{k},\lambda} i \left(\boldsymbol{k} \times \hat{\boldsymbol{e}}_{\boldsymbol{k},\lambda} \right) A_{\boldsymbol{k},\lambda} e^{i\boldsymbol{k}\cdot\boldsymbol{r}} + \text{c.c.} \right)^2 \Bigg]. \end{aligned} \tag{2.13}$$

Noting the orthonormality of the mode functions and the fact that the wavevectors $\boldsymbol{k}$ are orthogonal to the polarisation vectors $\hat{\boldsymbol{e}}_{\boldsymbol{k},\lambda}$, the above expression simplifies to

$$H = 2\epsilon_0 V \sum_{\boldsymbol{k},\lambda} \omega_{\boldsymbol{k}}^2 \left| A_{\boldsymbol{k},\lambda} \right|^2. \tag{2.14}$$

Since the Fourier coefficients $A_{\boldsymbol{k},\lambda}$ are generally complex values, we introduce two real variables, $Q_{\boldsymbol{k},\lambda}$ and $P_{\boldsymbol{k},\lambda}$, corresponding to the generalised coordinate and conjugate momenta, and with the Fourier coefficients written as

$$A_{\boldsymbol{k},\lambda} = \frac{1}{\sqrt{4\epsilon_0 V}} \left(Q_{\boldsymbol{k},\lambda} + i\omega_{\boldsymbol{k}}^{-1} P_{\boldsymbol{k},\lambda} \right), \tag{2.15}$$

the Hamiltonian for the electromagnetic field now resembles an infinite set of harmonic oscillators:

$$H = \sum_{\boldsymbol{k},\lambda} \frac{1}{2} \left(\omega_{\boldsymbol{k}} Q_{\boldsymbol{k},\lambda}^2 + P_{\boldsymbol{k},\lambda}^2 \right). \tag{2.16}$$

We make the final step of quantisation by converting the generalised coordinates and conjugate momenta into quantum mechanical operators,

$$Q_{\boldsymbol{k},\lambda} \longrightarrow \hat{q}_{\boldsymbol{k},\lambda}, \quad P_{\boldsymbol{k},\lambda} \longrightarrow \hat{p}_{\boldsymbol{k},\lambda}, \tag{2.17}$$

with the canonical commutation relation

$$[\hat{q}_{\boldsymbol{k},\lambda}, \hat{p}_{\boldsymbol{k}',\lambda'}] = i\hbar\delta_{\boldsymbol{k},\boldsymbol{k}'}\delta_{\lambda,\lambda'}. \tag{2.18}$$

We then introduce the *annihilation* and *creation* operators

$$\hat{a}_{\boldsymbol{k},\lambda} = \frac{1}{\sqrt{2\hbar\omega_{\boldsymbol{k}}}} \left(\omega_{\boldsymbol{k}} \hat{q}_{\boldsymbol{k},\lambda} + i\hat{p}_{\boldsymbol{k},\lambda} \right), \tag{2.19a}$$

$$\hat{a}^\dagger_{\boldsymbol{k},\lambda} = \frac{1}{\sqrt{2\hbar\omega_{\boldsymbol{k}}}} \left(\omega_{\boldsymbol{k}} \hat{q}_{\boldsymbol{k},\lambda} - i\hat{p}_{\boldsymbol{k},\lambda}\right), \tag{2.19b}$$

which, from Eq. (2.18), obey the boson commutation relations

$$[\hat{a}_{\boldsymbol{k},\lambda}, \hat{a}_{\boldsymbol{k}',\lambda'}] = [\hat{a}^\dagger_{\boldsymbol{k},\lambda}, \hat{a}^\dagger_{\boldsymbol{k}',\lambda'}] = 0, \tag{2.20a}$$

$$[\hat{a}_{\boldsymbol{k},\lambda}, \hat{a}^\dagger_{\boldsymbol{k}',\lambda'}] = \delta_{\boldsymbol{k},\boldsymbol{k}'}\delta_{\lambda,\lambda'}. \tag{2.20b}$$

Thus the Hamiltonian for the quantised electromagnetic field is finally cast in the form

$$\hat{H} = \sum_{\boldsymbol{k},\lambda} \hbar\omega_{\boldsymbol{k}} \left(\hat{a}^\dagger_{\boldsymbol{k},\lambda}\hat{a}_{\boldsymbol{k},\lambda} + \frac{1}{2}\right). \tag{2.21}$$

We can now solve the Heisenberg equation of motion for the annihilation operator,

$$\frac{\mathrm{d}}{\mathrm{d}t}\hat{a}_{\boldsymbol{k},\lambda} = \frac{1}{i\hbar}[\hat{a}_{\boldsymbol{k},\lambda}, \hat{H}] = -i\omega_{\boldsymbol{k}}\hat{a}_{\boldsymbol{k},\lambda}, \tag{2.22}$$

with solution

$$\hat{a}_{\boldsymbol{k},\lambda}(t) = e^{-i\omega_{\boldsymbol{k}}t}\hat{a}_{\boldsymbol{k},\lambda}(0), \tag{2.23}$$

to write the electric and magnetic fields as operators:

$$\hat{\boldsymbol{E}}(\boldsymbol{r},t) = i\sum_{\boldsymbol{k},\lambda}\sqrt{\frac{\hbar\omega_{\boldsymbol{k}}}{2\epsilon_0 V}}\left[\hat{\boldsymbol{e}}_{\boldsymbol{k},\lambda}\hat{a}_{\boldsymbol{k},\lambda}(t)e^{i\boldsymbol{k}\cdot\boldsymbol{r}} - \text{H.c.}\right], \tag{2.24a}$$

$$\hat{\boldsymbol{B}}(\boldsymbol{r},t) = i\sum_{\boldsymbol{k},\lambda}\sqrt{\frac{\hbar}{2\epsilon_0\omega_{\boldsymbol{k}}V}}\left[(\boldsymbol{k}\times\hat{\boldsymbol{e}}_{\boldsymbol{k},\lambda})\,\hat{a}_{\boldsymbol{k},\lambda}(t)e^{i\boldsymbol{k}\cdot\boldsymbol{r}} - \text{H.c.}\right]. \tag{2.24b}$$

2.1.3 Field mode states

Drawing on the quantum treatment of the harmonic oscillator (Ref. [23], ch. 2), we introduce the number operator $\hat{n}_{\boldsymbol{k}} = \hat{a}^\dagger_{\boldsymbol{k}}\hat{a}_{\boldsymbol{k}}$, with eigenvalue equation

$$\hat{n}_{\boldsymbol{k}}\,|n_{\boldsymbol{k}}\rangle = n_{\boldsymbol{k}}\,|n_{\boldsymbol{k}}\rangle\,, \tag{2.25}$$

where $\{|n_{\boldsymbol{k}}\rangle\}$ is a complete,

$$\sum_{n_{\boldsymbol{k}}} |n_{\boldsymbol{k}}\rangle\langle n_{\boldsymbol{k}}| = \mathbb{1}, \tag{2.26}$$

and orthogonal,

$$\langle m_{\boldsymbol{k}}|n_{\boldsymbol{k}}\rangle = \delta_{mn}, \tag{2.27}$$

set of states, known as the Fock states, with $m_{\boldsymbol{k}}, n_{\boldsymbol{k}} \in \mathbb{N}_0$ (Ref. [24], ch. 1). Considering only a single mode of the quantised field, the Hamiltonian Eq. (2.21) has discrete eigenvalues

$$\hat{H}\left|n_{\boldsymbol{k}}\right\rangle = \hbar\omega_{\boldsymbol{k}}\left(n_{\boldsymbol{k}} + \frac{1}{2}\right)\left|n_{\boldsymbol{k}}\right\rangle = E_n\left|n_{\boldsymbol{k}}\right\rangle. \tag{2.28}$$

The state $\hat{a}^\dagger_{\boldsymbol{k}}\left|n_{\boldsymbol{k}}\right\rangle$ is also an eigenstate of the Hamiltonian, with an eigenvalue equation

$$\hat{H}\hat{a}^\dagger_{\boldsymbol{k}}\left|n_{\boldsymbol{k}}\right\rangle = \left(E_n + \hbar\omega_{\boldsymbol{k}}\right)\hat{a}^\dagger_{\boldsymbol{k}}\left|n_{\boldsymbol{k}}\right\rangle, \tag{2.29}$$

where we have made use of the commutation relation Eq. (2.20b). In a similar way, we find that $\hat{a}_{\boldsymbol{k}}\left|n_{\boldsymbol{k}}\right\rangle$ is an eigenstate of $\hat{H}$ with the eigenvalue equation

$$\hat{H}\hat{a}_{\boldsymbol{k}}\left|n_{\boldsymbol{k}}\right\rangle = \left(E_n - \hbar\omega_{\boldsymbol{k}}\right)\hat{a}_{\boldsymbol{k}}\left|n_{\boldsymbol{k}}\right\rangle. \tag{2.30}$$

From these two eigenvalues we can see that the annihilation and creation operators have the actions

$$\hat{a}_{\boldsymbol{k}}\left|n_{\boldsymbol{k}}\right\rangle = \beta_1\left|n_{\boldsymbol{k}} - 1\right\rangle, \tag{2.31a}$$
$$\hat{a}^\dagger_{\boldsymbol{k}}\left|n_{\boldsymbol{k}}\right\rangle = \beta_2\left|n_{\boldsymbol{k}} + 1\right\rangle, \tag{2.31b}$$

where β_1 and β_2 are normalisation constants. To find these constants we use Eq. (2.25) to find

$$n_{\boldsymbol{k}}\left\langle n_{\boldsymbol{k}}|n_{\boldsymbol{k}}\right\rangle = \left\langle n_{\boldsymbol{k}}|\hat{a}^\dagger_{\boldsymbol{k}}\hat{a}_{\boldsymbol{k}}|n_{\boldsymbol{k}}\right\rangle = \beta_1^*\beta_1\left\langle n_{\boldsymbol{k}} - 1|n_{\boldsymbol{k}} - 1\right\rangle \Rightarrow |\beta_1|^2 = n_{\boldsymbol{k}}, \tag{2.32}$$

and

$$\left(n_{\boldsymbol{k}} + 1\right)\left\langle n_{\boldsymbol{k}}|n_{\boldsymbol{k}}\right\rangle = \left\langle n_{\boldsymbol{k}}|\hat{a}_{\boldsymbol{k}}\hat{a}^\dagger_{\boldsymbol{k}}|n_{\boldsymbol{k}}\right\rangle = \beta_2^*\beta_2\left\langle n_{\boldsymbol{k}} + 1|n_{\boldsymbol{k}} + 1\right\rangle \Rightarrow |\beta_2|^2 = n_{\boldsymbol{k}} + 1. \tag{2.33}$$

We see that $\hat{a}_{\boldsymbol{k}}$ and $\hat{a}^\dagger_{\boldsymbol{k}}$ are raising and lowering operators for the *ladder* of harmonic oscillator eigenstates:

$$\hat{a}_{\boldsymbol{k}}\left|n_{\boldsymbol{k}}\right\rangle = \sqrt{n_{\boldsymbol{k}}}\left|n_{\boldsymbol{k}} - 1\right\rangle, \tag{2.34a}$$
$$\hat{a}^\dagger_{\boldsymbol{k}}\left|n_{\boldsymbol{k}}\right\rangle = \sqrt{n_{\boldsymbol{k}} + 1}\left|n_{\boldsymbol{k}} + 1\right\rangle. \tag{2.34b}$$

It is often useful to decompose the electric field operator positive and negative frequency contributions:

$$\hat{\boldsymbol{E}}(\boldsymbol{r}, t) = \hat{\boldsymbol{E}}^{(+)}(\boldsymbol{r}, t) + \hat{\boldsymbol{E}}^{(-)}(\boldsymbol{r}, t), \tag{2.35}$$

with

$$\hat{\boldsymbol{E}}^{(+)}(\boldsymbol{r}, t) = i\sum_{\boldsymbol{k},\lambda}\sqrt{\frac{\hbar\omega_{\boldsymbol{k}}}{2\epsilon_0 V}}\hat{\boldsymbol{e}}_{\boldsymbol{k},\lambda}\hat{a}_{\boldsymbol{k},\lambda}(t)e^{i\boldsymbol{k}\cdot\boldsymbol{r}}, \tag{2.36a}$$
$$\hat{\boldsymbol{E}}^{(-)}(\boldsymbol{r}, t) = \left(\hat{\boldsymbol{E}}^{(+)}(\boldsymbol{r}, t)\right)^\dagger. \tag{2.36b}$$

2.1.4 Coherent States

Fock states form a useful basis for fields with small photon numbers but are not so suitable for high photon numbers such as can be found in a laser field. A state that is better suited to describing such fields is the *coherent state* [25]. Typically denoted by $|\alpha\rangle$, the coherent state is an eigenstate of the annihilation operator

$$\hat{a}_{\boldsymbol{k}} |\alpha\rangle = \alpha |\alpha\rangle , \tag{2.37}$$

and has the expansion in Fock states,

$$|\alpha\rangle = e^{-\frac{1}{2}|\alpha|^2} \sum_{n=0}^{\infty} \frac{\alpha^n}{\sqrt{n!}} |n\rangle . \tag{2.38}$$

Coherent states are not orthogonal, with overlap

$$\langle\beta|\alpha\rangle = e^{-|\alpha-\beta|^2}, \tag{2.39}$$

but they are complete, in fact overcomplete,

$$\frac{1}{\pi} \int \mathrm{d}^2\alpha \, |\alpha\rangle \langle\alpha| = \mathbb{1}. \tag{2.40}$$

2.2 Atom-Field Hamiltonian

The artificial atom used in the experiment by Gasparinetti et al. models a driven three-level ladder-type system [13] with ground state $|g\rangle$, excited state $|f\rangle$ and an intermediate state $|e\rangle$, and respective eigenfrequencies ω_g, ω_f, and ω_e, $\omega_g < \omega_e < \omega_f$. The two transitions of the atom, $|e\rangle \leftrightarrow |g\rangle$ and $|f\rangle \leftrightarrow |e\rangle$, are driven by a coherent laser at frequency ω_d. The direct transition from the ground state $|g\rangle$ to the excited state $|f\rangle$ is dipole forbidden.

In this section we will derive a mathematical model describing this system and its coupling to the electromagnetic field by making two important approximations: the *dipole* and *rotating wave* approximations.

2.2.1 Atom-field interaction: Dipole approximation

The Hamiltonian of an atom interacting with the transverse electromagnetic field is given by

$$\hat{H} = \hat{H}_F + \hat{H}_A + \hat{H}_I, \tag{2.41}$$

where the Hamiltonian describing the field, $\hat{H}_F$, is given by Eq. (2.21) with the ground state energy set to zero,

$$\hat{H}_F = \sum_{\boldsymbol{k},\lambda} \hbar\omega_{\boldsymbol{k}} \hat{a}^\dagger_{\boldsymbol{k},\lambda} \hat{a}_{\boldsymbol{k},\lambda}, \tag{2.42}$$

and letting $\{|l\rangle\}, l = 1, 2, \ldots, N$ be a complete set of orthonormal eigenstates of an N-level atom with the corresponding eigenfrequencies $\{\omega_i\}$, the free-atom Hamiltonian is

$$\hat{H}_A = \sum_{l}^{N} \hbar\omega_i \left|l\right\rangle \left\langle l\right| . \tag{2.43}$$

The interaction, $\hat{H}_I$, consists of many multipolar expansion terms. Comparing the magnitudes of these terms we find that the electric-dipole interaction is many orders of magnitude larger. We therefore make the *dipole approximation* and neglect the other terms, which leads us to the interaction

$$\hat{H}_I = -\hat{\boldsymbol{D}} \cdot \hat{\boldsymbol{E}} \left(\boldsymbol{r}_0\right), \tag{2.44}$$

with $\hat{\boldsymbol{E}}$ given by Eq. (2.24a) and the dipole operator $\hat{\boldsymbol{D}}$ by

$$\begin{aligned} \hat{\boldsymbol{D}} &= \sum_{l,m=1}^{N} \left|l\right\rangle \left\langle l\right| e \left(\hat{\boldsymbol{r}} - \boldsymbol{r}_0\right) \left|m\right\rangle \left\langle m\right| \\ &= \sum_{l,m=1}^{N} \boldsymbol{d}_{lm} \left|l\right\rangle \left\langle m\right| , \end{aligned} \tag{2.45}$$

with e the charge of an electron, $\hat{\boldsymbol{r}}$ the electron position operator, $\boldsymbol{r}_0$ the nuclear position, and dipole matrix element

$$\boldsymbol{d}_{lm} = \langle l| e \left(\hat{\boldsymbol{r}} - \boldsymbol{r}_0\right) \left|m\right\rangle . \tag{2.46}$$

We then assume that the wavelength of the field is large compared with the size of the atom so that, over the dimensions of the atom, the field is constant. We expand the spatial dependence of the electric field as

$$e^{i\boldsymbol{k}\cdot\hat{\boldsymbol{r}}} = e^{i\boldsymbol{k}\cdot\boldsymbol{r}_0} e^{i\boldsymbol{k}\cdot\left(\hat{\boldsymbol{r}}-\boldsymbol{r}_0\right)} = e^{i\boldsymbol{k}\cdot\boldsymbol{r}_0} \left[1 + i\boldsymbol{k}\cdot\left(\hat{\boldsymbol{r}} - \boldsymbol{r}_0\right) + \mathcal{O}\left(\left|\boldsymbol{k}\cdot\left(\hat{\boldsymbol{r}} - \boldsymbol{r}_0\right)\right|^2\right)\right], \tag{2.47}$$

and retain only the first term. Thus the complete Hamiltonian for an N-level atom interacting with the electromagnetic field in the dipole approximation is

$$\hat{H} = \sum_{\boldsymbol{k},\lambda} \hbar\omega_{\boldsymbol{k}} \hat{a}^{\dagger}_{\boldsymbol{k},\lambda} \hat{a}_{\boldsymbol{k},\lambda} + \sum_{l=1}^{N} \hbar\omega_l \left|l\right\rangle \left\langle l\right| + \sum_{l,m=1}^{N} \sum_{\boldsymbol{k},\lambda} \hbar \left|l\right\rangle \left\langle m\right| \left[g^{lm}_{\boldsymbol{k},\lambda} \hat{a}_{\boldsymbol{k},\lambda} + \left(g^{lm}_{\boldsymbol{k},\lambda}\right)^{*} \hat{a}^{\dagger}_{\boldsymbol{k},\lambda}\right], \tag{2.48}$$

with

$$g^{lm}_{\boldsymbol{k},\lambda} = -i\sqrt{\frac{\omega_{\boldsymbol{k}}}{2\hbar\epsilon_0 V}} \left(\boldsymbol{d}_{lm} \cdot \hat{\boldsymbol{e}}_{\boldsymbol{k},\lambda}\right) e^{i\boldsymbol{k}\cdot\boldsymbol{r}_0}. \tag{2.49}$$

For the three-level system of interest

$$\hat{H}_A = \hbar\omega_g \left|g\right\rangle \left\langle g\right| + \hbar\omega_e \left|e\right\rangle \left\langle e\right| + \hbar\omega_f \left|f\right\rangle \left\langle f\right| , \tag{2.50}$$

and

$$\begin{aligned}\hat{H}_I = &\sum_{\boldsymbol{k},\lambda} \hbar \left|g\right\rangle \left\langle e\right| \left[g^{ge}_{\boldsymbol{k},\lambda}\hat{a}_{\boldsymbol{k},\lambda} + \left(g^{ge}_{\boldsymbol{k},\lambda}\right)^* \hat{a}^\dagger_{\boldsymbol{k},\lambda}\right] + \hbar \left|e\right\rangle \left\langle g\right| \left[g^{eg}_{\boldsymbol{k},\lambda}\hat{a}_{\boldsymbol{k},\lambda} + \left(g^{eg}_{\boldsymbol{k},\lambda}\right)^* \hat{a}^\dagger_{\boldsymbol{k},\lambda}\right] \\ &+ \hbar \left|e\right\rangle \left\langle f\right| \left[g^{ef}_{\boldsymbol{k}\lambda}\hat{a}_{\boldsymbol{k},\lambda} + \left(g^{ef}_{\boldsymbol{k}\lambda}\right)^* \hat{a}^\dagger_{\boldsymbol{k},\lambda}\right] + \hbar \left|f\right\rangle \left\langle e\right| \left[g^{fe}_{\boldsymbol{k}\lambda}\hat{a}_{\boldsymbol{k},\lambda} + \left(g^{fe}_{\boldsymbol{k}\lambda}\right)^* \hat{a}^\dagger_{\boldsymbol{k},\lambda}\right].\end{aligned} \tag{2.51}$$

2.2.2 Rotating-wave approximation

We aim to transform this Hamiltonian into an interaction picture so that we are able to drop any rapidly oscillating terms. We thus make the *rotating wave approximation* by introducing the unitary evolution operator

$$\hat{U}(t) = e^{-\frac{i}{\hbar}\hat{H}_0 t} = e^{-\frac{i}{\hbar}(\hat{H}_F+\hat{H}_A)t} = e^{-i\omega_{\boldsymbol{k}} t\hat{a}^\dagger_{\boldsymbol{k},\lambda}\hat{a}_{\boldsymbol{k},\lambda}} e^{-i\omega_g t|g\rangle\langle g|} e^{-i\omega_e t|e\rangle\langle e|} e^{-i\omega_f t|f\rangle\langle f|}, \tag{2.52}$$

with $\hat{H}_F$ defined by Eq. (2.42) and $\hat{H}_A$ by Eq. (2.50). An operator $\hat{A}$ in this interaction picture is defined by the transformation $\hat{\tilde{A}}(t) = \hat{U}^\dagger(t)\hat{A}(0)\hat{U}(t)$. We therefore use the Baker-Campbell-Hausdorff Lemma [26],

$$e^{\lambda\hat{A}}\hat{B}e^{-\lambda\hat{A}} = \hat{B} + \lambda[\hat{A},\hat{B}] + \frac{\lambda^2}{2!}[\hat{A},[\hat{A},\hat{B}]] + \cdots, \tag{2.53}$$

to find the explicit time dependence of the operators in the interaction terms. For the Hamiltonian Eq. (2.51) we find

$$\hat{U}^\dagger(t)\hat{a}_{\boldsymbol{k},\lambda}\hat{U}(t) = e^{-i\omega_{\boldsymbol{k}} t}\hat{a}_{\boldsymbol{k},\lambda}, \tag{2.54a}$$

$$\hat{U}^\dagger(t)\hat{a}^\dagger_{\boldsymbol{k},\lambda}\hat{U}(t) = e^{i\omega_{\boldsymbol{k}} t}\hat{a}^\dagger_{\boldsymbol{k},\lambda}, \tag{2.54b}$$

$$\hat{U}^\dagger(t)\left|g\right\rangle\left\langle e\right|\hat{U}(t) = e^{-i\omega_{eg}t}\left|g\right\rangle\left\langle e\right|, \tag{2.54c}$$

$$\hat{U}^\dagger(t)\left|e\right\rangle\left\langle g\right|\hat{U}(t) = e^{i\omega_{eg}t}\left|e\right\rangle\left\langle g\right|, \tag{2.54d}$$

$$\hat{U}^\dagger(t)\left|e\right\rangle\left\langle f\right|\hat{U}(t) = e^{-i\omega_{fe}t}\left|e\right\rangle\left\langle f\right|, \tag{2.54e}$$

$$\hat{U}^\dagger(t)\left|f\right\rangle\left\langle e\right|\hat{U}(t) = e^{i\omega_{fe}t}\left|f\right\rangle\left\langle e\right|, \tag{2.54f}$$

where $\omega_{ij} = \omega_i - \omega_j$. The Hamiltonian in this interaction picture is now

$$\begin{aligned}\tilde{H}_I = &\sum_{\boldsymbol{k},\lambda} \hbar \left|g\right\rangle \left\langle e\right| \left[g^{ge}_{\boldsymbol{k},\lambda}\hat{a}_{\boldsymbol{k},\lambda}e^{-i\varpi^C_{eg}t} + \left(g^{ge}_{\boldsymbol{k}}\right)^* \hat{a}^\dagger_{\boldsymbol{k}}e^{i\varpi^R_{eg}t}\right] + \text{H.c.} \\ &+\hbar \left|e\right\rangle \left\langle f\right| \left[g^{ef}_{\boldsymbol{k},\lambda}\hat{a}_{\boldsymbol{k},\lambda}e^{-i\varpi^C_{fe}t} + \left(g^{ef}_{\boldsymbol{k},\lambda}\right)^* \hat{a}^\dagger_{\boldsymbol{k},\lambda}e^{i\varpi^R_{fe}t}\right] + \text{H.c}\end{aligned} \tag{2.55}$$

with the rotating and counter-rotating frequencies

$$\varpi^R_{ij} = \omega_{\boldsymbol{k}} - \omega_{ij}, \tag{2.56a}$$

$$\varpi^C_{ij} = \omega_{\boldsymbol{k}} + \omega_{ij}. \tag{2.56b}$$

Over the shortest time scale of the evolution of the system, the rapidly oscillating terms, those with frequencies ϖ_{ij}^{C}, will average to zero. The *rotating wave approximation* consists in neglecting these counter-rotating terms and leaving only the slower terms with frequencies ϖ_{ij}^{R}. Then after transforming back into the Schrödinger picture, we obtain the interaction

$$\hat{H}_I = \sum_{\boldsymbol{k},\lambda} \hbar \left(g_{\boldsymbol{k},\lambda} \hat{a}^\dagger_{\boldsymbol{k},\lambda} \left|g\right\rangle \left\langle e\right| + g^*_{\boldsymbol{k},\lambda} \hat{a}_{\boldsymbol{k},\lambda} \left|e\right\rangle \left\langle g\right| \right) + \hbar \left(\xi g_{\boldsymbol{k},\lambda} \hat{a}^\dagger_{\boldsymbol{k},\lambda} \left|e\right\rangle \left\langle f\right| + \left(\xi g_{\boldsymbol{k},\lambda}\right)^* \hat{a}_{\boldsymbol{k},\lambda} \left|f\right\rangle \left\langle e\right| \right), \quad (2.57)$$

with

$$g_{\boldsymbol{k},\lambda} = i \sqrt{\frac{\omega_{\boldsymbol{k}}}{2\hbar\epsilon_0 V}} \left(\boldsymbol{d}_{eg} \cdot \hat{\boldsymbol{e}}^*_{\boldsymbol{k},\lambda} \right) e^{-i\boldsymbol{k}\cdot\boldsymbol{r}_0}, \quad (2.58)$$

and the dipole moment ratio

$$\xi \equiv \frac{\boldsymbol{d}_{fe} \cdot \hat{\boldsymbol{e}}^*_{\boldsymbol{k},\lambda}}{\boldsymbol{d}_{eg} \cdot \hat{\boldsymbol{e}}^*_{\boldsymbol{k},\lambda}}. \quad (2.59)$$

Finally, the complete Hamiltonian for a three-level ladder-type atom interacting with the radiation field in the dipole and rotating-wave approximations is

$$\begin{aligned} \hat{H} = \sum_{\boldsymbol{k},\lambda} \hbar\omega_{\boldsymbol{k}} \hat{a}^\dagger_{\boldsymbol{k},\lambda} \hat{a}_{\boldsymbol{k},\lambda} + \hbar\omega_g \left|g\right\rangle \left\langle g\right| + \hbar\omega_e \left|e\right\rangle \left\langle e\right| + \hbar\omega_f \left|f\right\rangle \left\langle f\right| \\ + \sum_{\boldsymbol{k},\lambda} \hbar g_{\boldsymbol{k},\lambda} \hat{a}^\dagger_{\boldsymbol{k},\lambda} \left|g\right\rangle \left\langle e\right| + \hbar\xi g_{\boldsymbol{k},\lambda} \hat{a}^\dagger_{\boldsymbol{k},\lambda} \left|e\right\rangle \left\langle f\right| + \text{H.c.}. \end{aligned} \quad (2.60)$$

2.2.3 Coherent driving

We are interested in investigating the resonance fluorescence of an atom when driven on the two-photon transition. We therefore assume the atom is powered by a coherent driving laser of frequency ω_d. This can be accounted for by taking all but one mode of the field to be in the vacuum state, and a single mode, $\boldsymbol{k}_d$, with a single polarisation, in a highly populated coherent state $|\beta\rangle$, as defined by Eq. (2.38). We then replace the $\hat{a}_{\boldsymbol{k}}$ and $\hat{a}^\dagger_{\boldsymbol{k}}$ operators in Eq. (2.60) with complex numbers after transforming into an interaction picture (Ref. [27], p. 139):

$$\hat{a}_{\boldsymbol{k}_d} \longrightarrow \beta e^{-i\omega_d t}, \quad (2.61a)$$

$$\hat{a}^\dagger_{\boldsymbol{k}_d} \longrightarrow \beta^* e^{i\omega_d t}. \quad (2.61b)$$

We now have the time-dependent Hamiltonian

$$\begin{aligned} \hat{H} = \hbar\omega_g \left|g\right\rangle \left\langle g\right| + \hbar\omega_e \left|e\right\rangle \left\langle e\right| + \hbar\omega_f \left|f\right\rangle \left\langle f\right| + \hbar\frac{\Omega}{2} \left(\left|g\right\rangle \left\langle e\right| e^{i\omega_d t} + \left|e\right\rangle \left\langle g\right| e^{-i\omega_d t} \right) \\ + \hbar\xi\frac{\Omega}{2} \left(\left|e\right\rangle \left\langle f\right| e^{i\omega_d t} + \left|f\right\rangle \left\langle e\right| e^{-i\omega_d t} \right), \end{aligned} \quad (2.62)$$

with

$$\frac{\Omega}{2} \equiv g_{\boldsymbol{k}_d,\lambda} \beta. \quad (2.63)$$

Although the driving strength $g_{\boldsymbol{k}_d,\lambda}\beta$ is generally complex, we may adopt a phase convention such that Ω is a real parameter.

3 Quantum Open Systems

In the previous chapter we dealt with the interaction of an atom with the quantised electromagnetic field inside a "closed" system – that is, a system which does not experience energy gain or loss. Closed systems also have time-reversible evolutions governed only by the Hamiltonian. These two properties are not physically realisable in an experimental setting as the system will have some form of energy loss. We are interested in a driven system where energy is being pumped in and lost via spontaneous emission. This type of dissipative evolution can be modelled by a *master equation*. The atom will eventually reach a steady state, where the energy pumped in is balanced by the loss.

In this chapter we set out the formulation of a general master equation by considering an infinite number of degrees of freedom. We will use this approach to derive a master equation for the three-level system interacting with the vacuum electromagnetic field we are interested in, but by first omitting the driving field, only to reintroduce it after we have accounted for the loss mechanism. Using the master equation, we will then discuss how to recover the optical spectrum and photon-photon correlations of the atom using quantum regression. Finaly, we will consider a different approach to open quantum systems – *quantum trajectory theory*.

3.1 Lindblad Master Equation

We consider a system S coupled to an environment reservoir R through an interaction between S and R. We aim to derive an equation of motion that gives information about the evolution of the system with minimal dependence on the composite system $S \otimes R$. While we will start with a generic formulation for any system-reservoir coupling, we will ultimately consider the system to be the three-level atom, Eq. (2.50), the reservoir to be the electromagnetic field, Eq. (2.42), and the interaction between the two to be the dipole interaction in the rotating-wave approximation, Eq. (2.57).

Following the method of Carmichael (Ref. [28], ch. 1), we give only a general formulation of the derivation.

3.1.1 System plus reservoir approach

We begin with the general Hamiltonian

$$\hat{H} = \hat{H}_S + \hat{H}_R + \hat{H}_{SR}, \tag{3.1}$$

where $\hat{H}_S$, $\hat{H}_R$ and $\hat{H}_{SR}$ are Hamiltonians describing the system, the reservoir and the coupling between them, respectively. We introduce the density operator for the composite $S \otimes R$ system,

$\hat{\chi}(t)$, and then define the *reduced* density operator, $\hat{\rho}(t)$, by taking the trace over the reservoir states:

$$\hat{\rho}(t) \equiv \mathrm{tr}_R \left[\hat{\chi}(t)\right]. \tag{3.2}$$

We can calculate the average of an operator of S, $\hat{A}$, in the Schrödinger picture even if we only have knowledge of $\hat{\rho}(t)$:

$$\langle \hat{A}(t) \rangle = \mathrm{tr}_{S\otimes R}\left[\hat{A}\hat{\chi}(t)\right] = \mathrm{tr}_S\{\hat{A}\mathrm{tr}_R\left[\hat{\chi}(t)\right]\} = \mathrm{tr}_S\left[\hat{A}\hat{\rho}(t)\right]. \tag{3.3}$$

The time evolution of the density operator in the Schrödinger picture is given by

$$\frac{\mathrm{d}}{\mathrm{d}t}\hat{\chi} = \frac{1}{i\hbar}[\hat{H}, \hat{\chi}], \tag{3.4}$$

where $\hat{H}$ is the total Hamiltonian, Eq. (3.1). We transform the density operator into an interaction picture with the unitary evolution operator,

$$\hat{U}(t) = e^{-\frac{i}{\hbar}(\hat{H}_S + \hat{H}_R)t}, \tag{3.5}$$

by defining

$$\hat{\tilde{\chi}}(t) = \hat{U}^\dagger(t)\hat{\chi}(0)\hat{U}(t). \tag{3.6}$$

Transforming Eq. (3.4) into the interaction picture, we then obtain

$$\begin{aligned}\frac{\mathrm{d}}{\mathrm{d}t}\hat{\tilde{\chi}} &= -\frac{1}{i\hbar}\hat{\tilde{\chi}}\left(\hat{H}_S + \hat{H}_R\right) + \frac{1}{i\hbar}\left(\hat{H}_S + \hat{H}_R\right)\hat{\tilde{\chi}} + \hat{U}^\dagger(t)\frac{\mathrm{d}}{\mathrm{d}t}\hat{\chi}\hat{U}(t) \\ &= \frac{1}{i\hbar}[\hat{\tilde{H}}_{SR}, \hat{\tilde{\chi}}],\end{aligned} \tag{3.7}$$

where $\hat{H}_{SR}$ is given the time dependent form

$$\hat{\tilde{H}}_{SR}(t) = \hat{U}^\dagger(t)\hat{H}_{SR}\hat{U}(t). \tag{3.8}$$

Finally, we formally integrate Eq. (3.7) and substitute into the commutator (3.4):

$$\frac{\mathrm{d}}{\mathrm{d}t}\hat{\tilde{\chi}} = \frac{1}{i\hbar}[\hat{\tilde{H}}_{SR}, \hat{\tilde{\chi}}(0)] - \frac{1}{\hbar^2}\int_0^t \mathrm{d}t'[\hat{\tilde{H}}_{SR}(t), [\hat{\tilde{H}}_{SR}(t'), \hat{\tilde{\chi}}(t')]]. \tag{3.9}$$

3.1.2 Born and Markov approximations

We assume that at time $t = 0$, when the interaction is turned on, there are no correlations between S and R. The density operator can then be factorised as

$$\hat{\tilde{\chi}}(0) = \hat{\chi}(0) = \hat{\rho}(0)\hat{R}_0, \tag{3.10}$$

where $\hat{R}_0$ is the initial density operator for the reservoir. We now take the trace of Eq. (3.9) over the reservoir states to obtain the *master equation*

$$\frac{\mathrm{d}}{\mathrm{d}t}\hat{\tilde{\rho}} = -\frac{1}{\hbar^2}\int_0^t \mathrm{d}t' \mathrm{tr}_R \left\{ [\hat{\tilde{H}}_{SR}(t), [\hat{\tilde{H}}_{SR}(t'), \hat{\tilde{\chi}}(t')]] \right\}, \tag{3.11}$$

where we have assumed

$$\mathrm{tr}_R \left[\hat{\tilde{H}}_{SR}(t) \hat{R}_0 \right] = 0 \tag{3.12}$$

and neglected the first commutator term in Eq. (3.9). As the coupling between S and R is very weak we assume that the density operator can be factorised at all times. Thus we expand the density operator in powers of the coupling interaction,

$$\hat{\tilde{\chi}}(t) = \hat{\tilde{\rho}}(t)\hat{R}_0 + \mathcal{O}(\hat{H}_{SR}), \tag{3.13}$$

and make the *Born approximation* by neglecting terms higher than second-order in $\hat{H}_{SR}$,

$$\frac{\mathrm{d}}{\mathrm{d}t}\hat{\tilde{\rho}} = -\frac{1}{\hbar^2}\int_0^t \mathrm{d}t' \mathrm{tr}_R \left\{ [\hat{\tilde{H}}_{SR}(t), [\hat{\tilde{H}}_{SR}(t'), \hat{\tilde{\rho}}(t')\hat{R}_0]] \right\}. \tag{3.14}$$

Our equation of motion for the state $\hat{\tilde{\rho}}(t)$ now depends on the initial state of the reservoir. It also depends on the past behaviour of the system through the integration over $\hat{\tilde{\rho}}(t')$ in Eq. (3.14). We may nonetheless make the *Markov approximation* based on the assumption that the reservoir is much larger than the system; changes in R from its interaction with S are negligible. More specifically, there exist two very different time scales: a slow time scale for the evolution of S, and a rapid time scale of the decaying reservoir correlations. We then replace $\hat{\tilde{\rho}}(t')$ with $\hat{\tilde{\rho}}(t)$ to obtain the master equation in the Born-Markov approximation:

$$\frac{\mathrm{d}}{\mathrm{d}t}\hat{\tilde{\rho}} = -\frac{1}{\hbar^2}\int_0^t \mathrm{d}t' \mathrm{tr}_R \left\{ [\hat{\tilde{H}}_{SR}(t), [\hat{\tilde{H}}_{SR}(t'), \hat{\tilde{\rho}}(t)\hat{R}_0]] \right\}. \tag{3.15}$$

3.1.3 Three-level atom

We know from section 2.2.1 that the atom has two dipole transitions, $|f\rangle \leftrightarrow |e\rangle$ and $|e\rangle \leftrightarrow |g\rangle$, with respective raising (lowering) operators $\hat{\sigma}^+_{fe}$ $(\hat{\sigma}^-_{fe}) = |f\rangle\langle e|$ $\Big(|e\rangle\langle f|\Big)$ and $\hat{\sigma}^+_{eg}$ $(\hat{\sigma}^-_{eg}) = |e\rangle\langle g|$ $\Big(|g\rangle\langle e|\Big)$. These two dipole transitions couple to every mode in the electromagnetic field (reservoir). We then introduce the combined lowering operator

$$\hat{\Sigma} \equiv \hat{\sigma}^-_{eg} + \xi\hat{\sigma}^-_{fe}, \tag{3.16}$$

and returning to our specific interest in a three-level atom coupled to the electromagnetic field, we now adopt a more explicit model for the composite system, with Hamiltonians

$$\hat{H}_S = \hbar\omega_g |g\rangle\langle g| + \hbar\omega_e |e\rangle\langle e| + \hbar\omega_f |f\rangle\langle f|, \tag{3.17a}$$

$$\hat{H}_R = \sum_{\boldsymbol{k},\lambda} \hbar\omega_{\boldsymbol{k}} \hat{r}^\dagger_{\boldsymbol{k},\lambda} \hat{r}_{\boldsymbol{k},\lambda}, \tag{3.17b}$$

$$\hat{H}_{SR} = \sum_{\boldsymbol{k},\lambda} \hbar \left(g^*_{\boldsymbol{k},\lambda} \hat{\Sigma} \hat{r}^\dagger_{\boldsymbol{k},\lambda} + g_{\boldsymbol{k},\lambda} \hat{\Sigma}^\dagger \hat{r}_{\boldsymbol{k},\lambda} \right) = \hbar \left(\hat{\Sigma}\hat{\Gamma}^\dagger + \hat{\Sigma}^\dagger \hat{\Gamma} \right), \tag{3.17c}$$

where $\hat{H}_S$ is the free Hamiltonian of the atom, from Eq. (2.62), with the driving field turned off, and the reservoir Hamiltonian is described by a collection of harmonic oscillators with frequencies $\omega_{\boldsymbol{k}}$, creation and annihilation operators $\hat{r}^\dagger_{\boldsymbol{k},\lambda}$ and $\hat{r}_{\boldsymbol{k},\lambda}$, wavevectors $\boldsymbol{k}$ and polarisation λ. The interaction term, $\hat{H}_{SR}$, contains a product of reservoir operators and atomic operators with a coupling constant $g_{\boldsymbol{k},\lambda}$ as defined by Eq. (2.58), and we have defined

$$\hat{\Gamma}^\dagger \equiv \sum_{\boldsymbol{k},\lambda} g^*_{\boldsymbol{k},\lambda} \hat{r}^\dagger_{\boldsymbol{k},\lambda} \tag{3.18a}$$

$$\hat{\Gamma} \equiv \sum_{\boldsymbol{k},\lambda} g_{\boldsymbol{k},\lambda} \hat{r}_{\boldsymbol{k},\lambda}. \tag{3.18b}$$

We set the reservoir to be in thermal equilibrium at a temperature T, with the initial density operator

$$\hat{R}_0 = \prod_j e^{-\hbar\omega_{\boldsymbol{k}} \hat{r}^\dagger_{\boldsymbol{k},\lambda} \hat{r}_{\boldsymbol{k},\lambda}/k_B T} \left(1 - e^{-\hbar\omega_{\boldsymbol{k}}/k_B T} \right), \tag{3.19}$$

where k_B is Boltzmann's constant. The explicit form of the master equation in the Born-Markov approximation is then

$$\begin{aligned} \frac{\mathrm{d}}{\mathrm{d}t}\hat{\tilde{\rho}}(t) = -\int_0^t \mathrm{d}t' \Big\{ & \left[\hat{\tilde{\Sigma}}(t)\hat{\tilde{\Sigma}}(t')\hat{\tilde{\rho}}(t) - \hat{\tilde{\Sigma}}(t')\hat{\tilde{\rho}}(t)\hat{\tilde{\Sigma}}(t) \right] \langle \hat{\tilde{\Gamma}}(t)\hat{\tilde{\Gamma}}(t') \rangle_R + \text{H.c.} \\ & + \left[\hat{\tilde{\Sigma}}^\dagger(t)\hat{\tilde{\Sigma}}^\dagger(t')\hat{\tilde{\rho}}(t) - \hat{\tilde{\Sigma}}^\dagger(t')\hat{\tilde{\rho}}(t)\hat{\tilde{\Sigma}}^\dagger(t) \right] \langle \hat{\tilde{\Gamma}}^\dagger(t)\hat{\tilde{\Gamma}}^\dagger(t') \rangle_R + \text{H.c.} \\ & + \left[\hat{\tilde{\Sigma}}(t)\hat{\tilde{\Sigma}}^\dagger(t')\hat{\tilde{\rho}}(t) - \hat{\tilde{\Sigma}}^\dagger(t')\hat{\tilde{\rho}}(t)\hat{\tilde{\Sigma}}(t) \right] \langle \hat{\tilde{\Gamma}}(t)\hat{\tilde{\Gamma}}^\dagger(t') \rangle_R + \text{H.c.} \\ & + \left[\hat{\tilde{\Sigma}}^\dagger(t)\hat{\tilde{\Sigma}}(t')\hat{\tilde{\rho}}(t) - \hat{\tilde{\Sigma}}(t')\hat{\tilde{\rho}}(t)\hat{\tilde{\Sigma}}^\dagger(t) \right] \langle \hat{\tilde{\Gamma}}^\dagger(t)\hat{\tilde{\Gamma}}(t') \rangle_R + \text{H.c.} \Big\}, \end{aligned} \tag{3.20}$$

where the system and reservoir operators in the interaction picture are

$$\hat{\tilde{\Sigma}}(t) = \hat{U}^\dagger(t)\hat{\Sigma}(0)\hat{U}(t) = e^{-i\omega_{eg}t} |g\rangle\langle e| + e^{-i\omega_{fe}t}\xi |e\rangle\langle f|, \tag{3.21a}$$

$$\hat{\tilde{\Sigma}}^\dagger(t) = \hat{U}^\dagger(t)\hat{\Sigma}^\dagger(0)\hat{U}(t) = e^{i\omega_{eg}t} |e\rangle\langle g| + e^{i\omega_{ef}t}\xi |f\rangle\langle e|, \tag{3.21b}$$

$$\hat{\tilde{\Gamma}}(t) = \hat{U}^\dagger(t)\hat{\Gamma}(0)\hat{U}(t) = \sum_{\boldsymbol{k},\lambda} g_{\boldsymbol{k},\lambda} \hat{r}_{\boldsymbol{k},\lambda} e^{-i\omega_{\boldsymbol{k}}t}, \tag{3.21c}$$

$$\hat{\tilde{\Gamma}}^\dagger(t) = \hat{U}^\dagger(t)\hat{\Gamma}^\dagger(0)\hat{U}(t) = \sum_{\boldsymbol{k},\lambda} g^*_{\boldsymbol{k},\lambda} \hat{r}^\dagger_{\boldsymbol{k},\lambda} e^{i\omega_{\boldsymbol{k}}t}, \tag{3.21d}$$

and the explicit reservoir correlation functions, $\langle \hat{A}\hat{B} \rangle_R = \mathrm{tr}_R \left[\hat{R}_0 \hat{A}\hat{B}\right]$, are

$$\begin{aligned}
\langle \hat{\tilde{\Gamma}}(t)\hat{\tilde{\Gamma}}(t')\rangle &= \sum_{\boldsymbol{k},\boldsymbol{k}'}\sum_{\lambda,\lambda'} g_{\boldsymbol{k},\lambda} g_{\boldsymbol{k}',\lambda'} e^{-i\omega_{\boldsymbol{k}}t} e^{-i\omega_{\boldsymbol{k}'}t'} \mathrm{tr}_R \left[\hat{R}_0 \hat{r}_{\boldsymbol{k},\lambda}\hat{r}_{\boldsymbol{k}',\lambda'}\right] \\
&= 0, \qquad (3.22a)\\
\langle \hat{\tilde{\Gamma}}^\dagger(t)\hat{\tilde{\Gamma}}^\dagger(t')\rangle &= \sum_{\boldsymbol{k},\boldsymbol{k}'}\sum_{\lambda,\lambda'} g^*_{\boldsymbol{k},\lambda} g^*_{\boldsymbol{k}',\lambda'} e^{i\omega_{\boldsymbol{k}}t} e^{i\omega_{\boldsymbol{k}'}t'} \mathrm{tr}_R \left[\hat{R}_0 \hat{r}^\dagger_{\boldsymbol{k},\lambda}\hat{r}^\dagger_{\boldsymbol{k}',\lambda'}\right] \\
&= 0 \qquad (3.22b)\\
\langle \hat{\tilde{\Gamma}}(t)\hat{\tilde{\Gamma}}^\dagger(t')\rangle &= \sum_{\boldsymbol{k},\lambda} |g_{\boldsymbol{k},\lambda}|^2 e^{-i\omega_{\boldsymbol{k}}(t-t')} \left[\hat{R}_0 \hat{r}_{\boldsymbol{k},\lambda}\hat{r}^\dagger_{\boldsymbol{k}',\lambda'}\right], \\
&= \sum_{\boldsymbol{k},\lambda} |g_{\boldsymbol{k},\lambda}|^2 e^{-i\omega_{\boldsymbol{k}}(t-t')} \left[\bar{n}(\omega_{\boldsymbol{k}},T)+1\right], \qquad (3.22c)\\
\langle \hat{\tilde{\Gamma}}^\dagger(t)\hat{\tilde{\Gamma}}(t')\rangle &= \sum_{\boldsymbol{k},\lambda} |g_{\boldsymbol{k},\lambda}|^2 e^{i\omega_{\boldsymbol{k}}(t-t')} \mathrm{tr}_R \left[\hat{R}_0 \hat{r}^\dagger_{\boldsymbol{k},\lambda}\hat{r}_{\boldsymbol{k},\lambda}\right] \\
&= \sum_{\boldsymbol{k},\lambda} |g_{\boldsymbol{k},\lambda}|^2 e^{i\omega_{\boldsymbol{k}}(t-t')} \bar{n}(\omega_{\boldsymbol{k}},T), \qquad (3.22d)
\end{aligned}$$

where

$$\bar{n}(\omega_{\boldsymbol{k}},T) = \frac{e^{-\hbar\omega_{\boldsymbol{k}}/k_BT}}{1-e^{-\hbar\omega_{\boldsymbol{k}}/k_BT}} \qquad (3.23)$$

is the mean thermal photon number at temperature T of reservoir modes of frequency $\omega_{\boldsymbol{k}}$. If we change the summation over modes to an integral by introducing the density of states $\varrho(\boldsymbol{k})$ and making use of the dispersion relation, $\omega_{\boldsymbol{k}} = kc$, the master equation becomes

$$\begin{aligned}
\frac{\mathrm{d}}{\mathrm{d}t}\hat{\tilde{\rho}} = -\int_0^t \mathrm{d}t' \Bigg\{ &\left[\hat{\tilde{\Sigma}}(t)\hat{\tilde{\Sigma}}^\dagger(t')\hat{\tilde{\rho}} - \hat{\tilde{\Sigma}}^\dagger(t')\hat{\tilde{\rho}}\hat{\tilde{\Sigma}}(t)\right]\langle \hat{\tilde{\Gamma}}^\dagger(t)\hat{\tilde{\Gamma}}(t')\rangle_R + \mathrm{H.c.} \\
&+ \left[\hat{\tilde{\Sigma}}^\dagger(t)\hat{\tilde{\Sigma}}(t')\hat{\tilde{\rho}} - \hat{\tilde{\Sigma}}(t')\hat{\tilde{\rho}}\hat{\tilde{\Sigma}}^\dagger(t)\right]\langle \hat{\tilde{\Gamma}}(t)\hat{\tilde{\Gamma}}^\dagger(t')\rangle_R + \mathrm{H.c.}\Bigg\},
\end{aligned} \qquad (3.24)$$

with the reservoir correlation functions

$$\langle \hat{\tilde{\Gamma}}^\dagger(t)\hat{\tilde{\Gamma}}(t')\rangle_R = \sum_\lambda \int \mathrm{d}^3\boldsymbol{k} e^{i\omega_{\boldsymbol{k}}(t-t')} \varrho(\boldsymbol{k}) |g(\boldsymbol{k},\lambda)|^2 \bar{n}(\boldsymbol{k},T), \qquad (3.25a)$$

$$\langle \hat{\tilde{\Gamma}}(t)\hat{\tilde{\Gamma}}^\dagger(t')\rangle_R = \sum_\lambda \int \mathrm{d}^3\boldsymbol{k} e^{-i\omega_{\boldsymbol{k}}(t-t')} \varrho(\boldsymbol{k}) |g(\boldsymbol{k},\lambda)|^2 \left[\bar{n}(\boldsymbol{k},T)+1\right]. \qquad (3.25b)$$

The decay operator $\hat{\tilde{\Sigma}}(t)$ in the interaction picture is the sum of two separate operators which oscillate at different frequencies. Equation (3.24) then involves sixteen terms as well as their Hermitian conjugates. To simplify this problem we will assume the reservoir is in a vacuum state and set $\bar{n}(\omega,T) \to 0$, thereby retaining only the second term of Eq. (3.24). This still leaves us with eight terms plus Hermitian conjugates with different combinations of frequency dependence. We

may nevertheless assume that over the range of fluorescence frequencies of the atom the density of states, $\varrho(\boldsymbol{k})$, and the field-atom coupling, $g(\boldsymbol{k},\lambda)$, are constant. We evaluate these functions at the average resonance frequency – the two-photon transition frequency $\omega = \omega_{fg}/2$ - and adopt spherical coordinates in $\boldsymbol{k}$-space to write the density states as

$$\varrho \boldsymbol{k} \mathrm{d}^3\boldsymbol{k} = \frac{(\omega_{fg}/2)^2 V}{8\pi^3 c^3} \mathrm{d}\omega \mathrm{d}\Omega. \tag{3.26}$$

Substituting the coupling constant, Eq. (2.58), the correlation function, Eq. (3.25b), becomes

$$\langle \hat{\tilde{\Gamma}}(t) \hat{\tilde{\Gamma}}^\dagger(t') \rangle_R = \pi \sum_\lambda \frac{(\omega_{fg}/2)^3}{16\hbar\pi^3 c^3 \epsilon_0} \int \mathrm{d}\Omega \left(\boldsymbol{d}_{eg} \cdot \hat{\boldsymbol{e}}_{\boldsymbol{k},\lambda}\right)^2 \delta\left(t - t'\right). \tag{3.27}$$

We may now evaluate the time integral in Eq. (3.24) to obtain the master equation in the interaction picture

$$\frac{\mathrm{d}}{\mathrm{d}t}\hat{\tilde{\rho}} = \frac{\gamma}{2}\left(2\hat{\tilde{\Sigma}}(t)\hat{\tilde{\rho}}\hat{\tilde{\Sigma}}^\dagger(t) - \hat{\tilde{\Sigma}}^\dagger(t)\hat{\tilde{\Sigma}}(t)\hat{\tilde{\rho}} - \hat{\tilde{\rho}}\hat{\tilde{\Sigma}}^\dagger(t)\hat{\tilde{\Sigma}}(t)\right), \tag{3.28}$$

with decay rate

$$\gamma \equiv 2\pi \sum_\lambda \frac{(\omega_{fg}/2)^3}{16\hbar\pi^3 c^3 \epsilon_0} \int \mathrm{d}\Omega \left(\boldsymbol{d}_{eg} \cdot \hat{\boldsymbol{e}}_{\boldsymbol{k},\lambda}\right)^2. \tag{3.29}$$

Although a master equation like Eq. (3.28) would generally also contain dispersive (frequency shift) terms, these have been eliminated at the level of the approximations used. We choose to neglect these terms, as we aim only for a phenomenological treatment of damping in an artificial atom (transmon), rather than a first-principles treatment of a model system. After transforming back into the Schrödinger picture, we thus obtain the *Lindblad* master equation for a three-level atom with spontaneous emission:

$$\frac{\mathrm{d}}{\mathrm{d}t}\hat{\rho} = \frac{1}{i\hbar}[\hat{H}_S, \hat{\rho}] + \frac{\gamma}{2}\left(2\hat{\Sigma}\hat{\rho}\hat{\Sigma}^\dagger - \hat{\Sigma}^\dagger\hat{\Sigma}\hat{\rho} - \hat{\rho}\hat{\Sigma}^\dagger\hat{\Sigma}\right). \tag{3.30}$$

Finally, we make the extension to an atom driven by a coherent laser, to which end we replace the system Hamiltonian, Eq. (3.17a), by

$$\begin{aligned}\hat{H}_S = \hbar\omega_g |g\rangle\langle g| + \hbar\omega_e |e\rangle\langle e| + \hbar\omega_f |f\rangle\langle f| + \hbar\frac{\Omega}{2}\left(|g\rangle\langle e| e^{i\omega_d t} + |e\rangle\langle g| e^{-i\omega_d t}\right) \\ + \hbar\xi\frac{\Omega}{2}\left(|e\rangle\langle f| e^{i\omega_d t} + |f\rangle\langle e| e^{-i\omega_d t}\right).\end{aligned} \tag{3.31}$$

3.2 Two-Time Correlation Functions

The focus of this thesis is on the fluorescence emitted from a three-level atom and the photon-photon correlations of this fluorescence. The optical spectrum of a stationary field $\hat{E}(t)$ can be

calculated by taking the Fourier transform of the first-order correlation function (Ref. [23], Sect. 3.3)

$$G^{(1)}(\tau) = \lim_{t\to\infty} \langle \hat{\boldsymbol{E}}^{(-)}(t)\hat{\boldsymbol{E}}^{(+)}(t+\tau)\rangle. \tag{3.32}$$

This first order correlation quantifies the coherence of two electric fields. Experiments such as Young's double slit experiment were very important in determining the duality of light by showing such interference patterns. On the other hand, the second order correlation,

$$G^{(2)}(\tau) = \lim_{t\to\infty} \langle \hat{\boldsymbol{E}}^{(-)}(t)\hat{\boldsymbol{E}}^{(-)}(t+\tau)\hat{\boldsymbol{E}}^{(+)}(t+\tau)\hat{\boldsymbol{E}}^{(+)}(t)\rangle, \tag{3.33}$$

provides information on the likelihood of detecting a second photon at a time delay τ after a first photon detection. Hanbury Brown and Twiss performed an important experiment showing bunching of such delayed photon coincidences [6]. There will be a more detailed discussion of the two orders of coherence in the following chapters.

The master equation we have developed allows us to solve for the density operator of a system interacting with a reservoir as a function of time. It also allows us to solve for one-time averages of an operator $\hat{A}$ computed by the standard formula

$$\langle \hat{A}(t)\rangle = \mathrm{tr}[\hat{A}\hat{\rho}(t)]. \tag{3.34}$$

What it cannot directly provide are two-time or multi-time averages. Resonance fluorescence and photon correlations – which are our interest – rely on computing two-time operator averages. We now discuss how the master equation can be used to compute these averages.

3.2.1 Quantum Regression

We start by considering the Lindblad master equation, Eq. (3.30), recast in the form

$$\frac{\mathrm{d}}{\mathrm{d}t}\hat{\rho} = \mathcal{L}\hat{\rho}, \tag{3.35}$$

with Liouvillian superoperator

$$\mathcal{L}\bullet = \frac{1}{i\hbar}[\hat{H},\bullet] + \frac{\gamma}{2}\left(2\hat{\Sigma}\bullet\hat{\Sigma}^\dagger - \hat{\Sigma}^\dagger\hat{\Sigma}\bullet - \bullet\hat{\Sigma}^\dagger\hat{\Sigma}\right). \tag{3.36}$$

For two operators, $\hat{A}$ and $\hat{B}$, which both satisfy the Heisenberg equations of motion, the two-time average is

$$\langle \hat{A}(t)\hat{B}(t+\tau)\rangle = \mathrm{tr}_{S\otimes R}\left[\hat{\chi}(0)\hat{A}(t)\hat{B}(t+\tau)\right], \tag{3.37}$$

where we consider the case $\tau \geq 0$. If we then solve the Heisenberg equations of motion formally, writing

$$\hat{A}(t) = \hat{U}^\dagger(t)\hat{A}(0)\hat{U}(t) \tag{3.38}$$

and

$$\hat{B}(t+\tau) = \hat{U}^\dagger(t+\tau)\hat{B}(0)\hat{U}(t+\tau) \tag{3.39}$$

with $\hat{U}(t)$ the time evolution operator, we may use the cyclic property of the trace and the Born-Markoff approximation (see Ref. [28], Sect. 1.5.1) to obtain

$$\langle \hat{A}(t)\hat{B}(t+\tau)\rangle = \mathrm{tr}_S\left[\hat{B}(0)e^{\mathcal{L}\tau}\left(\hat{\rho}(t)\hat{A}(0)\right)\right]. \tag{3.40}$$

Following a similar procedure, we can also calculate the correlation function of three operators from the quantum regression formula

$$\langle \hat{A}(t)\hat{B}(t+\tau)\hat{C}(t)\rangle = \mathrm{tr}_S\left[\hat{B}(0)e^{\mathcal{L}\tau}\left(\hat{C}(0)\hat{\rho}(t)\hat{A}(0)\right)\right]. \tag{3.41}$$

3.3 Quantum Trajectory Theory

When we derived the master we traced over the reservoir, causing us to lose information about the entanglement between the system and the reservoir. We can recover some of this information by *disentangling* the system from the reservoir, rather than tracing over the reservoir. We are able to do this by considering a situation where an ideal detector is placed in the reservoir which detects photons lost from the system. When considering the master equation, the Markov and Born approximation protects the system evolution from being affected by the presence of the detector; however, by disentangling, there will be some effect due to measurement backaction on the future evolution of the system state. In order to uncover this more detailed view of the dynamics, we aim to "unravel" the density operator into a collection of possible measurement records – or "trajectories" [29].

3.3.1 Unravelling the density operator

Following the treatment of Carmichael (Ref. [30], ch. 17), we separate the Liouvillian superoperator, Eq. (3.36), into two parts, writing $\mathcal{L} = (\mathcal{L} - \mathcal{S}) + \mathcal{S}$, with interaction term

$$\mathcal{S} \equiv \gamma\hat{\Sigma}\bullet\hat{\Sigma}^\dagger, \tag{3.42}$$

such that

$$\begin{aligned}\mathcal{L} - \mathcal{S} &= \frac{1}{i\hbar}[\hat{H},\bullet] - \frac{\gamma}{2}\left(\hat{\Sigma}^\dagger\hat{\Sigma}\bullet + \bullet\,\hat{\Sigma}^\dagger\hat{\Sigma}\right)\\ &= \frac{1}{i\hbar}\left(\hat{H}'\bullet - \bullet\,\hat{H}'^\dagger\right),\end{aligned} \tag{3.43}$$

which governs the free evolution of the system, with the non-Hermitian Hamiltonian

$$\hat{H}' = \hat{H} - i\hbar\frac{\gamma}{2}\hat{\Sigma}^\dagger\hat{\Sigma}. \tag{3.44}$$

Transforming into an effective "interaction picture", Eq. (3.35) becomes

$$\frac{\mathrm{d}}{\mathrm{d}t}\hat{\tilde{\rho}} = e^{-(\mathcal{L}-\mathcal{S})t}\mathcal{S}e^{(\mathcal{L}-\mathcal{S})t}\hat{\tilde{\rho}}, \tag{3.45}$$

with

$$\hat{\tilde{\rho}} = e^{-(\mathcal{L}-\mathcal{S})t}\hat{\rho}(t). \tag{3.46}$$

This differential equation has the formal solution

$$\hat{\tilde{\rho}}(t) = \hat{\rho}(0) + \int_0^t \mathrm{d}t' e^{-(\mathcal{L}-\mathcal{S})t'}\mathcal{S}e^{(\mathcal{L}-\mathcal{S})t'}\hat{\rho}(0). \tag{3.47}$$

We may then proceed with a Dyson expansion to obtain

$$\hat{\rho}(t) = \sum_{n=0}^{\infty}\left\{\int_0^t \mathrm{d}t_n \int_0^{t_n} \mathrm{d}t_{n-1}\cdots\int_0^{t_2}\mathrm{d}t_1 e^{(\mathcal{L}-\mathcal{S})(t-t_n)}\mathcal{S}e^{(\mathcal{L}-\mathcal{S})(t_n-t_{n-1})}\mathcal{S}\cdots\mathcal{S}e^{(\mathcal{L}-\mathcal{S})t_1}\hat{\rho}(0)\right\}, \tag{3.48}$$

where we have reversed the transformation, Eq. (3.46). We now rewrite the density operator as

$$\hat{\rho}(t) = \sum_{n=0}^{\infty}\int_0^t \mathrm{d}t_n \int_0^{t_n} \mathrm{d}t_{n-1}\cdots\int_0^{t_2}\mathrm{d}t_1 P_{\mathrm{REC}}(t)\left|\psi_{\mathrm{REC}}(t)\right\rangle\left\langle\psi_{\mathrm{REC}}(t)\right|, \tag{3.49}$$

with normalised conditional state

$$\left|\psi_{\mathrm{REC}}(t)\right\rangle = \frac{\left|\tilde{\psi}_{\mathrm{REC}}(t)\right\rangle}{\sqrt{\langle\tilde{\psi}_{\mathrm{REC}}(t)|\tilde{\psi}_{\mathrm{REC}}(t)\rangle}}, \tag{3.50}$$

conditional probability

$$P_{\mathrm{REC}}(t) = \langle\tilde{\psi}_{\mathrm{REC}}(t)|\tilde{\psi}_{\mathrm{REC}}(t)\rangle, \tag{3.51}$$

and unnormalised state

$$\left|\tilde{\psi}_{\mathrm{REC}}(t)\right\rangle = e^{-\frac{i}{\hbar}\hat{H}'(t-t_n)}\hat{J}_\gamma e^{-\frac{i}{\hbar}\hat{H}'(t_n-t_{n-1})}\hat{J}_\gamma\cdots\hat{J}_\gamma e^{-\frac{i}{\hbar}\hat{H}'t_1}\left|\psi(0)\right\rangle, \tag{3.52}$$

where we have introduced the jump operator

$$\hat{J}_\gamma = \sqrt{\gamma}\,\hat{\Sigma}. \tag{3.53}$$

The photon detector will produce a record of detection times, $t_1, t_2, \ldots, t_n$, which we refer to with the REC label. The Dyson expansion in Eq. (3.48) then refers to the sum over all possible numbers of photon detections recorded in an experiment, while the integral covers all possible times in the interval $[0, t]$ at which the detections occur. The state, $|\tilde{\psi}_{\mathrm{REC}}(t)\rangle$, is governed by the non-Hermitian evolution Hamiltonian, $\hat{H}'$, with intermittent jumps, $\hat{J}$, acting on an initial pure state

$|\psi(0)\rangle$. The probability for a particular path leading to state $|\tilde{\psi}_{\mathrm{REC}}(t)\rangle$ is given by

$$P_{\mathrm{REC}}(t)\mathrm{d}t_1\mathrm{d}t_2\cdots\mathrm{d}t_n = \langle\tilde{\psi}_{\mathrm{REC}}(t)|\tilde{\psi}_{\mathrm{REC}}(t)\rangle\,\mathrm{d}t_1\mathrm{d}t_2\cdots\mathrm{d}t_n. \tag{3.54}$$

3.3.2 Monte Carlo simulations

We are able to compute stochastic realisations of the states, $|\tilde{\psi}(t)\rangle$, of a quantum trajectory by using a Monte Carlo algorithm. We consider the time interval of the trajectory, $[0,t]$, to be broken into discrete steps of size $\mathrm{d}t$. At each time step the trajectory has two possible paths it might take: free evolution governed by the non-Hermitian Hamiltonian $\hat{H}'$, or a jump executed by the operator $\hat{J}$:

$$|\tilde{\psi}_{\mathrm{REC}}(t+\mathrm{d}t)\rangle = \begin{cases} \text{either} & e^{-\frac{i}{\hbar}\hat{H}\mathrm{d}t}\,|\tilde{\psi}_{\mathrm{REC}}(t)\rangle \\ \text{or} & \hat{J}_\gamma\,|\tilde{\psi}_{\mathrm{REC}}(t)\rangle\,. \end{cases} \tag{3.55}$$

The decision to evolve freely or jump is made by comparing the conditional probabilities for either of the two events for a given photon detection record. Using Bayesian inference, the conditional probability to evolve freely in interval $(t, t+\mathrm{d}t]$, given the detection record up to time t, is

$$\begin{aligned} \mathrm{Prob(free\ evolution)} &= \frac{\mathrm{Prob}\left(e^{-\frac{i}{\hbar}\hat{H}\mathrm{d}t}\,|\tilde{\psi}_{\mathrm{REC}}(t)\rangle\right)}{P_{\mathrm{REC}}(t)} \\ &= \langle\psi_{\mathrm{REC}}(t)|e^{-\frac{i}{\hbar}(\hat{H}'^{\dagger}-\hat{H}')\mathrm{d}t}|\psi_{\mathrm{REC}}(t)\rangle \\ &= \langle\psi_{\mathrm{REC}}(t)|e^{-\gamma\hat{\Sigma}^{\dagger}\hat{\Sigma}\mathrm{d}t}|\psi_{\mathrm{REC}}(t)\rangle\,, \end{aligned} \tag{3.56}$$

and the conditional probability for a jump to occur is

$$\begin{aligned} \mathrm{Prob(jump)} &= \frac{\mathrm{Prob}\left(\hat{J}_\gamma\,|\tilde{\psi}_{\mathrm{REC}}(t)\rangle\right)}{P_{\mathrm{REC}}(t)}\mathrm{d}t \\ &= \langle\psi_{\mathrm{REC}}(t)|\hat{J}_\gamma^{\dagger}\hat{J}_\gamma|\psi_{\mathrm{REC}}(t)\rangle\mathrm{d}t \\ &= \gamma\,\langle\psi_{\mathrm{REC}}(t)|\hat{\Sigma}^{\dagger}\hat{\Sigma}|\psi_{\mathrm{REC}}(t)\rangle\,\mathrm{d}t, \end{aligned} \tag{3.57}$$

where we note that the $P_{\mathrm{REC}}(t)$ in the denominator converts unnormalised bras and kets into normalized bras and kets. We choose $\mathrm{d}t$ to be sufficiently small that in each time step only a single action occurs. Physically this means that the photon detector we have set up will only register at most one photon detection in the interval $(t, t+\mathrm{d}t]$. We now see that the probabilities add to unity as

$$\begin{aligned} \mathrm{Prob(free\ evolution)} &\approx \langle\psi_{\mathrm{REC}}(t)|1-\gamma\mathrm{d}t\hat{\Sigma}^{\dagger}\hat{\Sigma}|\psi_{\mathrm{REC}}(t)\rangle \\ &= 1-\gamma\mathrm{d}t\,\langle\psi_{\mathrm{REC}}(t)|\hat{\Sigma}^{\dagger}\hat{\Sigma}|\psi_{\mathrm{REC}}(t)\rangle \\ &= 1-\mathrm{Prob(jump)}. \end{aligned} \tag{3.58}$$

The probability for a jump to occur is the only information required in order to decide how the system evolves from one time step to another. Now that we have all the pieces, the trajectory simulation can be simplified into four steps [31]:

Step 1. Compute the probability for a jump to occur.

Step 2. Generate a random number $z \in [0, 1)$.

Step 3. Compare with the probability for a jump to occur:

3.a. If $z \geq$ Prob(jump) then freely evolve with $\hat{H}'$ so

$$|\tilde{\psi}(t + \mathrm{d}t)\rangle = e^{-\frac{i}{\hbar}\hat{H}'\mathrm{d}t}\,|\tilde{\psi}_{\mathrm{REC}}(t)\rangle\,; \tag{3.59}$$

3.b. If $z <$ Prob(jump) then a jump occurs so

$$|\tilde{\psi}(t + \mathrm{d}t)\rangle = \hat{J}_\gamma\,|\tilde{\psi}_{\mathrm{REC}}(t)\rangle\,. \tag{3.60}$$

Step 4. Renormalise the state and go back to Step 1.

An operator expectation in a single trajectory can be computed in the usual way as

$$\langle \hat{A}(t)\rangle_{\mathrm{REC}} = \langle \psi_{\mathrm{REC}}(t)|\hat{A}|\psi_{\mathrm{REC}}(t)\rangle\,, \tag{3.61}$$

while an ensemble average is given by the sum over N independent quantum trajectories

$$\overline{\langle \hat{A}(t)\rangle}_{\mathrm{REC}} = \frac{1}{N}\sum_{\{\mathrm{REC}\}_N} \langle \psi_{\mathrm{REC}}(t)|\hat{A}|\psi_{\mathrm{REC}}(t)\rangle\,, \tag{3.62}$$

where the $\{\mathrm{REC}\}_N$ label refers to an ensemble of N realised trajectory records. Taking the limit $N \to \infty$ is equivalent to averaging over all possible trajectories, resulting in the same operator average we would expect from the density operator:

$$\lim_{N\to\infty} \overline{\langle \hat{A}(t)\rangle}_{\mathrm{REC}} \longrightarrow \langle \hat{A}(t)\rangle = \mathrm{tr}\left[\hat{A}\hat{\rho}(t)\right]. \tag{3.63}$$

In a similar fashion, if we compute the time average of a trajectory record for a sufficiently long time, we will also arrive at the same result given that quantum trajectories are ergodic [32, 33].

4 Atomic Dynamics

The motivation for this thesis comes from the work of Gasparinetti et al. and their experiments on a three-level ladder-type artificial atom [12, 13]. Up to this point we have modelled a real atom interacting with the electromagnetic field in free space, whereas the Gasparinetti experiment was conducted on a superconducting circuit. In recent times, circuit quantum electrodynamics (QED) has been a way to achieve experimental results for cavity QED studies.

Here we will give a brief overview of circuit QED, as an analogue and extension of cavity QED, as well as a review of the experimental set up that forms the basis of this thesis. We will remove the time dependence from the Hamiltonian Eq. (3.31) by transforming into a frame rotating at the drive frequency. This allows us to restate the Hamiltonian in simpler terms. Finally, we will investigate the steady states of the atom in different parameter regimes.

4.1 From Cavity to Circuit QED

Cavity quantum electrodynamics (QED) is the study of an atom interacting with a quantised electromagnetic field inside a cavity. In the past decade, superconducting circuits have been used to successfully model the dynamics of a cavity QED setting. This makes circuit QED a very popular candidate for quantum computing and quantum technology [11, 34].

4.1.1 Circuit QED: A brief review

In place of a real atom, circuit QED experiments "engineer" artificial atoms using superconducting circuits that utilise the quantum tunnelling of pairs of electrons – Cooper pairs – between two coupled superconducting plates. This effect, known as the Josephson effect [35, 36], is the main component in the three main types of qubits: charge qubits [37], flux qubit [38], and phase qubits [39].

One of the first realised artificial atoms was the Cooper pair box [40, 41], which consists of an "island" of superconducting material which is coupled to a grounded reservoir via a Josephson junction [42]. The use of superconducting materials requires the experiments to be performed at very low temperatures, on the order of mK. At such low temperatures the effect of thermal noise is also minimised. This is important as these artificial atoms usually "emit" radiation in the range of 1-30 GHz and, even at 20 mK, the peak blackbody radiation is approximately 1.2 GHz [43].

The experiments this thesis is based on (Refs. [12, 13, 44]) were performed on a transmon superconducting circuit. A transmon is a Cooper pair box operating in the strong coupling regime – where the Josephson tunnelling energy is much greater than the charging energy [45, 46]. Transmons are anharmonic oscillators which have many unequally spaced energy levels, and this makes them

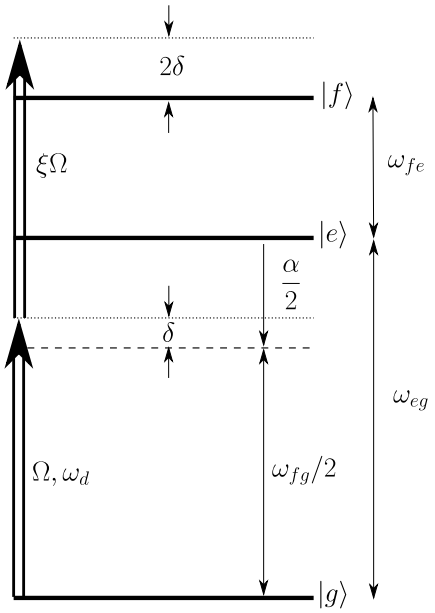

Figure 4.1: Energy level diagram of the three-level artificial atom: ω_{ge} and ω_{ef} are single-photon resonance frequencies, ω_{fg} is the two-photon resonance frequency, δ and $\alpha/2$ are detunings, Ω and $\xi\Omega$ are Rabi frequencies, and ω_d is the drive frequency.

good candidates for artificial atoms. The transmon is typically coupled to a *coplanar transmission line* which acts like a waveguide in a traditional optical setting. "Cavities" are created by making a break in the transmission line, where two capacitors act as traditional mirrors. The output of this circuit is then transmitted to a waveguide. In a cavity QED setting, the atom spontaneously emits into a random mode in three-dimensional space; however, in the circuit QED setting, with coupling to a waveguide, the energy is emitted into a single (transverse) spatial mode.

4.1.2 Time independent Hamiltonian

While the experiments this work is based on were conducted on an artificial atom we model our approach on a real atom where the laser is is replaced by a coherent microwave drive. Although largely phenomenological, carrying over Lindblad master equations from a fundamental quantum optics model to circuit QED is a common practice and has been found to work very well, even at a quantitative level (see, e.g., Refs. [12, 44, 47]). We wish to restate the Hamiltonian Eq. (3.31) in terms of useful parameters from a circuit QED setting by removing the time dependence. To this end we may decompose the Hamiltonian in the form

$$\hat{H} = \hat{H}_0' + \left(\hat{H} - \hat{H}_0'\right), \tag{4.1}$$

with

$$\hat{H}_0' = \lambda_g |g\rangle\langle g| + \lambda_e |e\rangle\langle e| + \lambda_f |f\rangle\langle f|, \tag{4.2}$$

where $\lambda_g, \lambda_e, \lambda_f$ are parameters. We then transform into a frame rotating at frequency ω_d with the unitary evolution operator

$$\hat{U}(t) = e^{-\frac{i}{\hbar}\hat{H}_0' t}, \tag{4.3}$$

fixing the adjustable parameters so as to accomplish our aim. In the Hamiltonian, Eq. (3.31), we generate time dependence in the new interaction picture with

$$\hat{U}^\dagger \left(e^{i\omega_d t} |g\rangle \langle e| \right) \hat{U} = e^{i\omega_d t} e^{-i(\lambda_e - \lambda_g)t} |g\rangle \langle e| , \tag{4.4a}$$

$$\hat{U}^\dagger \left(e^{i\omega_d t} |e\rangle \langle f| \right) \hat{U} = e^{i\omega_d t} e^{-i\left(\lambda_f - \lambda_e\right)t} |e\rangle \langle f| . \tag{4.4b}$$

To remove this time dependence we now choose λ_g, λ_e, and λ_f to satisfy

$$\lambda_e - \lambda_g = \omega_d, \tag{4.5a}$$

$$\lambda_f - \lambda_e = \omega_d, \tag{4.5b}$$

and by setting the ground state energy to zero, $\lambda_g - \omega_g = 0$, we obtain the time-independent Hamiltonian for a driven three-level ladder-type atom

$$\hat{H} = -\hbar \left(\frac{\alpha}{2} + \delta \right) |e\rangle \langle e| - 2\hbar\delta |f\rangle \langle f| + \hbar \frac{\Omega}{2} \Big(|g\rangle \langle e| + |e\rangle \langle g| \Big) + \hbar\xi \frac{\Omega}{2} \Big(|e\rangle \langle f| + |f\rangle \langle e| \Big), \tag{4.6}$$

where, following Gasparinetti et al. (Refs. [12, 13]), we have defined the *anharmonicity* of the $|e\rangle \to |g\rangle$ and $|f\rangle \to |e\rangle$ transitions,

$$\alpha = \omega_{fe} - \omega_{eg}, \tag{4.7}$$

and the *drive detuning from two-photon resonance*

$$2\delta = 2\omega_d - \omega_{fg}. \tag{4.8}$$

For this thesis we take the anharmonicity of the transmon to be negative [13]. In fact, to consider two-photon resonance, the anharmonicity must be very high compared with the linewidth, $|\alpha|/\gamma \gg 1$. If $\alpha \approx 0$, the atom would be able to able to transition from $|g\rangle$ to $|f\rangle$ via $|e\rangle$ in two separate absorption events. We are interested in the case where the atom can only be excited to the $|f\rangle$ state by absorbing two photons simultaneously. Figure 4.1 shows how this can happen via a virtual state and how the different parameters we have defined relate to one another.

4.2 Steady States

In this section we use numerical methods to solve the master equation and survey the effects each of the parameters in our model have on the steady state of the atom. We then use a simplified model where we have adiabatically removed the intermediate state, $|e\rangle$, to derive analytic expressions for the steady states. From these expressions we are able to qualitatively clarify the observations we

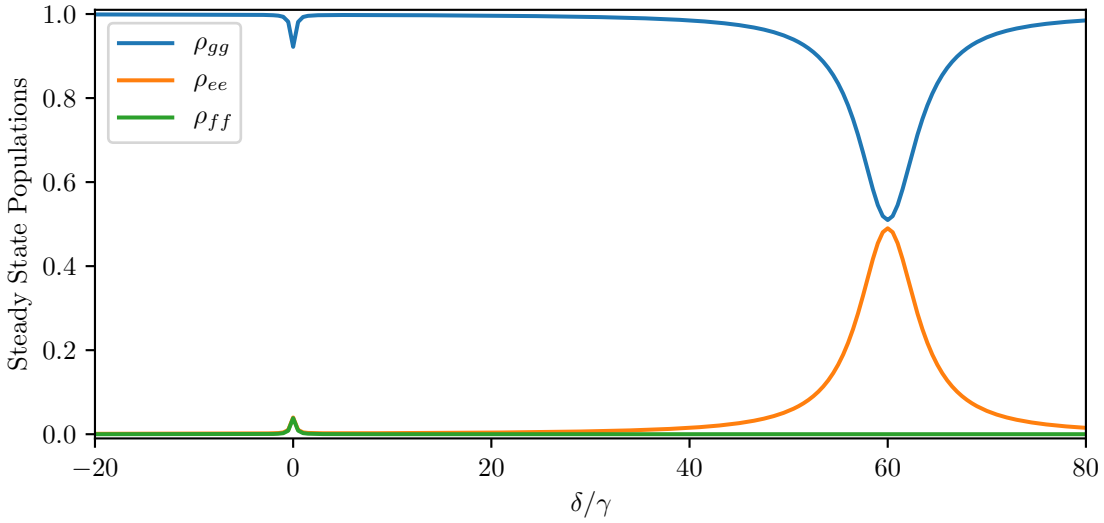

Figure 4.2: Steady state populations for $|g\rangle$ (blue), $|e\rangle$ (orange), and $|f\rangle$ (green) plotted against the two-photon resonance detuning parameter δ. There are peaks at the single-photon ($\delta/\gamma = 60.0$) and two-photon ($\delta/\gamma = 0.0$) resonances. Parameters are $(\Omega/\gamma, \alpha/\gamma, \xi) = (5.0, -120.0, 1.0)$.

have made from our numerical calculations.

4.2.1 Numerical survey of populations in steady state

For very weak drives, we expect the atom to remain largely in state $|g\rangle$. At two-photon resonance, however, there is a peak in the probability to occupy states $|e\rangle$ and $|f\rangle$, as the atom simultaneously absorbs two photons of frequency $\omega_{fg}/2$ to excite $|f\rangle$, and then decays to the ground state via a *cascade decay* through $|e\rangle$. There is also a large peak in the probability to occupy state $|e\rangle$ at the single-photon resonance $\delta = -\alpha/2$, as the drive is resonant with the lower $|g\rangle \leftrightarrow |e\rangle$ transition. These resonance effects are illustrated in Fig. 4.2.

While this thesis is concerned with the case where $|\alpha|/\gamma \gg 1$, let us for a moment consider the case where $\alpha = 0$, as in Fig. 4.3a. Then, if the field driving this harmonic three-level ladder is resonant with the two-photon transition, $\delta = 0$, it is also resonant with both the $|g\rangle \leftrightarrow |e\rangle$ and $|e\rangle \leftrightarrow |f\rangle$ transitions. Population is able to move into the state $|f\rangle$ by two-photon absorption, as well as by two single-photon absorptions, first into state $|e\rangle$ and then into state $|f\rangle$. Due to the single-photon resonance with the state $|e\rangle$, away from $\delta = 0$, the state $|e\rangle$ is more populated than state $|f\rangle$.

If we increase the anharmonicity to $\alpha/\gamma = -120$, we see, in Fig. 4.3b, that the region of detuning with significant population in the states $|e\rangle$ and $|f\rangle$ has narrowed. This becomes more apparent in Fig. 4.3c, where $\alpha/\gamma = -500$. We see that there is an effective two-photon drive for a $|g\rangle \leftrightarrow |f\rangle$ transition that is inversely proportional to α. For a fixed Ω, as we increase $|\alpha|$, the effective two-photon drive becomes weaker. Fig. 4.3, with the exception of the $\alpha/\gamma = -120$ case,

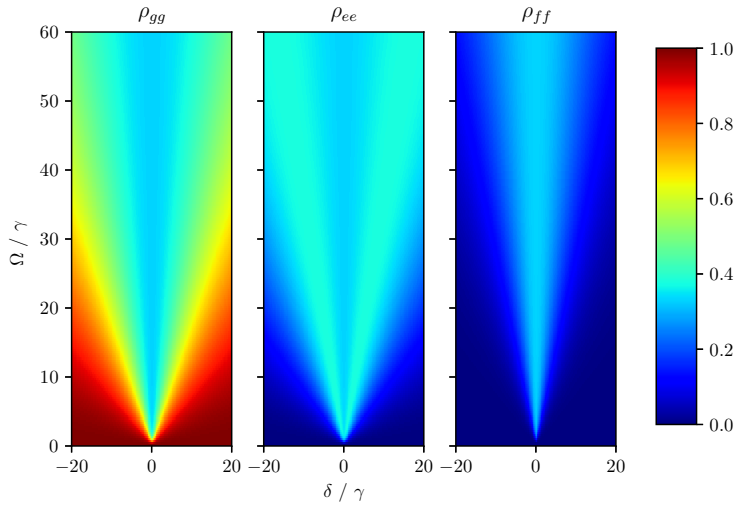

(a) $\alpha/\gamma = 0.0$

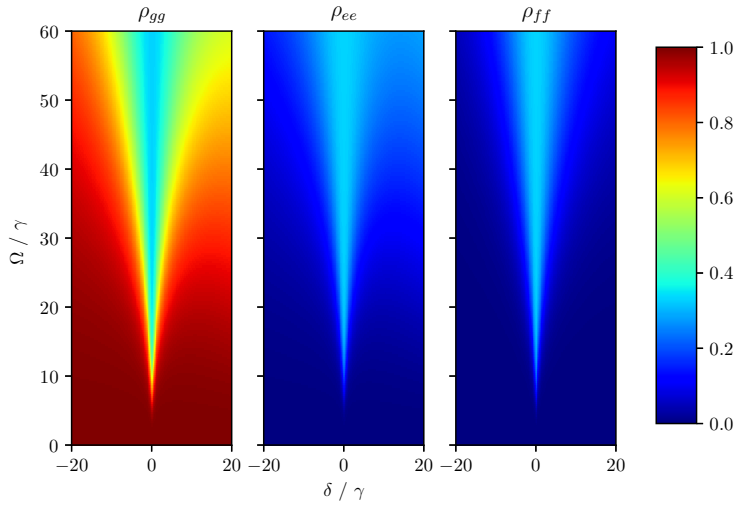

(b) $\alpha/\gamma = -120.0$

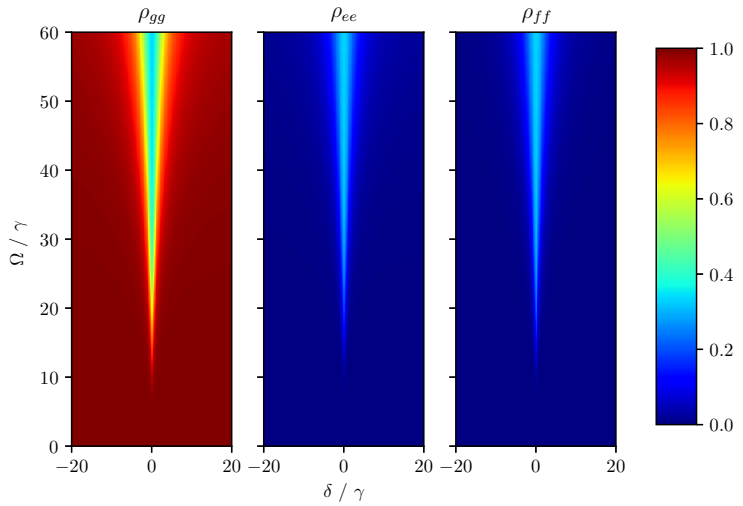

(c) $\alpha/\gamma = -500.0$

Figure 4.3: Steady state population plotted as a function of detuning from two-photon resonance for three different values of anharmonicity α. We have set $\xi = 1.0$.

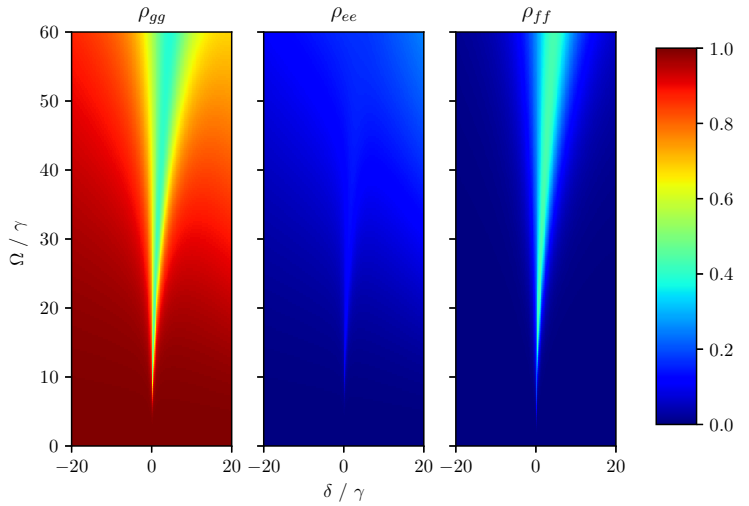

(a) $\xi = 0.5$

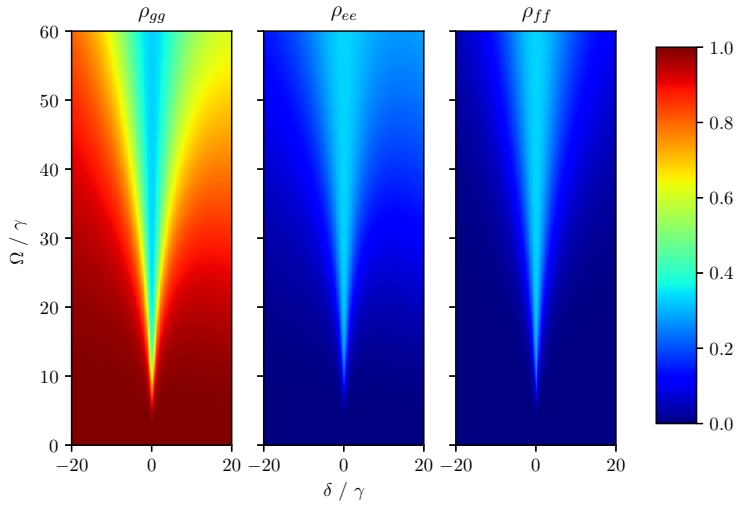

(b) $\xi = 1.0$

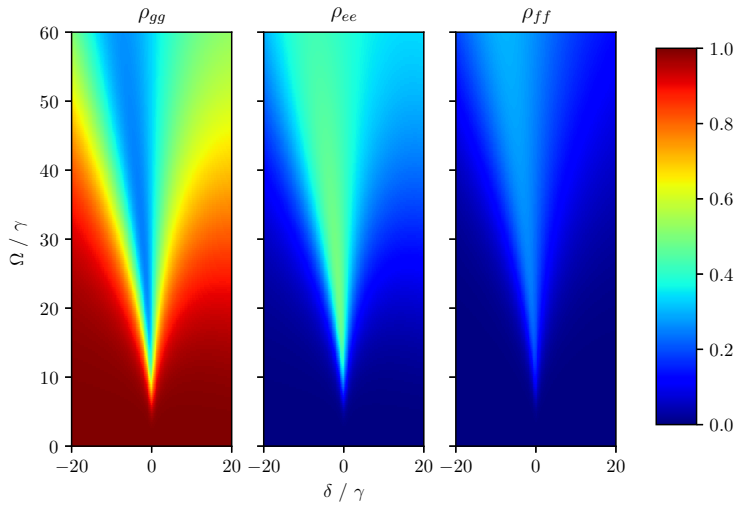

(c) $\xi = 1.5$

Figure 4.4: Steady state populations plotted as a function of detuning from the two-photon resonance for three different values of the dipole moment ratio ξ. We have set $\alpha/\gamma = -120.0$.

show a symmetry about the two-photon resonance. The symmetry in Fig. 4.3b breaks down as the effects of the single-photon resonance, at $\delta = 60$, start to appear. This also occurs for $\alpha/\gamma = -500$, but we would have to expand the range of the drive strength and the detuning to see it. Only for the case of zero anharmonicity is there a complete symmetry due to the single-photon and double-photon resonances being the same.

One other parameter that plays a significant role in the evolution of the atom is the dipole moment ratio ξ. This ratio plays two important roles: first, it determines the ratio of Rabi frequencies (drive strengths) for the $|g\rangle \to |e\rangle$ and $|e\rangle \to |f\rangle$ transitions; and, second, it determines the ratio of the decay rates from the upper states of these transitions. By increasing this ratio we not only allow the atom to be excited to the state $|f\rangle$ with a stronger drive, but we also increase the rate at which population decays from $|f\rangle$ to $|e\rangle$ by a factor of ξ^2. We see in Fig. 4.4c that, due to the increased decay rate, more steady state population accumulates in $|e\rangle$ than $|f\rangle$ for stronger drives. The opposite can also be seen in Fig. 4.4a where, for a lower ξ, there is more population in $|f\rangle$. We already know from Fig. 4.3c that, for $\xi = 1$, the steady state populations of $|e\rangle$ and $|f\rangle$ are approximately the same, so we can conclude that they must be proportional to each other with some dependence on ξ.

The symmetry seen in Fig. 4.3 is lost as we change the dipole moment ratio. For an increasing ξ, the region of two-photon resonance appears to shift towards negative values of δ, while for a decreasing ξ, this region shifts towards positive δ. Not only is there an effective two-photon drive, but there also appears to be an effective two-photon resonance that shifts as the drive strength increases. While the symmetry for these two parameters is lost, there is one important effect on the steady state that these two parameters share; it is that the effective two-photon drive appears to be dependent on both. Not only is it apparent that the effective two-photon drive is inversely proportional on the anharmonicity, but it also appears to be directly proportional to ξ. As we increase the dipole moment ratio, the region of two-photon resonance also increases, as we see in Fig. 4.4.

4.2.2 Simplified model: adiabatic elimination of the intermediate state

We now employ a "secular approximation" of the atom and adiabatically eliminate the intermediate state $|e\rangle$ to obtain an effective two-level atom [48, 49]. We begin by solving Schrödinger's equation for the Hamiltonian Eq. (4.6), where for the pure state

$$|\psi(t)\rangle = c_g(t)\,|g\rangle + c_e(t)\,|e\rangle + c_f(t)\,|f\rangle\,, \tag{4.9}$$

we obtain three coupled differential equations $\left(\dot{x} = \frac{\mathrm{d}}{\mathrm{d}t}x\right)$:

$$\dot{c}_g = -i\frac{\Omega}{2}c_e(t), \tag{4.10a}$$

$$\dot{c}_e = -i\frac{\Omega}{2}c_g(t) + i\left(\frac{\alpha}{2} + \delta\right)c_e(t) - i\xi\frac{\Omega}{2}c_f(t), \tag{4.10b}$$

$$\dot{c}_f = -i\xi\frac{\Omega}{2}c_e(t) + 2i\delta c_f(t). \tag{4.10c}$$

In order to adiabatically eliminate the $|e\rangle$ state, we set the time derivative to zero in Eq. (4.10b), rearrange to solve for c_e, and substitute back into the remaining expressions, leaving us with the pair of coupled equations

$$\dot{c}_g = -i\left(\frac{\Omega}{2}\right)^2\frac{1}{\alpha/2+\delta}c_g(t) - i\xi\left(\frac{\Omega}{2}\right)^2\frac{1}{\alpha/2+\delta}c_f(t), \tag{4.11a}$$

$$\dot{c}_f = -i\xi\left(\frac{\Omega}{2}\right)^2\frac{1}{\alpha/2+\delta}c_g(t) - i\left[\left(\frac{\xi\Omega}{2}\right)^2\frac{1}{\alpha/2+\delta} - 2\delta\right]c_f(t). \tag{4.11b}$$

From these equations, we construct the effective Hamiltonian

$$\hat{H}_{\text{eff}} = \hbar\delta_g\left|g\right\rangle\left\langle g\right| + \hbar\left(-2\delta+\delta_f\right)\left|f\right\rangle\left\langle f\right| + \hbar\frac{\Omega_{\text{eff}}}{2}\Big(\left|g\right\rangle\left\langle f\right| + \left|f\right\rangle\left\langle g\right|\Big), \tag{4.12}$$

with *effective two-photon drive*

$$\frac{\Omega_{\text{eff}}}{2} = \xi\left(\frac{\Omega}{2}\right)^2\frac{1}{\alpha/2+\delta}. \tag{4.13}$$

and frequency shifts due to the Stark effect [50–52]

$$\delta_g = \left(\frac{\Omega}{2}\right)^2\frac{1}{\alpha/2+\delta}, \tag{4.14a}$$

$$\delta_f = \left(\xi\frac{\Omega}{2}\right)^2\frac{1}{\alpha/2+\delta}. \tag{4.14b}$$

From Eqs. (4.13) and (4.14) we clearly see that this aproximation will not hold when the atom is driven at single-photon resonance. We therefore assume that the atom is driven near two-photon resonance and that the ratio $(\Omega/2)^2/(\alpha/2)^2$ is much less than one. The level shifts clearly cause a shift in the two-photon resonance frequency as well. If the drive is resonant with the bare two-photon resonant frequency, it may not be resonant with the shifted frequency. We therefore define the *effective detuning from two-photon resonance*:

$$2\Delta_{\text{eff}} = -2\delta + \delta_f - \delta_g = -2\delta + \left(\frac{\Omega}{2}\right)^2\frac{1}{\alpha/2+\delta}\left(\xi^2-1\right). \tag{4.15}$$

Equations (4.13) and (4.15) have already confirmed two of the observations made in the previous section. For this approximate model, we see that the effective two-photon drive is proportional to ξ and inversely proportional to α, confirming what we see in Figs. 4.3 and 4.4. It is also clear that, when both dipole moments are equal we get the symmetrical steady states in Fig. 4.3. The levels shift further from their bare frequencies as the drive strength increases; however, if $\xi = 1$, the shift is zero.

To find analytic expressions for the steady state populations, we may take the approximation

one step further. While we have adiabatically removed the state $|e\rangle$ from the excitation process, it is still required for the cascade decay. Considering that we have assumed the anharmonicity of the atom is large, the factors in the master equation, Eq. (3.30), oscillating at frequency $|\omega_{eg} - \omega_{fe}|$ average to zero (Ref. [27], p. 173). The cross terms which arise from multiplying $\hat{\Sigma}$ and $\hat{\Sigma}^\dagger$ can then be neglected, leaving us with the master equation in the secular approximation

$$\begin{aligned}\frac{\mathrm{d}}{\mathrm{d}t}\hat{\rho} = \frac{1}{i\hbar}[\hat{H}_{\text{eff}}, \hat{\rho}] + \frac{\gamma}{2}\left(2\hat{\sigma}^-_{eg}\hat{\rho}\hat{\sigma}^+_{eg} - \hat{\sigma}^+_{eg}\hat{\sigma}^-_{eg}\hat{\rho} - \hat{\rho}\hat{\sigma}^+_{eg}\hat{\sigma}^-_{eg}\right) \\ + \frac{\gamma}{2}\xi^2\left(2\hat{\sigma}^-_{fe}\hat{\rho}\hat{\sigma}^+_{fe} - \hat{\sigma}^+_{fe}\hat{\sigma}^-_{fe}\hat{\rho} - \hat{\rho}\hat{\sigma}^+_{fe}\hat{\sigma}^-_{fe}\right),\end{aligned} \tag{4.16}$$

with separate decay operators $\hat{\sigma}^-_{eg}\ \left(\hat{\sigma}^+_{eg}\right) = |g\rangle\langle e|\ \left(\ |e\rangle\langle g|\ \right)$ and $\hat{\sigma}^-_{fe}\ \left(\hat{\sigma}^+_{fe}\right) = |e\rangle\langle f|\ \left(\ |f\rangle\langle e|\ \right)$. We then expand the density operator in the form

$$\hat{\rho}(t) = \sum_{i,j\in\{g,e,f\}} \rho_{ij}(t)\,|i\rangle\langle j|\,, \tag{4.17}$$

and obtain nine coupled differential equations for the density matrix elements. Using the fact that $\rho_{ff} = 1 - \rho_{gg} - \rho_{ee}$, we are able to reduce these to two sets of four coupled differential equations $\left(\frac{\mathrm{d}}{\mathrm{d}t}x = \dot{x}\right)$:

$$\dot{\rho}_{gg} = i\frac{\Omega_{\text{eff}}}{2}\rho_{gf}(t) + \gamma\rho_{ee}(t) - i\frac{\Omega_{\text{eff}}}{2}\rho_{fg}(t), \tag{4.18a}$$

$$\dot{\rho}_{gf} = 2i\frac{\Omega_{\text{eff}}}{2}\rho_{gg}(t) - \left(\frac{\gamma}{2}\xi^2 - i\Delta_{\text{eff}}\right)\rho_{gf} + i\frac{\Omega_{\text{eff}}}{2}\rho_{ee}(t) - i\frac{\Omega_{\text{eff}}}{2}, \tag{4.18b}$$

$$\dot{\rho}_{ee} = -\gamma\xi^2\rho_{gg}(t) - \gamma\left(1+\xi^2\right)\rho_{ee}(t) + \gamma\xi^2, \tag{4.18c}$$

$$\dot{\rho}_{fg} = -2i\frac{\Omega_{\text{eff}}}{2}\rho_{gg}(t) - i\frac{\Omega_{\text{eff}}}{2}\rho_{ee}(t) - \left(\frac{\gamma}{2}\xi^2 + i\Delta_{\text{eff}}\right)\rho_{fg}(t) + i\frac{\Omega_{\text{eff}}}{2}, \tag{4.18d}$$

and

$$\dot{\rho}_{ge} = -\left(\frac{\gamma}{2} + i\delta_g\right)\rho_{ge}(t) - i\frac{\Omega_{\text{eff}}}{2}\rho_{fe}(t), \tag{4.19a}$$

$$\dot{\rho}_{eg} = -\left(\frac{\gamma}{2} - i\delta_g\right)\rho_{eg}(t) + i\frac{\Omega_{\text{eff}}}{2}\rho_{ef}(t), \tag{4.19b}$$

$$\dot{\rho}_{ef} = i\frac{\Omega_{\text{eff}}}{2}\rho_{eg}(t) - \left(\frac{\gamma}{2}\left(1+\xi^2\right) - i\left(\delta_f - 2\delta\right)\right)\rho_{ef}(t), \tag{4.19c}$$

$$\dot{\rho}_{fe} = -i\frac{\Omega_{\text{eff}}}{2}\rho_{ge}(t) - \left(\frac{\gamma}{2}\left(1+\xi^2\right) + i\left(\delta_f - 2\delta\right)\right)\rho_{fe}(t). \tag{4.19d}$$

Solving for the steady state by setting the derivatives to zero, we find the following solutions:

$$\rho^{ss}_{gg} = \frac{1}{Z}\left[\left(\frac{\Omega_{\text{eff}}}{2}\right)^2 + \Delta^2_{\text{eff}} + \frac{\gamma^2}{2}\xi^4\right], \tag{4.20a}$$

$$\rho^{ss}_{ee} = \frac{1}{Z}\xi^2\left(\frac{\Omega_{\text{eff}}}{2}\right)^2, \tag{4.20b}$$

$$\rho_{ff}^{ss} = \frac{1}{Z}\left(\frac{\Omega_{\text{eff}}}{2}\right)^2, \tag{4.20c}$$

$$\rho_{gf}^{ss} = \frac{1}{Z}\left(\frac{\Omega_{\text{eff}}}{2}\right)\left[-\Delta_{\text{eff}} + i\frac{\xi^2}{2}\right], \tag{4.20d}$$

$$\rho_{ge}^{ss} = 0, \tag{4.20e}$$

$$\rho_{ef}^{ss} = 0, \tag{4.20f}$$

and

$$\rho_{ij}^{ss} = \left(\rho_{ji}^{ss}\right)^*, \tag{4.20g}$$

with denominator

$$Z = \left(\frac{\Omega_{\text{eff}}}{2}\right)^2 \left(2 + \xi^2\right) + \Delta_{\text{eff}}^2 + \frac{\gamma^2}{2}\xi^4. \tag{4.21}$$

We have assumed

$$2\left(\frac{\Omega}{2}\right)^2 \frac{\left(\xi^2 - 1\right)}{\left(\alpha/2\right)^2} < 1. \tag{4.22}$$

We therefore expect, for a fixed α, that, as the drive strength increases, the analytic results diverge from the correct numerical results. We clearly see this in Fig. 4.5 where $\xi \neq 1$. When $\xi = 1$, however, the analytic expressions tend to agree as Ω increases.

The analytic expressions confirm many of the observations made. As we expect, the steady state populations of the states $|e\rangle$ and $|f\rangle$ are dependent on the effective two-photon drive. We also see that the steady state population of the state $|e\rangle$ is directly proportional to that of state $|f\rangle$ with proportionality factor ξ^2. When $\xi = 1$, we see that they are exactly the same, as demonstrated in Fig. 4.3c.

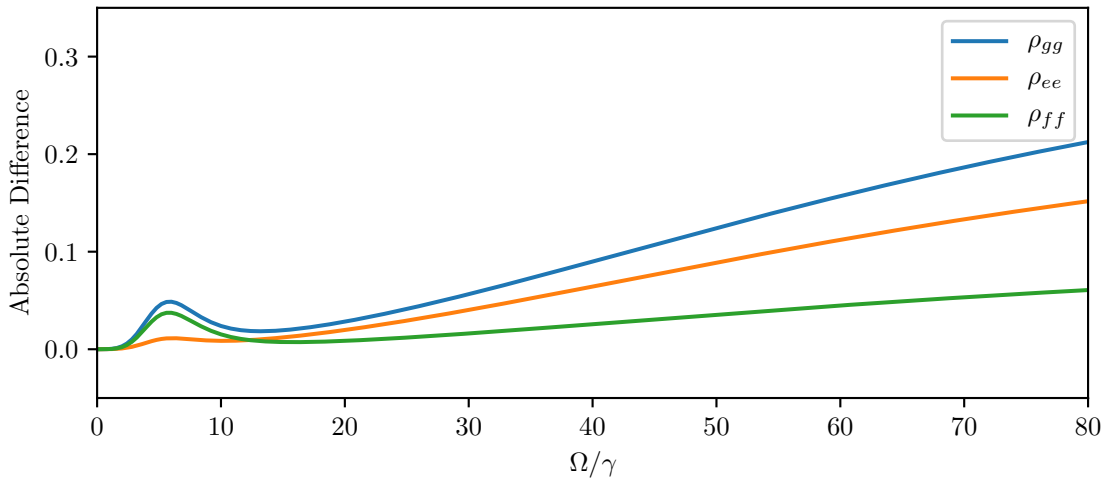

(a) $\xi = 0.5$

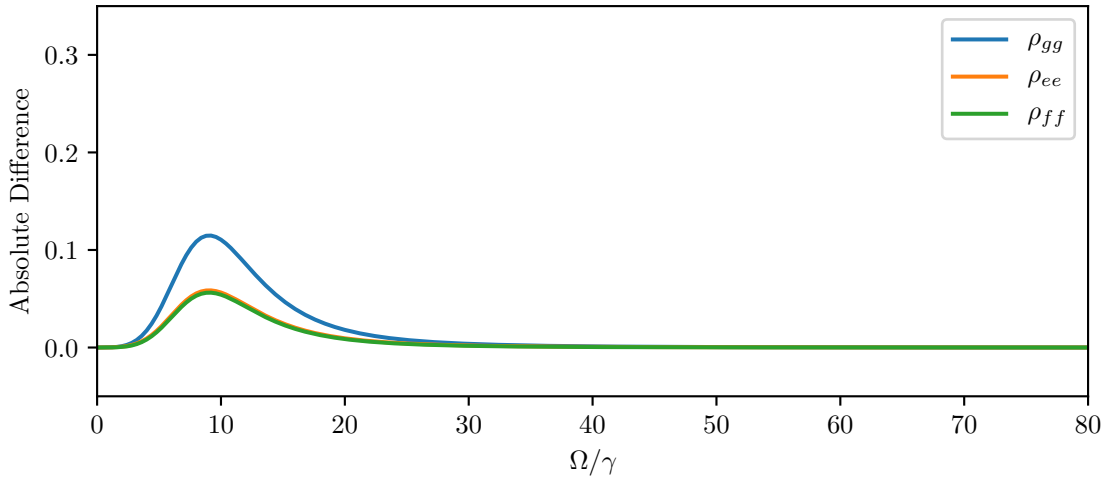

(b) $\xi = 1.0$

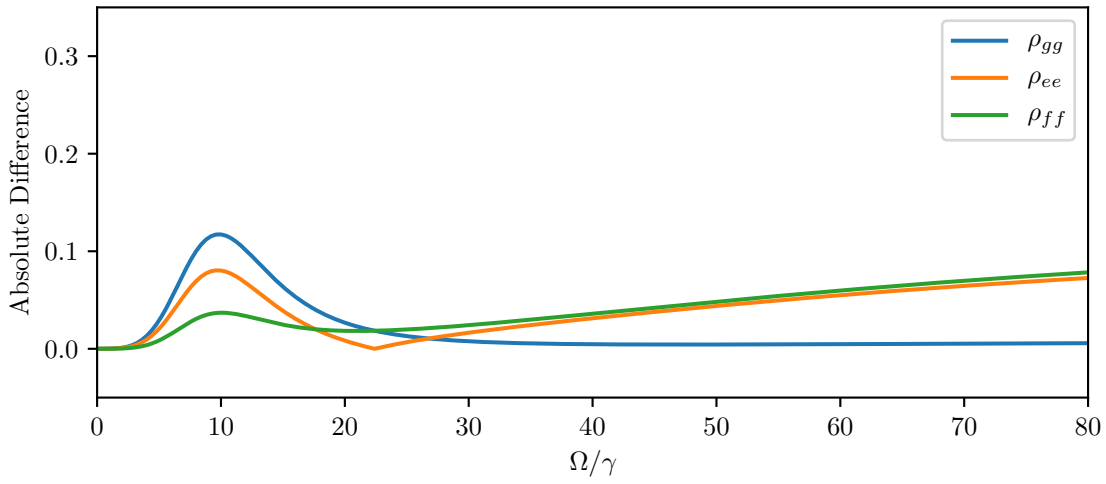

(c) $\xi = 1.5$

Figure 4.5: The absolute difference between the numerical steady states and the analytic expressions at two-photon resonance. The parameters are $(\delta/\gamma, \alpha/\gamma) = (0.0, -120.0)$

5 Optical Spectrum

In previous chapters, we have mentioned that our three-level atom of interest undergoes a cascaded decay. In this chapter we will see that the atom not only decays from the state $|f\rangle$ to $|e\rangle$ and then from $|e\rangle$ to the state $|g\rangle$, but, if the drive is strong enough, it will also make transitions between what are called *dressed states*. We start this chapter with a discussion on the dressed state picture and then we derive an expression for the dressed states of our three-level atom driven at two-photon resonance. In order to look at the fluorescence spectrum, we will then show how the electric field operator, as defined in Eq. (2.24a), can be expressed in terms of the atomic decay operator $\hat{\Sigma}$, Eq. (3.16). Making this substitution in the first-order correlation function, Eq. (3.32), we use the Wiener-Khintchine theorem (Ref. [53], pp. 56-60) and calculate the power spectrum of the fluorescence. Following the steps of the previous chapter, we then investigate how the fluorescence spectrum changes as the different parameters are varied.

5.1 Dressed States

The bare states of the atom, $|g\rangle, |e\rangle$, and $|f\rangle$, are eigenstates of the bare Hamiltonian, Eq. (2.43). They are not, however, eigenstates of the full Hamiltonian, Eq. (4.6). The eigenstates of the full Hamiltonian, including the interaction with the coherent driving field, are the so-called dressed states. In this section we will derive expressions for the dressed states and their respective eigenfrequencies at two-photon resonance.

5.1.1 Analytic expression

We adopt the bare states of the atom as basis states and identify them with the basis vectors:

$$|g\rangle \longrightarrow \begin{pmatrix} 1 \\ 0 \\ 0 \end{pmatrix}, \quad |e\rangle \longrightarrow \begin{pmatrix} 0 \\ 1 \\ 0 \end{pmatrix}, \quad |f\rangle \longrightarrow \begin{pmatrix} 0 \\ 0 \\ 1 \end{pmatrix}. \tag{5.1}$$

Thus we restate the time-independent Hamiltonian, Eq. (4.6), in matrix form:

$$\hat{H} \longrightarrow \hbar \begin{pmatrix} 0 & \frac{\Omega}{2} & 0 \\ \frac{\Omega}{2} & -\frac{\alpha}{2} - \delta & \xi\frac{\Omega}{2} \\ 0 & \xi\frac{\Omega}{2} & -2\delta \end{pmatrix}. \tag{5.2}$$

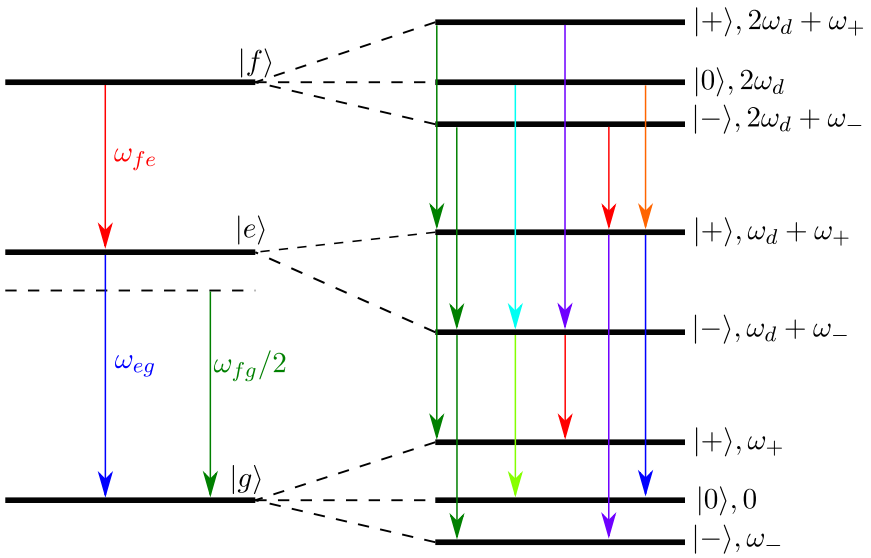

Figure 5.1: Dressed states of the atom at two-photon resonance, $\delta = 0$, with all possible decay transitions shown. As the driving field increases (dashed lines), the $|g\rangle$ and $|f\rangle$ states split to acquire three dressed state components: $|+\rangle, |-\rangle$, and $|0\rangle$. The intermediate state $|e\rangle$ splits to acquire only $|+\rangle$ and $|-\rangle$ components.

We then solve for the dressed states by diagonalising the Hamiltonian matrix, beginning with the characteristic polynomial

$$\lambda^3 + \left(\frac{\alpha}{2} + 3\delta\right)\lambda^2 + \left[(\alpha + 2\delta)\,\delta - \left(\frac{\Omega}{2}\right)^2 (1 + \xi^2)\right]\lambda - 2\delta\left(\frac{\Omega}{2}\right)^2 = 0. \tag{5.3}$$

Being cubic, this polynomial has a complicated general solution, and therefore, to simplify, we specialize to the case of primary interest, two-photon resonance, where for $\delta = 0$ the three eigenfrequencies are

$$\omega_0 = 0, \tag{5.4a}$$

$$\omega_\pm = -\frac{\alpha}{4} \pm \sqrt{\left(\frac{\alpha}{4}\right)^2 + \left(\frac{\Omega}{2}\right)^2 (1 + \xi^2)}, \tag{5.4b}$$

with corresponding eigenvectors defining the dressed states:

$$|0\rangle \longrightarrow \frac{1}{\sqrt{1 + \xi^2}} \begin{pmatrix} \xi \\ 0 \\ -1 \end{pmatrix}, \tag{5.5a}$$

$$|\pm\rangle \longrightarrow \frac{1}{\sqrt{4\omega_\pm^2 + \Omega^2 (1 + \xi^2)}} \begin{pmatrix} \Omega \\ 2\omega_\pm \\ \xi\Omega \end{pmatrix}. \tag{5.5b}$$

We now invert the transformation made in Sect. 4.1.2 with the unitary evolution operator

$$\hat{U}(t) = e^{-i\omega_d t|e\rangle\langle e|} e^{-2i\omega_d t|f\rangle\langle f|}, \tag{5.6}$$

which is Eq. (4.3), with ground state energy set to zero, and then consider how the dressed states evolve with time:

$$|0\rangle \to \frac{e^{-i\omega_0 t}}{\sqrt{1+\xi^2}}\Big(\xi\,|g\rangle - e^{-2i\omega_d t}\,|f\rangle\Big), \tag{5.7a}$$

$$|\pm\rangle \to \frac{e^{-i\omega_\pm t}}{\sqrt{4\omega_\pm^2 + \Omega^2\,(1+\xi^2)}}\Big(\Omega\,|g\rangle + 2\omega_\pm e^{-i\omega_d t}\,|e\rangle + \xi\Omega e^{-2i\omega_d t}\,|f\rangle\Big). \tag{5.7b}$$

For a standard energy eigenket, $|E\rangle$, with energy $\hbar\omega$, we expect it to evolve as $e^{-i\omega t}$. We see this is the case in Eq. (5.7), but with the dressed state time-evolution from the interaction picture adding to the free evolution of the time-dependent states $e^{-i\omega_d t}\,|e\rangle$ and $e^{-2i\omega_d t}\,|f\rangle$. We thus see that the frequencies appearing in Eq. (5.7) are combinations of the dressed state frequencies, Eq. (5.4), and the drive frequency ω_d which comes from the transformation out of the interaction picture. These eight frequencies are shown in Fig. 5.1, in an energy-level like diagram, where $2\omega_d = \omega_{fg}$. We expect twelve possible transitions to occur, with seven distinct frequencies:

$$\omega_0 = \omega_d, \tag{5.8a}$$

$$\omega_{1,2} = \omega_d \pm \omega_+, \tag{5.8b}$$

$$\omega_{3,4} = \omega_d \pm \omega_-, \tag{5.8c}$$

$$\omega_{5,6} = \omega_d \pm (\omega_+ - \omega_-)\,. \tag{5.8d}$$

We therefore expect to see seven peaks in the fluorescence spectrum, which is quite different from the two expected transitions from the bare states cascade decay; first $|f\rangle \to |e\rangle$ with transition frequency ω_{fe}; and then $|e\rangle \to |g\rangle$ with transition frequency ω_{eg}. If we consider a weak driving field, we find the dressed state frequencies

$$\omega_0 = 0, \quad \omega_+ \approx -\frac{\alpha}{2}, \quad \omega_- \approx 0, \tag{5.9}$$

where $\alpha < 0$. In this limit there are only three distinct transition frequencies:

$$\omega_0' = \omega_d, \quad \omega_1' = \omega_d + \omega_+ = \omega_{eg}, \quad \omega_2' = \omega_d - \omega_+ = \omega_{fe}, \tag{5.10}$$

which correspond to the cascade decay of the bare states and elastic scattering ($\omega_0' = \omega_d$). As the drive strength increases and the dressed frequencies separate further, more possible decay transitions become available to the atom. The dressed state picture is able to give us the frequencies of the peaks of the fluorescence spectrum; however, it can not tell us anything about relative heights of the peaks. For us to do that we require a detailed quantum-mechanical treatment.

5.2 First-Order Coherence

The coherence of light has long been an important topic in optics, both in classical and quantum optics. While there exist many orders of coherence (Ref. [23], p. 35), in this section we will consider only the first-order correlation function – originating from the discussion of fringe visibility from interfering fields (Ref. [24], Sect. 4.2). We use this section to set out the background for the following section where we discuss the optical spectrum of the light emitted from the coherently driven three-level atom.

5.2.1 First-order correlation function

From a classical optics perspective, coherence was associated with interference fringes from two superposed fields. The simplest example of this is Young's double slit experiment, where a field is passed through two closely spaced pinholes, interfering at a point on a screen. In this context we introduce the first-order correlation function,

$$G^{(1)}(\boldsymbol{r}, t, \boldsymbol{r}', t') = \langle \hat{\boldsymbol{E}}^{(-)}(\boldsymbol{r}, t)\hat{\boldsymbol{E}}^{(+)}(\boldsymbol{r}', t')\rangle, \tag{5.11}$$

which "correlates" the electric field at two different points in space, $\boldsymbol{r}$ and $\boldsymbol{r}'$, and at times t and t' (Ref. [54], p. 221). From here we see the difference between the two main forms of coherence usually discussed: *temporal* coherence and *spatial* coherence. Typically, from a quantum optics perspective, we consider a single point detector, with $\boldsymbol{r} = \boldsymbol{r}'$, thereby considering only the temporal coherence of the field. Adopting this restriction, from Schwarz's inequality, we find that the magnitude of $G^{(1)}(t, t')$ is bounded by

$$|G^{(1)}(t, t')| \leq |G^{(1)}(t, t)G^{(1)}(t', t')|^{1/2}. \tag{5.12}$$

Then defining the time variable $\tau \equiv t - t'$, we introduce the normalised first-order correlation function

$$g^{(1)}(\tau) = \frac{\langle \hat{\boldsymbol{E}}^{(-)}(t)\hat{\boldsymbol{E}}^{(+)}(t+\tau)\rangle}{\sqrt{\langle \hat{\boldsymbol{E}}^{(-)}(t)\hat{\boldsymbol{E}}^{(+)}(t)\rangle\langle \hat{\boldsymbol{E}}^{(-)}(t+\tau)\hat{\boldsymbol{E}}^{(+)}(t+\tau)\rangle}}, \tag{5.13}$$

which has a range of

$$|g^{(1)}(\tau)| \leq 1. \tag{5.14}$$

If the fields are coherent then $|g^{(1)}(\tau)| = 1$, whereas, if the fields are uncorrelated $g^{(1)}(\tau) = 0$ (Ref. [55], p. 73).

5.2.2 Radiated electric field

So far we have only considered the correlation of a generic electric field, but we would like to focus our interest on the electric field radiated from our three-level atom. In order for us to do that, we must first consider how the electric field may be expressed in terms of operators referring to the field source, namely, the atom. We therefore now aim to derive an expression for the electric

field operator, Eq. (2.24a), in the Heisenberg picture in terms of the atomic operator $\hat{\Sigma}$.

We begin by recalling the total Hamiltonian, Eq. (3.17), where we have set the coherent driving to zero. Under the approximation adopted in Sec. 3.1.3, this Hamiltonian governs the evolution of the quantised electric field, Eq. (2.36a). We begin with the Heisenberg equation of motion for the field mode operator

$$\frac{\mathrm{d}}{\mathrm{d}t}\hat{a}_{\boldsymbol{k},\lambda} = -i\omega_{\boldsymbol{k}}\hat{a}_{\boldsymbol{k},\lambda}(t) - ig^{*}_{\boldsymbol{k},\lambda}\hat{\Sigma}, \tag{5.15}$$

where

$$\hat{a}_{\boldsymbol{k},\lambda}(t) = \hat{\tilde{a}}_{\boldsymbol{k},\lambda}e^{-i\omega_{\boldsymbol{k}}t}, \tag{5.16a}$$

$$\hat{\Sigma}(t) = \hat{\tilde{\sigma}}^{-}_{eg}(t)e^{-i\omega_{eg}t} + \xi\hat{\tilde{\sigma}}^{-}_{fe}(t)e^{-i\omega_{fe}t}. \tag{5.16b}$$

We formally integrate Eq. (5.15) to obtain

$$\begin{aligned}\hat{\tilde{a}}_{\boldsymbol{k},\lambda}(t) = \hat{a}_{\boldsymbol{k},\lambda}(0) &- ig^{*}_{\boldsymbol{k},\lambda}\int_0^t \mathrm{d}t'\hat{\tilde{\sigma}}^{-}_{eg}(t')e^{i(\omega_{\boldsymbol{k}}-\omega_{eg})t'} \\ &- i\xi g^{*}_{\boldsymbol{k},\lambda}\int_0^t \mathrm{d}t'\hat{\tilde{\sigma}}^{-}_{fe}(t')e^{i\left(\omega_{\boldsymbol{k}}-\omega_{fe}\right)t'}.\end{aligned} \tag{5.17}$$

Substituting this expression into Eq. (2.36a), we may decompose the electric field into two components,

$$\hat{\boldsymbol{E}}^{(+)}(\boldsymbol{r},t) = \hat{\boldsymbol{E}}^{(+)}_{f}(\boldsymbol{r},t) + \hat{\boldsymbol{E}}^{(+)}_{s}(\boldsymbol{r},t), \tag{5.18}$$

where

$$\hat{\boldsymbol{E}}^{(+)}_{f}(\boldsymbol{r},t) = i\sum_{\boldsymbol{k},\lambda}\sqrt{\frac{\hbar\omega_{\boldsymbol{k}}}{2\epsilon_0 V}}\hat{\boldsymbol{e}}_{\boldsymbol{k},\lambda}\hat{a}_{\boldsymbol{k},\lambda}(0)e^{-i(\omega_{\boldsymbol{k}}t-\boldsymbol{k}\cdot\boldsymbol{r})}, \tag{5.19}$$

describes the free evolution of the electric field, and

$$\hat{\boldsymbol{E}}^{(+)}_{s}(\boldsymbol{r},t) = \sum_{\boldsymbol{k},\lambda}\sqrt{\frac{\hbar\omega_{\boldsymbol{k}}}{2\epsilon_0 V}}\hat{\boldsymbol{e}}_{\boldsymbol{k},\lambda}g^{*}_{\boldsymbol{k},\lambda}e^{i\boldsymbol{k}\cdot\boldsymbol{r}}\int_0^t \mathrm{d}t' e^{i\omega_{\boldsymbol{k}}(t-t')}\left(\hat{\tilde{\sigma}}^{-}_{eg}(t')e^{-i\omega_{eg}t'} + \xi\hat{\tilde{\sigma}}^{-}_{fe}e^{-i\omega_{fe}t'}\right), \tag{5.20}$$

describes the electric field radiating from the atom. This expression is the same as that which we would expect from a single dipole, i.e. a two-level atom. We follow through the same calculation from Carmichael (Ref. [28], Sect. 2.3.1), but with an additional dipole moment attached. Recalling that the density of states, Eq. (3.26), is frequency independent over the range of fluorescence, we obtain the electric field operator for the field radiated by the atom,

$$\hat{\boldsymbol{E}}^{(+)}_{s}(\boldsymbol{r},t) = -\frac{\left(\omega_{fg}/2\right)^2}{4\pi\epsilon_0 c^2\boldsymbol{r}}\left(\boldsymbol{d}_{eg}\times\hat{r}\right)\times\hat{r}\hat{\Sigma}\left(t-r/c\right) \tag{5.21}$$

The first-order correlation function can now be restated as

$$G^{(1)}(t+r/c, t+r/c+\tau) \propto \langle\hat{\Sigma}^{\dagger}(t)\hat{\Sigma}(t+\tau)\rangle, \tag{5.22}$$

with normalised correlation function in the steady state limit

$$g^{(1)}(\tau) = \lim_{t\to\infty} \frac{\langle \hat{\Sigma}^\dagger(t)\hat{\Sigma}(t+\tau)\rangle}{\left[\langle \hat{\Sigma}^\dagger(t)\hat{\Sigma}(t)\rangle\langle \hat{\Sigma}^\dagger(t+\tau)\hat{\Sigma}(t+\tau)\rangle\right]^{1/2}} = \frac{\langle \hat{\Sigma}^\dagger(0)\hat{\Sigma}(\tau)\rangle_{ss}}{\langle \hat{\Sigma}^\dagger(0)\hat{\Sigma}(0)\rangle_{ss}}. \tag{5.23}$$

5.3 Fluorescence Spectrum

Here we present the method used to numerically calculate the fluorescence spectrum of the atom, where we first discuss the difference between *coherent* and *incoherent* scattering, otherwise known as *elastic* and *inelastic* scattering (Ref. [23], pp. 207-208). Having discussed how we calculate our results, we then provide a survey of the fluorescence spectrum and how it changes as parameters are varied.

5.3.1 Coherent and incoherent scattering

In classical optics, the intensity spectrum of a field can be calculated from the Fourier transform of the correlation function, which is a form of the *Wiener-Khintchine* theorem (Ref. [56], pp. 511-513) . Introducing the correlation function for the atomic source of the field, Eq. (5.23), we then define the normalised power spectrum of the field (Ref. [55], p. 73)

$$S(\omega) = \frac{1}{2\pi}\int_{-\infty}^{\infty} \mathrm{d}\tau e^{-i\omega\tau} g^{(1)}(\tau). \tag{5.24}$$

Since there exist quantum fluctuations in the steady state, described by (Ref. [28], p. 57)

$$\Delta\hat{\Sigma} = \hat{\Sigma} - \langle\hat{\Sigma}\rangle_{ss}, \tag{5.25a}$$
$$\Delta\hat{\Sigma}^\dagger = \hat{\Sigma}^\dagger - \langle\hat{\Sigma}^\dagger\rangle_{ss}, \tag{5.25b}$$

we decompose the power spectrum as

$$S(\omega) = S(\omega)_{\mathrm{coh}} + S(\omega)_{\mathrm{inc}}, \tag{5.26}$$

with coherent component, corresponding to elastic scattering,

$$S(\omega)_{\mathrm{coh}} = \frac{1}{2\pi}\frac{1}{\langle\hat{\Sigma}^\dagger\hat{\Sigma}\rangle_{ss}}\int_{-\infty}^{\infty} \mathrm{d}\tau e^{i\omega\tau}\langle\hat{\Sigma}^\dagger\rangle_{ss}\langle\hat{\Sigma}\rangle_{ss}, \tag{5.27}$$

and incoherent component, corresponding to inelastic scattering,

$$S(\omega)_{\mathrm{inc}} = \frac{1}{2\pi}\frac{1}{\langle\hat{\Sigma}^\dagger\hat{\Sigma}\rangle_{ss}}\int_{-\infty}^{\infty} \mathrm{d}\tau e^{i\omega\tau}\langle\Delta\hat{\Sigma}^\dagger(0)\Delta\hat{\Sigma}(\tau)\rangle_{ss}. \tag{5.28}$$

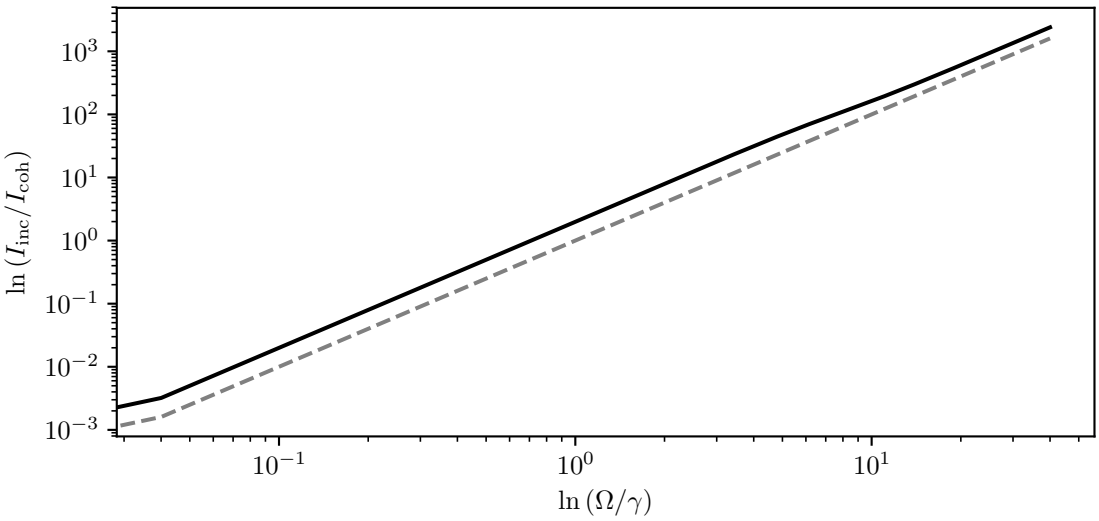

Figure 5.2: Coherent and incoherent intensity ratio (solid) compared with $(\Omega/\gamma)^2$ (dashed). Parameters are $(\alpha/\gamma, \delta/\gamma, \xi) = (-120.0, 0.0, 1.0)$.

Evaluating the steady state expectations in Eq. (5.27), we find that the operator average, $\langle\hat{\Sigma}\rangle_{ss}$, is proportional to the steady state coherences, or off-diagonal elements of the density operator, whereas $\langle\hat{\Sigma}^\dagger\hat{\Sigma}\rangle_{ss}$ is proportional to the steady state populations, ρ_{ee} and ρ_{ff}. Recalling the simplified adiabatic model, Eq. (4.20), the steady state two-photon coherences are proportional to a single power of the effective two-photon drive, while the populations are proportional to the square of the effective drive. We find the intensity ratio of coherent to incoherent scattering is

$$\frac{I_{\rm inc}}{I_{\rm coh}} = \frac{\langle\Delta\hat{\Sigma}^\dagger\Delta\hat{\Sigma}\rangle_{ss}}{\langle\hat{\Sigma}^\dagger\rangle_{ss}\langle\hat{\Sigma}\rangle_{ss}} = \frac{\langle\hat{\Sigma}^\dagger\hat{\Sigma}\rangle_{ss} - \langle\hat{\Sigma}^\dagger\rangle_{ss}\langle\hat{\Sigma}\rangle_{ss}}{\langle\hat{\Sigma}^\dagger\rangle_{ss}\langle\hat{\Sigma}\rangle_{ss}}.$$

We see in Fig. 5.2 that this intensity ratio increases proportionally with $(\Omega/\gamma)^2$. We therefore expect, at weak drives, for coherent scattering to dominate. As the drive strength increases, however, inelastic scattering of the radiation dominates. This works in parallel with the development of the incoherent spectrum, where for weak drives we expect to see only the two transition frequencies, ω_{eg} and ω_{fe}, and for strong drives, we see the dressed state "splitting".

5.3.2 Single-photon resonance

We have seen in Fig. 4.2 that if the driving field is resonant with the ω_{eg} transition we achieve single-photon resonance, which behaves similar to a driven two-level atom. The fluorescence spectrum of a driven two-level atom has been widely studied in the past. It is, in general, a much simpler version of the model we are looking at. The driven two-level atom has simpler dressed states, with corresponding eigenfrequencies that account for three peaks in the fluorescence spectrum: ω_d and $\omega_d \pm \Omega/2$ (Ref. [57], pp. 187-188). We expect for a very weak drive that the scattering of the

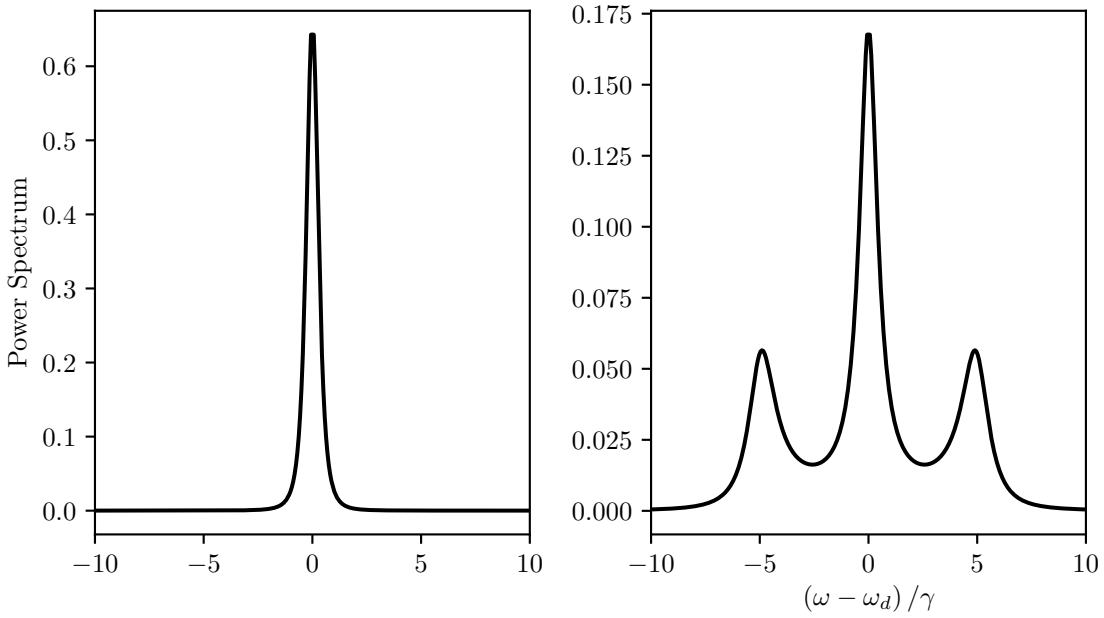

Figure 5.3: Incoherent fluorescence spectrum for a drive field $\Omega/\gamma = 0.0001$ (**Left**) and $\Omega/\gamma = 5.0$ (**Right**). Parameters are $(\alpha/\gamma, \delta/\gamma, \xi) = (-120.0, 60.0, 1.0)$.

field will be entirely coherent, resulting in a delta function centred on the drive frequency. As the drive strength increases, incoherent scattering dominates and sidebands appear at $\pm\Omega$, producing a three peak spectrum known as the Mollow triplet [15]. Both of these spectral features are shown in Fig. 5.3.

5.3.3 Near two-photon resonance

Single-photon resonance in this system is useful in that we can reproduce results for a known model, that being a two-level atom. We now take one step closer to the region we are most interested in – two-photon resonance. Before we investigate the resonance case, we first consider the effect that the drive detuning has on the fluorescence.

We know from our previous discussion on coherent and incoherent scattering that, for low drive strengths, elastic scattering dominates the power spectrum. For very weak drive fields, we see peaks in the small incoherent component of the power spectrum corresponding to the two transition frequencies, ω_{eg} and ω_{fe}. In Fig. 5.4, this corresponds to peaks at $\omega_d \pm (\alpha/2 + \delta)$. We expect the two fluorescence peaks to converge near the single-photon resonance $\delta = -\alpha/2$, as only the ω_{eg} transition frequency appears.

It is important to mention how the incoherent fluorescence spectrum is calculated. In the previous section we mentioned that we are interested in the *normalised* first-order correlation function. The Fourier transform of the normalised correlation function results in a normalised

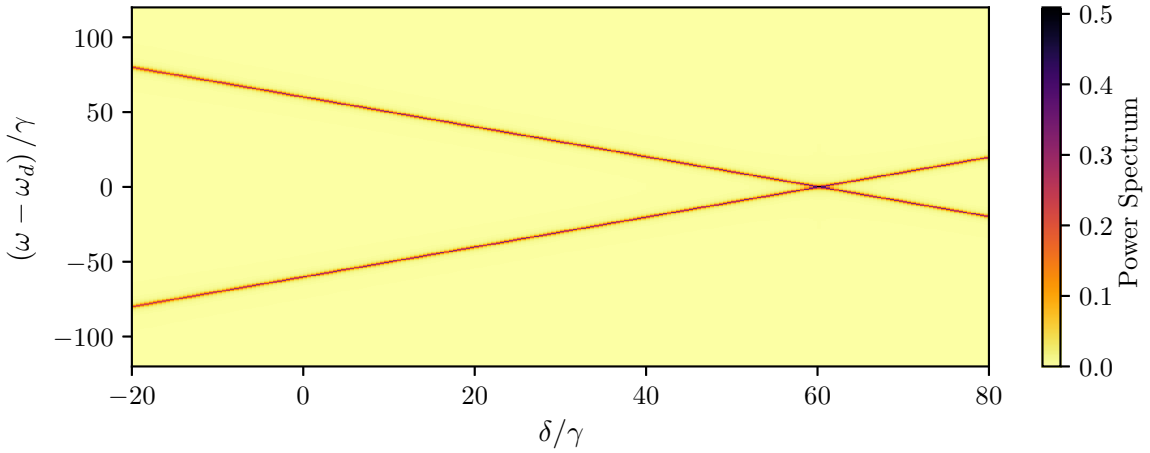

Figure 5.4: Incoherent fluorescence spectrum as a function of drive detuning and emission frequency for a weak drive field $\Omega/\gamma = 0.0001$. Parameters are $(\alpha/\gamma, \xi) = (-120.0, 1.0)$.

power spectrum

$$\int_{-\infty}^{\infty} \mathrm{d}\omega S(\omega) = 1. \tag{5.29}$$

For a very weak drive field that is far off two-photon resonance, the effective two-photon drive, Eq. (4.13), is also very weak, leading to a very small steady-state population in the state $|f\rangle$. It is still possible for the two-photon transition to occur, however, leading to a cascade decay via the state $|e\rangle$. If we were to evaluate the non-normalised correlation function, we would expect the intensity of the fluorescence peaks to decrease for the very weak and off resonant drives. When comparing power spectra for near resonant drive frequencies, as in Fig. 5.4, it would be difficult to see the peaks on the same scale. Therefore, we use the normalised correlation function, allowing the fluorescence peaks to be easily compared.

We shift our attention now to the case of a strong driving field where, as Ω increases, we see, in Fig. 5.5, the spectrum peaks split. It appears that the peaks split evenly whereas, if the drive is closer to resonance, the spectrum splits into three distinct groups. In Fig. 5.6, for $\delta = 5.0$, the central drive peak is clearly split into a triplet. The large peaks either side of this triplet are close to where the bare cascade transitions occur for a weak drive. Therefore, when the peaks split, they are most likely related to $|f\rangle \to |e\rangle$ and $|e\rangle \to |g\rangle$ transitions. We can infer that, for larger detunings, this grouping of peaks by relation to the ω_{eg}, ω_{fe}, and ω_d frequencies, still holds, even if they do not appear to be grouped.

We expect the drive frequency transition to increase in intensity closer to two-photon resonance, which we see in Fig. 5.7. An important dependency in this effect is the dependency on dipole moment ratio, which appears in the shift of the two-photon resonance, Eq. (4.15). We saw, in Fig. 4.4, that, for $\xi < 1$, the two-photon resonance shifts towards positive values of δ while the opposite occurs for $\xi > 1$. This effect is also shown in the spectra, where it determines the detuning

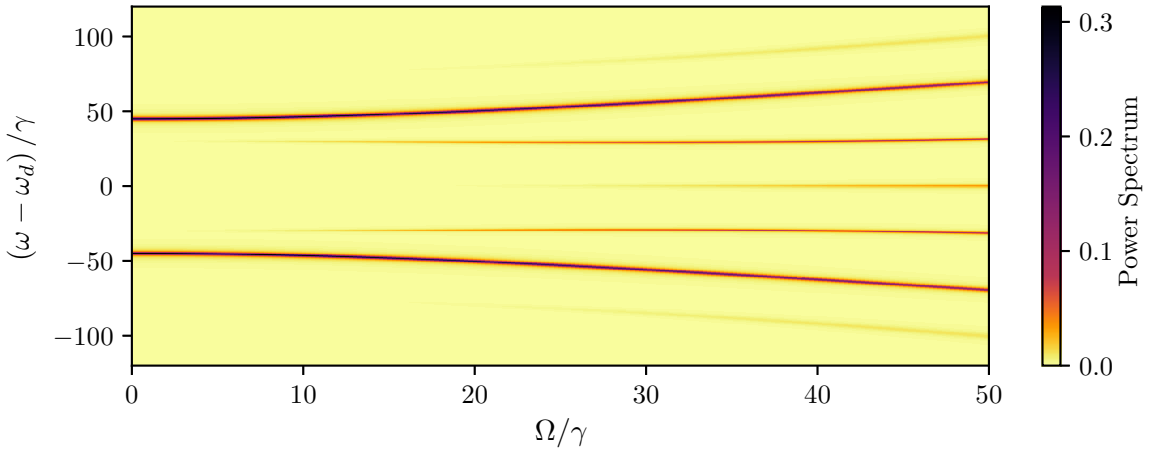

Figure 5.5: Incoherent fluorescence spectrum for $\delta = 15.0$ as a function of drive strength. Parameters are $(\alpha/\gamma, \xi) = (-120.0, 1.0)$.

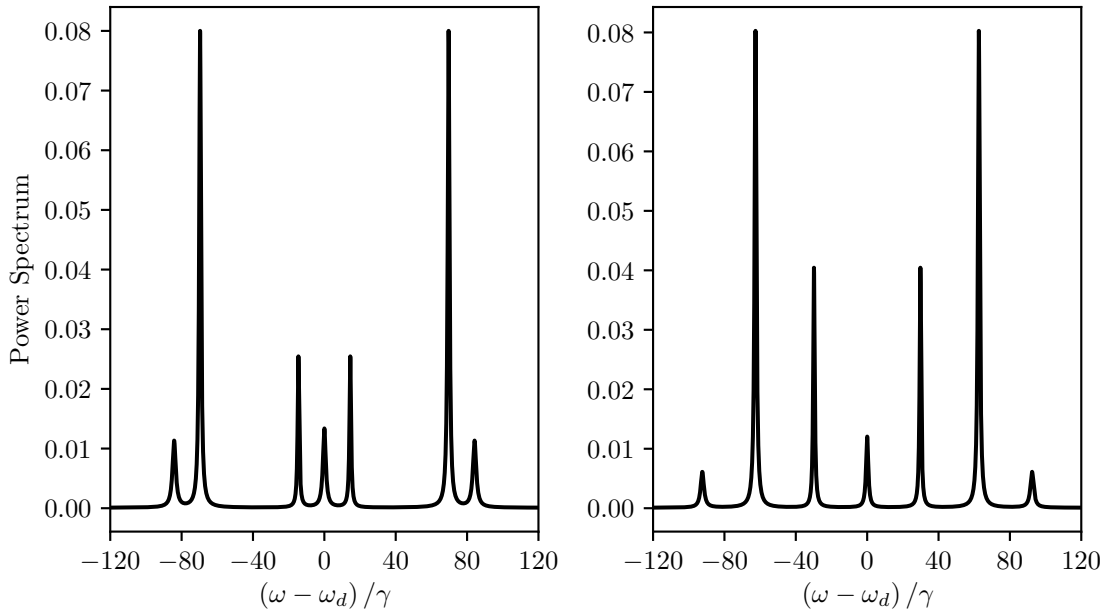

Figure 5.6: Incoherent fluorescence spectrum for $\delta = 5.0$ (**Left**) and $\delta = 15.0$ (**Right**). Parameters are $(\Omega/\gamma, \alpha/\gamma, \xi) = (50.0, -120.0, 1.0)$.

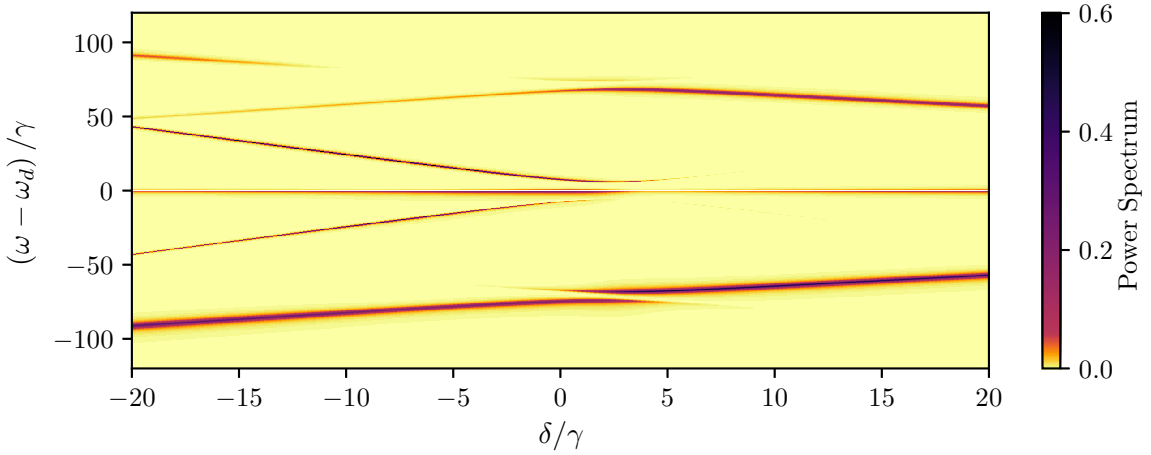

(a) $\xi = 0.5$

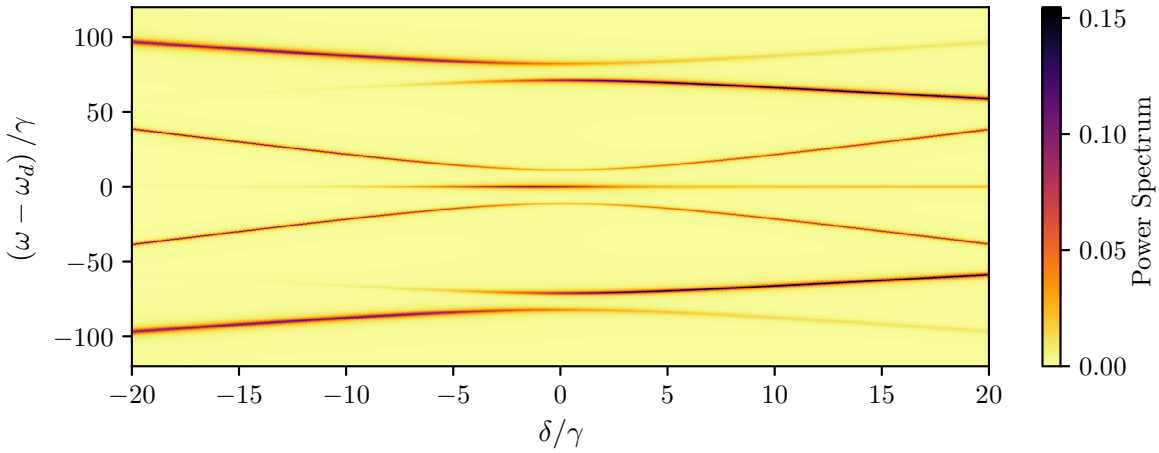

(b) $\xi = 1.0$

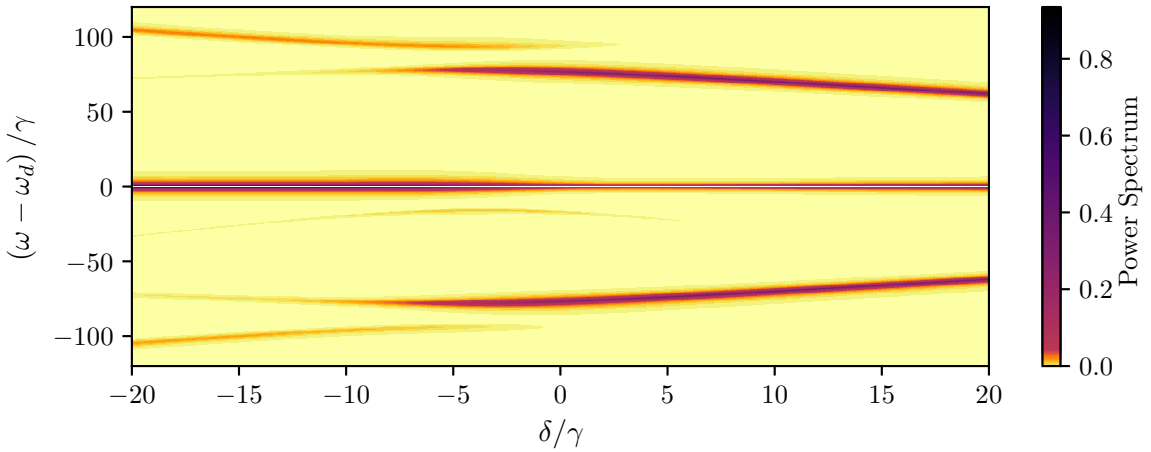

(c) $\xi = 1.5$

Figure 5.7: Incoherent fluorescence spectrum as a function of drive detuning and emission frequency for three different values of dipole moment ratio. Parameters are $(\Omega/\gamma, \alpha/\gamma) = (40.0, -120.0)$

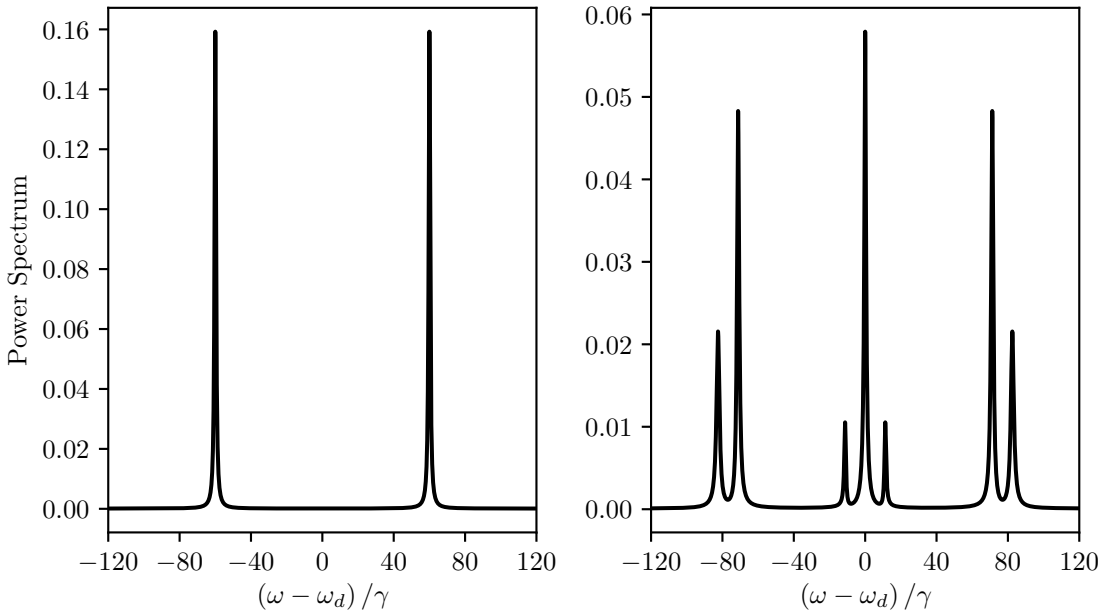

Figure 5.8: Incoherent fluorescence spectrum for a drive field $\Omega/\gamma = 0.0001$ (**Left**) and $\Omega/\gamma = 40.0$ (**Right**). Parameters are $(\alpha/\gamma, \delta/\gamma, \xi) = (-120.0, 0.0, 1.0)$.

where the central peak is most intense. The dipole moment ratio also appears to affect how far detuned the drive frequency can be for the splitting to appear; for an increasing ξ, the region where splitting occurs also increases. Recalling the derived expression for the effective two-photon drive, Eq. (4.13), we would expect a stronger effective drive for a large ξ – even for a large detuning.

5.3.4 Two-photon resonance

We have now arrived at the main focus of this thesis – two-photon resonance. When $\delta = 0$, the spectrum behaves very similarly to what has been discussed so far. One of the important differences in describing this case, however, is that we have simple expressions for the dressed states and their eigenfrequencies, respectively Eqs. (5.5) and (5.4). It has already been mentioned that transitions between the dressed states determine the positions of the peaks in the fluorescence spectrum. Having the explicit form of the dressed states, we are able to confidently explain the spectrum.

In Fig. 5.8 we see the stark contrast between the weak and strong driving limits. As we have established, for the weak drive field, we see two peaks centred on the bare transition frequencies, ω_{eg} and ω_{fe}. Then, for a strong drive field, the two single-photon peaks are Stark shifted away and split into a doublet [12, 58], while a central triplet emerges around the drive frequency, $\omega_{fg}/2$.

Which transitions, then, are responsible for the peaks? For the resonance case, we need only look at Fig. 5.1 to answer this. For a sufficiently weak drive, the left most peak coincides in frequency with the transition between the states $|f\rangle$ and $|e\rangle$, with frequency $\omega_{fe} = \omega_d + \alpha/2$. Similarly, the

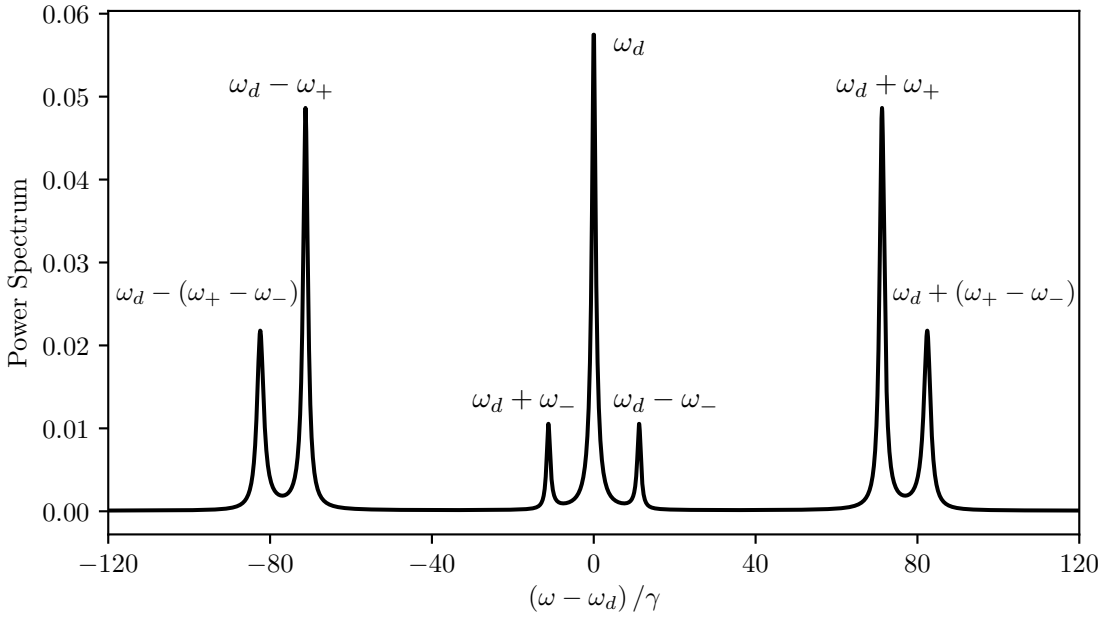

Figure 5.9: Split spectrum at two-photon resonance with labelled transitions from Fig. 5.8. Parameters are $(\Omega/\gamma, \alpha/\gamma, \delta/\gamma, \xi) = (40.0, -120.0, 0.0, 1.0)$.

right most peaks corresponds to the next transition in the cascaded decay, between the states $|e\rangle$ and $|f\rangle$, with frequency $\omega_{eg} = \omega_d - \alpha/2$.

As the drive strength increases the dressed state energies split and the degeneracy of the $|0\rangle$ and $|-\rangle$ states is lifted, allowing for more possible transitions to occur as the atom decays to the ground state. The transition frequencies of each peak, as labelled in Fig. 5.9, are a direct result of transitions amongst the dressed states. With the degeneracy of the dressed states lifted, the left most doublet arises from two transitions: $|-\rangle$ to $|+\rangle$ and $|0\rangle$ to $|+\rangle$. In order to conserve energy, these transitions are immediately followed by either a $|+\rangle$ to $|-\rangle$ or $|+\rangle$ to $|0\rangle$ transition. Moving to the central triplet we see the emergence of an intense central peak corresponding to the drive frequency. We see that there are four possible transitions with frequency ω_d. The surrounding sidepeaks of this central triplet, with frequencies $\omega_d \pm \omega_-$, are a result of the $|0\rangle$ to $|-\rangle$ to $|0\rangle$ cascade transition.

We clearly see the emergences of the dressed state splitting in Fig. 5.10. When $\xi \neq 1$ the split spectrum appears to be asymmetrical. We see this more clearly in Fig. 5.11 where we have also illustrated the spectrum when the drive is resonant with the shifted two-photon resonance. For a lower dipole ratio, the fluorescence peaks corresponding to the $\boldsymbol{d}_{eg}$ transitions are amplified, while for a higher dipole ratio, the $\boldsymbol{d}_{fe}$ transitions are amplified. When the drive is resonant with the *shifted* two-photon resonance this effect is even more pronounced. Looking at the central triplet, one of the peaks is almost completely suppressed. Holm and Sargent suggest that this effect is due to the Stark shift of the energy levels [59].

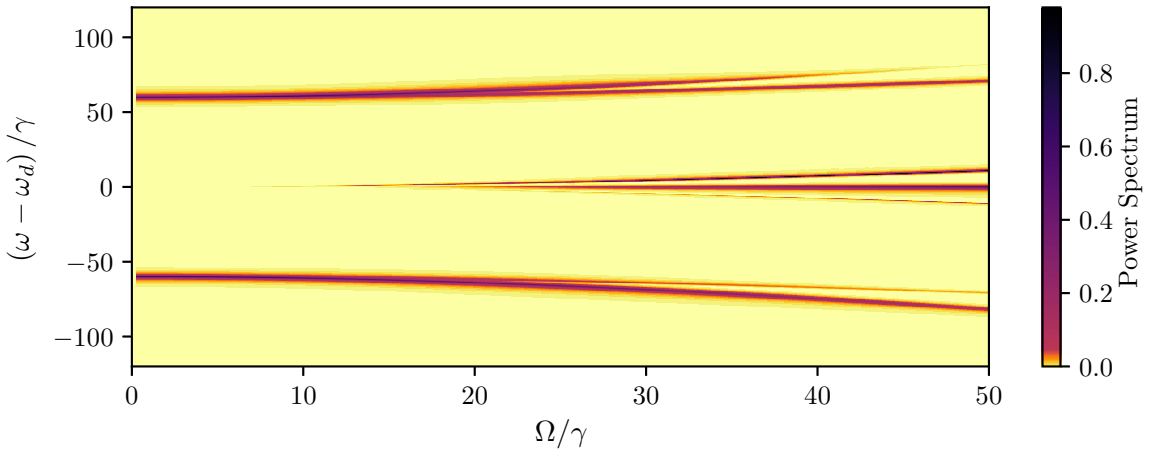

(a) $\xi = 0.5$

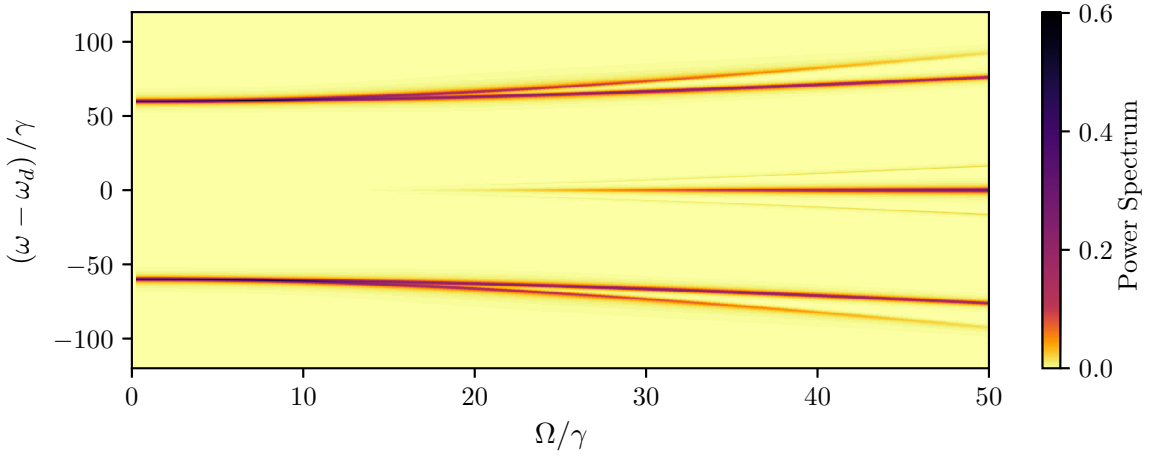

(b) $\xi = 1.0$

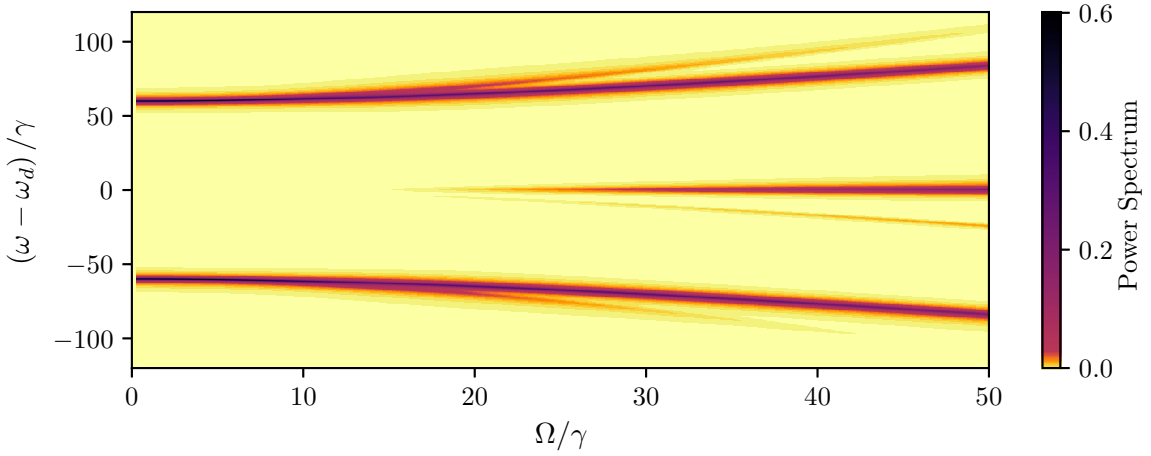

(c) $\xi = 1.5$

Figure 5.10: Incoherent fluorescence spectrum as a function of drive strength and emission frequency for three different values of dipole moment ratio. Parameters are $(\alpha/\gamma, \delta/\gamma) = (-120.0, 0.0)$.

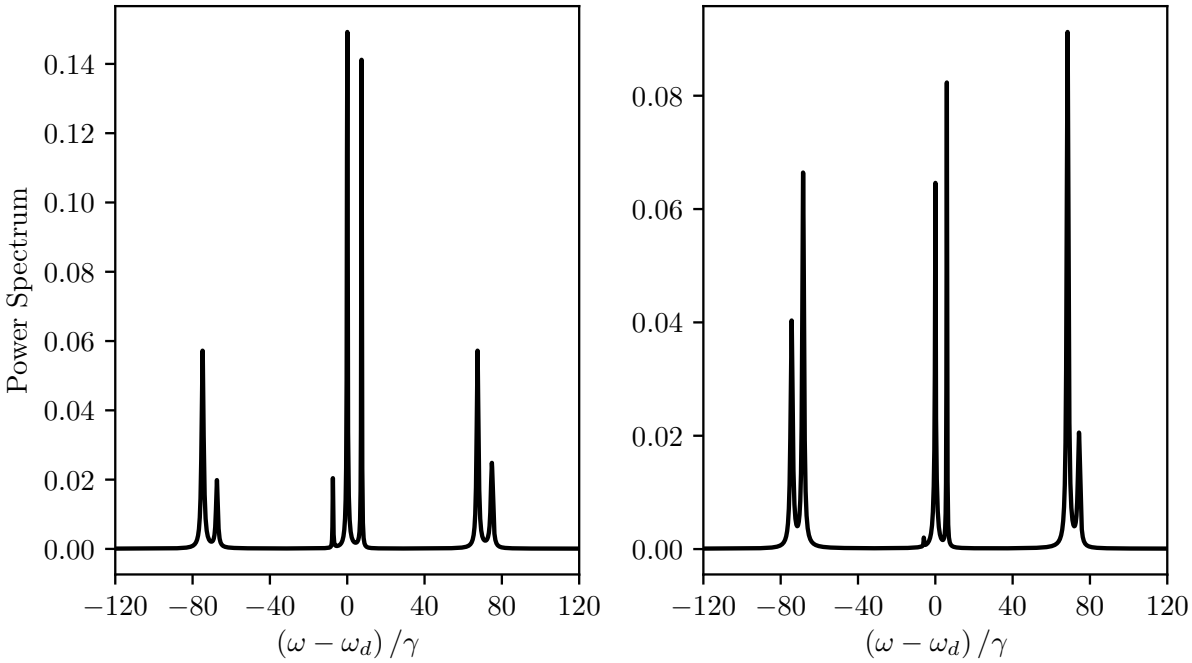

(a) $\delta = 0$ (**Left**) and $\Delta_{\text{eff}} = 0$ (**Right**). $\xi = 0.5$

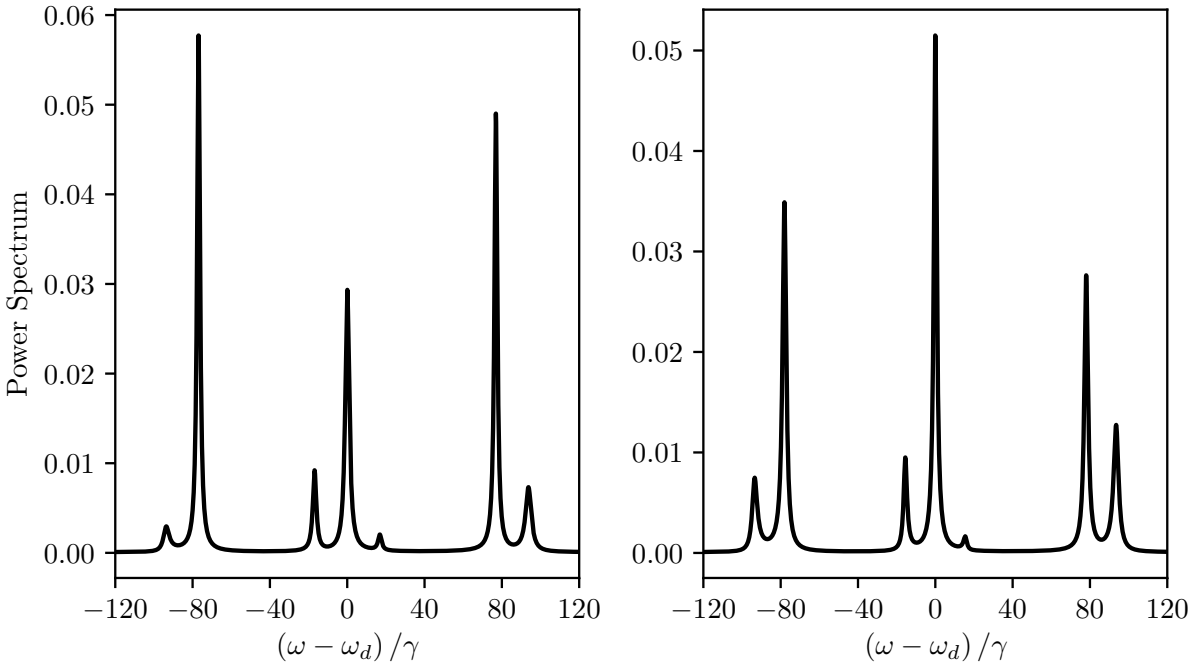

(b) $\delta = 0$ (**Left**) and $\Delta_{\text{eff}} = 0$ (**Right**). $\xi = 1.5$

Figure 5.11: Incoherent fluorescence spectrum with the drive detuning resonant with the two-photon transition, $\delta = 0$ (Left), and the drive detuning resonant with the shifted two-photon transition, $\Delta_{\text{eff}} = 0$ (Right), given by Eq. (4.15). Parameters are $(\Omega/\gamma, \alpha/\gamma) = (40.0, -120.0)$.

6 Photon-Photon Correlations

So far we have seen how the electric field radiated from the atom fluctuates with time, giving us the fluorescence spectrum. In this chapter we will investigate how the intensity of the electric field fluctuates by looking at the second-order correlation function. By treating the system and its interaction as a photon-counting experiment, we see that the second-order correlation is related to the likelihood of detecting two photons separated by a time τ.

We first describe what it means for light to have second-order coherence in both a classical and quantum sense. We then discuss what "bunched" and "anti-bunched" light is, highlighting the difference between classical and non-classical light. With these definitions in mind, we survey how the second-order correlation is affected by changing parameters. We consider the total dipole operator $\hat{\Sigma}$, Eq.(3.16), and the separate dipole operators that, together, compose $\hat{\Sigma}$.

Next we set out a method that will allow us to frequency filter the fluorescence of the atom. We do this by adding a cavity resonator, modelling a transmission filter. We introduce the theory of cascaded open system where the output field of the atom is the input field to the cavity [60]. This allows us to calculate the second-order correlations of individual transitions of the cascaded decay and characterise the emitted light.

Finally we take the method one step further by introducing a second filter cavity. With this second filter we can calculate second-order *cross-correlations*. Given an emission from cavity a, we find the likelihood of detecting an emission from cavity b. From the cross-correlations we set out to characterise the cascaded decay and see if the dressed state cascade decay sufficiently describes the several peaks we see in the incoherent fluorescence spectrum.

6.1 Photon Counting Statistics

In this section we will give an overview of what the second-order correlation function is and what it quantifies. We then describe the three main results we would expect from the second-order correlation function – *bunched*, *coherent*, and *anti-bunched* light – with physical examples of each.

6.1.1 Second-order correlation

In classical optics, the second-order correlation function measures the fluctuations in intensity (Ref. [54], p. 229):

$$g^{(2)}(\tau) = \frac{\langle I(t)I(t+\tau)\rangle}{\langle I(t)\rangle\langle I(t+\tau)\rangle}, \tag{6.1}$$

where $I(t)$ is the intensity of a field at a time t. We consider a statistically stationary source such that $\langle I(t)\rangle = \langle I(t+\tau)\rangle = \langle I\rangle$, with fluctuations

$$\Delta I(t) = I(t) - \langle I\rangle, \tag{6.2}$$

as in Eq. (5.25). The correlation function now becomes

$$\begin{aligned} g^{(2)}(\tau) &= \frac{\langle I\rangle^2 + \langle I\rangle\langle\Delta I(t)\rangle + \langle I\rangle\langle\Delta I(t+\tau)\rangle + \langle\Delta I(t)\Delta I(t+\tau)\rangle}{\langle I\rangle\langle I\rangle} \\ &= \frac{\langle I(t)\rangle^2 + \langle\Delta I(t)\Delta I(t+\tau)\rangle}{\langle I\rangle^2} \\ &= 1 + \frac{\langle\Delta I(t)\Delta I(t+\tau)\rangle}{\langle I\rangle^2}, \end{aligned} \tag{6.3}$$

where $\langle\Delta I(t)\rangle$ is zero by definition. In the long time delay limit, $\tau \to \infty$, the intensity fluctuations will be completely uncorrelated and

$$g^{(2)}(\tau \to \infty) = 1. \tag{6.4}$$

Using Cauchy's inequality, for zero time delay we find the correlation is bounded by

$$g^{(2)}(0) = \frac{\langle I^2\rangle}{\langle I\rangle^2} \geq 1. \tag{6.5}$$

6.1.2 Bunching and antibunching

Returning to familiar notation, we introduce the quantum-mechanical version of the second-order correlation function (Ref. [61], p. 212):

$$g^{(2)}(\tau) = \frac{\langle\hat{\boldsymbol{E}}^{(-)}(t)\hat{\boldsymbol{E}}^{(-)}(t+\tau)\hat{\boldsymbol{E}}^{(+)}(t+\tau)\hat{\boldsymbol{E}}^{(+)}(\tau)\rangle}{\langle\hat{\boldsymbol{E}}^{(-)}(t)\hat{\boldsymbol{E}}^{(+)}(t)\rangle\langle\hat{\boldsymbol{E}}^{(-)}(t+\tau)\hat{\boldsymbol{E}}^{(+)}(t+\tau)\rangle}. \tag{6.6}$$

This correlation function can be generalised to the nth order, corresponding to the response where n photons are detected in a time-ordered sequence.

The Hanbury Brown and Twiss experiment (Ref. [2]), which was one of the first quantum optics experiments, investigates intensity correlations of a beam of light. A light beam is split by a 50:50 beam splitter, and thus equally divided onto two detectors, as shown in Fig. 6.1a. The detector count is proportional to the intensity of the incoming beam, and therefore we write the second-order correlation function in terms of photon number operator:

$$g^{(2)}(\tau) = \frac{\langle:\hat{n}_1(t)\hat{n}_2(t+\tau):\rangle}{\langle\hat{n}_1(t)\rangle\langle\hat{n}_2(t+\tau)\rangle} = \frac{\langle\hat{a}_1^\dagger(t)\hat{a}_2^\dagger(t+\tau)\hat{a}_2(t+\tau)\hat{a}_1(t)\rangle}{\langle\hat{a}_1^\dagger(t)\hat{a}_1(t)\rangle\langle\hat{a}_2^\dagger(t+\tau)\hat{a}_2(t+\tau)\rangle}, \tag{6.7}$$

where $\hat{n}_i$ is the number operator for the ith detector; $\langle:\cdots:\rangle$ denotes normal ordering and time ordering, where the $\hat{a}^\dagger$ terms are to the left of the $\hat{a}$ terms and the earliest times are on the outside.

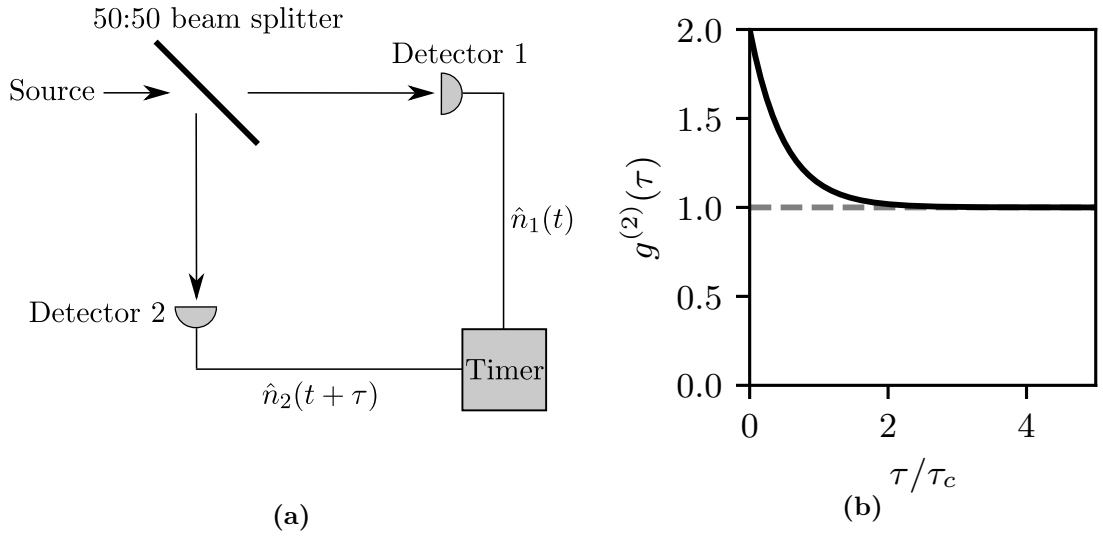

Figure 6.1: Schematic of a Hanbury Brown experiment (a) and the resulting second-order correlation (b) for chaotic light (solid) and coherent light (dashed).

If the field is in a coherent state the second-order correlation is unity for all τ. For a classical field, when τ is less than the coherence time τ_c there is increased correlation due to intensity fluctuations, which results in a higher initial second-order correlation. In the case of thermal light source (Ref. [23], p. 40)

$$g^{(2)}(0) = 1 + |g^{(1)}(0)|^2 = 2, \tag{6.8}$$

as show in Fig. 6.1b. The probability that a photon is detected at detector one is higher when the intensity fluctuations are high, hence there is a high probability that a photon is also detected at the same time, or at least within a correlation time, at detector two.

Now consider a source with long time intervals separating photon emissions. Individual photons arriving at the beam splitter have a 50% chance of being detected by detector one. If a photon is detected by detector one, due to the long time intervals there will be no recorded events from detector two at the same time, leading to a second-order correlation $g^{(2)}(0) = 0$ – clearly a non-classical result!

These results lead us to the following classification: *bunched light*, with $g^{(2)}(0) > 1$; *coherent light*, with $g^{(2)}(0) = 1$; and *anti-bunched light*, with $g^{(2)}(0) < 1$ [9, 62, 63]. In the context of a photon detection experiment, bunched light is light where photons arrive grouped or "bunched"; when a photon is detected, there is a high probability to detect another one at the same time. Coherent light has Poissonian photon statistics, where there are random time intervals between photon detections. Lastly, anti-bunched light has photons that are regularly spaced in time. The three cases are illustrated in Fig. 6.2.

An important example of antibunching is the coherently driven two-level atom [7, 8]. The atom can only store a single quantum of energy at any time, so when it decays to the ground

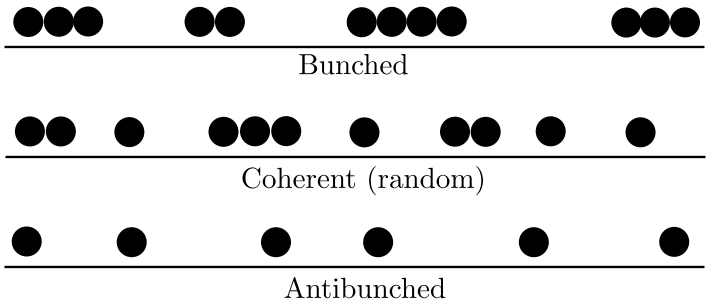

Figure 6.2: Comparison of photon streams for bunched, coherent (random), and anti-bunched light.

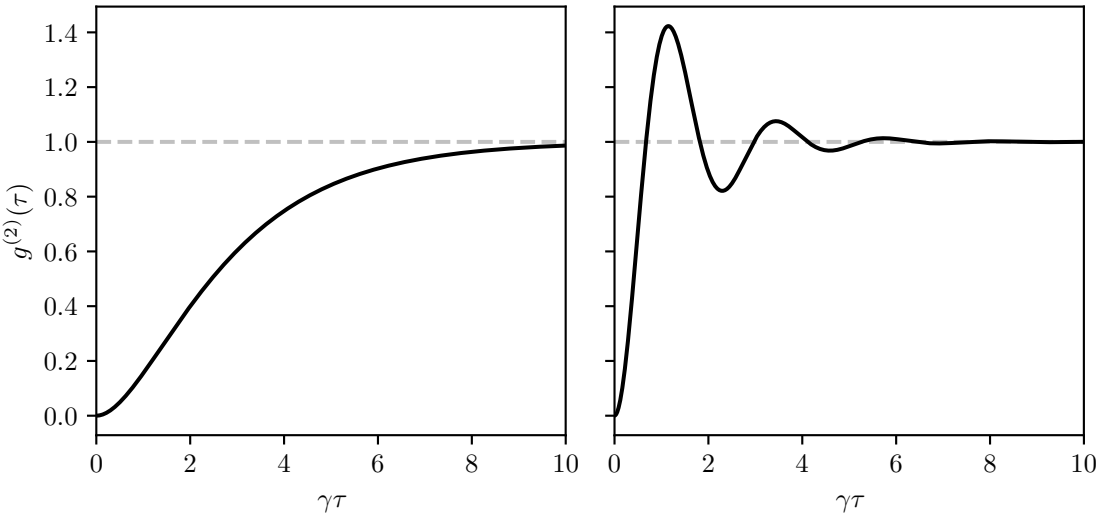

Figure 6.3: Second-order correlation for the atom driven at single-photon resonance for $\Omega/\gamma = 0.0001$ (**Left**) and $\Omega/\gamma = 2.75$ (**Right**). Parameters are $(\alpha/\gamma, \delta/\gamma, \xi) = (-120.0, 60.0, 1.0)$.

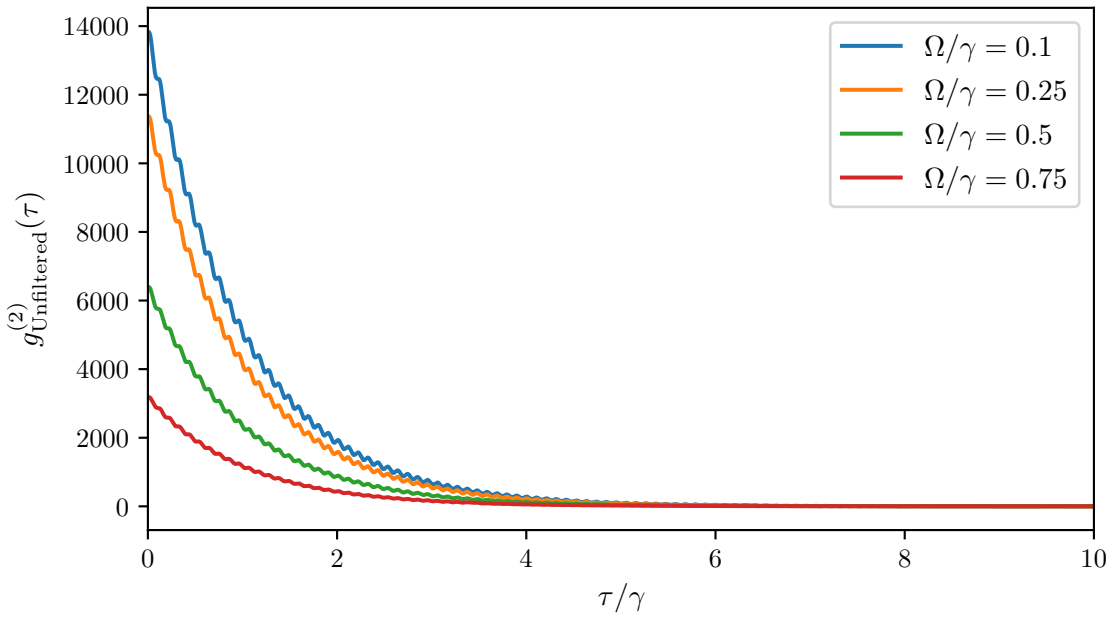

Figure 6.4: Second-order photon correlations for weak drive fields. Parameters are $(\alpha/\gamma, \delta/\gamma, \xi) = (-120.0, 0.0, 1.0)$.

state, emitting a photon, it must be excited again before emitting another. This leads to an initial correlation value of $g^{(2)}(0) = 0$, defying the boundary defined for a classical system (Fig. 6.3).

6.2 Unfiltered Photon Correlations

Now that we have defined the three main classes for second-order correlations, we investigate the characteristics of the emitted light from our driven three-level atom. We start by considering the total radiated field, Eq. (5.21), which is characterized by the dipole operator $\hat{\Sigma} = \hat{\sigma}^{-}_{eg} + \xi\hat{\sigma}^{-}_{fe}$, and survey the effects that changing parameters has on the nature of the emitted light. We then decompose $\hat{\Sigma}$ into its separate dipole operator components, allowing us to investigate the *cross-correlations* of the two components.

6.2.1 Total radiated field

Following the calculation of the first-order correlation function from the previous chapter, we substitute Eq. (5.21) into Eq. (6.6), obtaining the *normalised second-order correlation function for the three-level atom*:

$$g^{(2)}_{\text{Unfiltered}}(\tau) = \frac{\langle \hat{\Sigma}^{\dagger}(0)\hat{\Sigma}^{\dagger}(\tau)\hat{\Sigma}(\tau)\hat{\Sigma}(0)\rangle_{ss}}{\langle \hat{\Sigma}^{\dagger}\hat{\Sigma}\rangle^{2}_{ss}}. \tag{6.9}$$

This correlation function is proportional to the probability of an emission occurring a time τ after a first emission has been detected at $\tau = 0$. The total operator Σ is a combination of the decay

operators for the two dipoles, so an emission can be from either the $|f\rangle$ to $|e\rangle$ transition, or the $|e\rangle$ to $|g\rangle$ transition. The probability for a jump to occur in a time interval $[t, t + \mathrm{d}t]$ is then

$$\gamma\langle\hat{\Sigma}^\dagger\hat{\Sigma}\rangle\mathrm{d}t = \gamma\left(\rho_{ee} + \xi^2\rho_{ff}\right)\mathrm{d}t, \tag{6.10}$$

which is directly proportional to the population in the states $|e\rangle$ and $|f\rangle$.

In the previous chapter we showed that, by driving the atom at the single-photon resonance ($\omega_d = \omega_{eg}$) we obtain the spectrum of a driven two-level atom. It comes as no surprise, then, that we would obtain the second-order correlation of the driven two-level atom as well. At single-photon resonance, most of the steady state population is in either the state $|g\rangle$ or state $|e\rangle$, with a negligible amount in the state $|f\rangle$. If a photon is detected from the atom, the decay operator moves the $|e\rangle$ state population into the state $|g\rangle$. Immediately following an emission, there will be no population in the $|e\rangle$ state, so no emission can occur, regardless of the driving field strength, as we see in Fig. 6.3. As τ increases, the probability of the atom being in the $|e\rangle$ state increases and the second-order correlation approaches unity. For sufficiently strong drive fields, the atom state oscillates between $|g\rangle$ and $|e\rangle$, a process known as *Rabi oscillation*. We see the oscillations in Fig. 6.3, where $g^{(2)}(\tau)$ oscillates at the Rabi frequency Ω.

Considering now driving the atom at two-photon resonance we see things are very different from the two-level case. If the atom is excited to the $|f\rangle$ state, it needs to emit two photons in order to decay to the ground state, so we no longer expect to see any antibunching. This is most noticeable when the drive field is very weak, as shown in Fig. 6.4. For a very weak drive field, the effective two-photon drive is also very weak. It is, however, still possible for the field to excite the atom to the state $|f\rangle$. As the atom decays, the photons are emitted in pairs separated in time by approximately an atomic lifetime and the pairs, for a weak drive, are separated by a much greater time. Thus, detecting a first photon tells us that there is a much higher probability (than on average) to detect another photon within the next atomic lifetime. As the drive strength increases, the average time between detections decreases, causing the emitted photons to appear less "bunched". This effect is what causes the initial correlation value to increase for lower drive strengths in Fig. 6.4. Note that as the correlations decay to unity they also oscillate at a frequency equal to the detuning from single-photon resonance, $\alpha/2 + \delta$, which is an effect we would expect from the example of a two-level atom driven off resonance.

For an increased drive strength, we start to see behaviour similar to that of a driven two-level atom discussed earlier. The correlation function oscillates in a fashion similar to the Rabi oscillation of the two-level atom. In this regime the effective two-photon drive is strong enough to almost constantly excite the atom to the $|f\rangle$ state. The correlations for three different values of ξ are shown in Figs. 6.5, where we see three main differences due to the different dipole moment ratios. Firstly, the oscillations increase in frequency as ξ increases. We find, in fact, that this frequency is the dressed frequency $|\omega_-|/2\pi$, Eq. (5.4). Figures 5.1 and 5.9 show that the most prominent beat frequency of the different transitions is $|\omega_-|$, which grows larger as ξ increases. Similarly, the much more rapid oscillations have a frequency $|\omega_+|/2\pi$, another expected beat frequency.

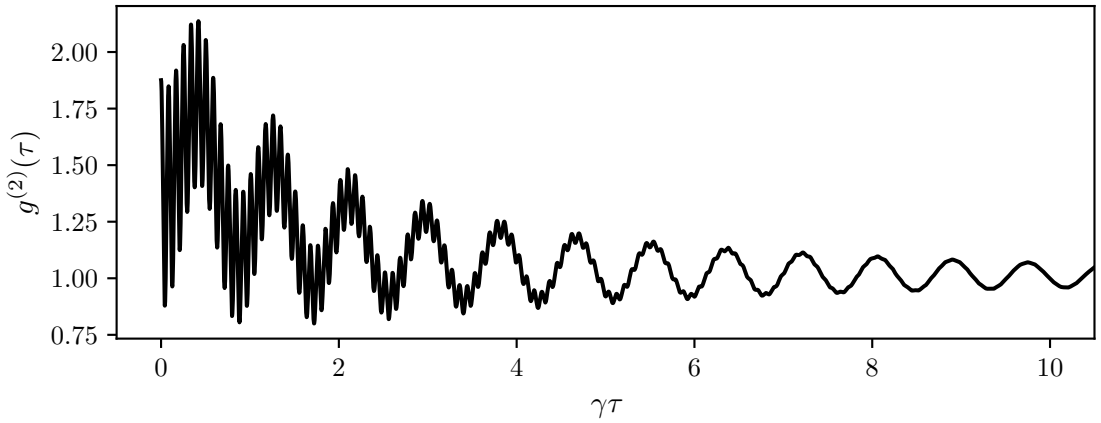

(a) $\xi = 0.5$

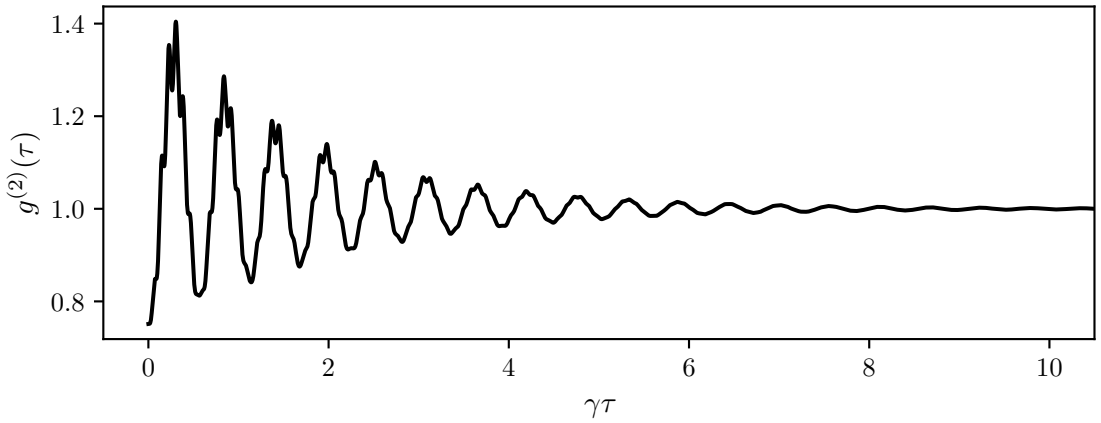

(b) $\xi = 1.0$

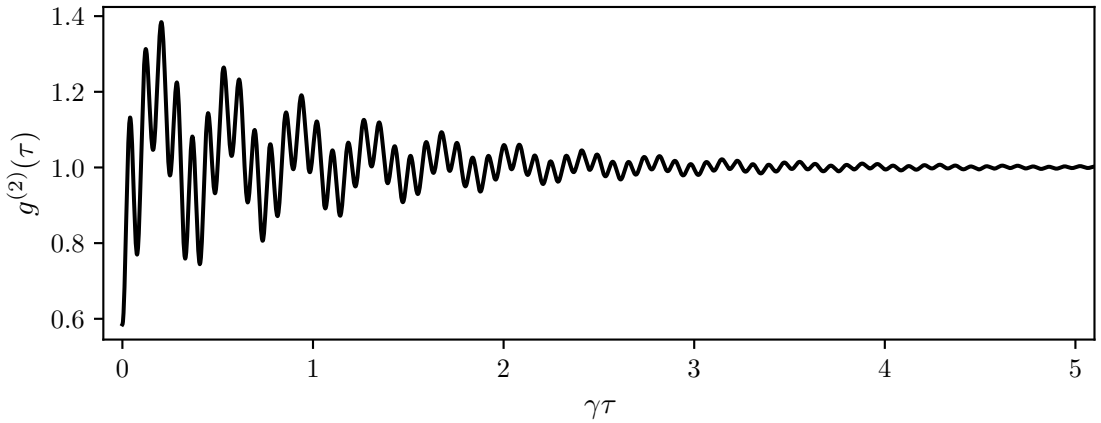

(c) $\xi = 1.5$

Figure 6.5: Second-order correlations for three different values of ξ. Parameters are $(\Omega/\gamma, \alpha/\gamma, \delta/\gamma) = (40.0, -120.0, 0.0)$.

The second observation is that the rate at which the correlations decay to unity depends on ξ. The $|f\rangle$ to $|e\rangle$ transition decays at a rate $\gamma\xi^2$, rather than γ, therefore affecting the average time taken to reach the steady-state after an emission. For $\xi > 1$, then, the photon correlation is expected to decay to unity faster than $\xi < 1$, as is clearly shown in Fig. 6.5.

Finally, the initial correlation value also appears to depend on the dipole moment ratio. We saw in Fig. 4.4 and from the analytic steady-state density operator, Eq. (4.20), that the steady state population of the state $|e\rangle$ depends on ξ^2. For $\xi < 1$, Fig. 4.4a, most of the population is in either the $|g\rangle$ or $|f\rangle$ states. After an emission occurs, the atom will be in state $|e\rangle$, giving a very high probability of another emission to occur, therefore $g^{(2)}(0) > 1$ and the emitted light is bunched, as shown in Fig. 6.5a. For $\xi > 1$, Fig. 6.5c, most of the population is either in the $|g\rangle$ and $|e\rangle$ states. Therefore, after an emission occurs the atom will more likely be in state $|g\rangle$, and there is a low probability of another emission occurring leading to more anti-bunched light.

6.2.2 Separate dipole components

Let us for a moment consider the non-normalised second-order correlation function

$$G^{(2)}(\tau) = \langle \hat{\Sigma}^\dagger(0)\hat{\Sigma}^\dagger(\tau)\hat{\Sigma}(\tau)\hat{\Sigma}(0)\rangle. \tag{6.11}$$

Substituting in the explicit form of $\hat{\Sigma}$, Eq. (3.16), and expanding, the non-normalised correlation becomes

$$\begin{aligned} G^{(2)}(\tau) = {} & \langle \hat{\sigma}^+_{eg}(0)\hat{\sigma}^+_{eg}(\tau)\hat{\sigma}^-_{eg}(\tau)\hat{\sigma}^-_{eg}(0)\rangle_{ss} + \xi^4\langle \hat{\sigma}^+_{fe}(0)\hat{\sigma}^+_{fe}(\tau)\hat{\sigma}^-_{fe}(\tau)\hat{\sigma}^-_{fe}(0)\rangle_{ss} \\ & + \xi^2\langle \hat{\sigma}^+_{fe}(0)\hat{\sigma}^+_{eg}(\tau)\hat{\sigma}^-_{eg}(\tau)\hat{\sigma}^-_{fe}(0)\rangle_{ss} + \xi^2\langle \hat{\sigma}^+_{eg}(0)\hat{\sigma}^+_{fe}(\tau)\hat{\sigma}^-_{fe}(\tau)\hat{\sigma}^-_{eg}(0)\rangle_{ss}, \end{aligned} \tag{6.12}$$

plus non-symmetrical terms. The second-order correlation of $\hat{\Sigma}$ is then the sum of four correlations for the separate dipole operators, which we classify under two groups: *auto-correlations* and *cross-correlations*. We define the auto-correlation function for the $\boldsymbol{d}_{eg}$ dipole as

$$g^{(2)}_{eg}(\tau) = \frac{\langle \hat{\sigma}^+_{eg}(0)\hat{\sigma}^+_{eg}(\tau)\hat{\sigma}^-_{eg}(\tau)\hat{\sigma}^-_{eg}(0)\rangle_{ss}}{\langle \hat{\sigma}^+_{eg}\hat{\sigma}^-_{eg}\rangle^2_{ss}}, \tag{6.13}$$

and similarly for the $\boldsymbol{d}_{fe}$ dipole

$$g^{(2)}_{fe}(\tau) = \frac{\langle \hat{\sigma}^+_{fe}(0)\hat{\sigma}^+_{fe}(\tau)\hat{\sigma}^-_{fe}(\tau)\hat{\sigma}^-_{fe}(0)\rangle_{ss}}{\langle \hat{\sigma}^+_{fe}\hat{\sigma}^-_{fe}\rangle^2_{ss}}. \tag{6.14}$$

At weak drive strengths the dipole operators directly correspond to the two cascade transitions, $|f\rangle \rightarrow |e\rangle$ and $|e\rangle \rightarrow |g\rangle$. Just like the two-level atom, after emitting a photon each dipole must be excited before it can emit again. We see this in Fig. 6.6 where, for both dipole operators, $g^{(2)}(0) = 0.0$. The main difference between these two correlations and that of a two-level atom, in Fig. 6.3 (**Left**), is that correlations in Fig. 6.6 also oscillate at a rapid frequency. This frequency

is in fact the detuning of the drive frequency from the respective dipole frequency, $\alpha/2$, which is what we would expect from a two-level system driven off resonance.

At strong drive strengths the atom no longer has transitions between the bare states. We can expand the bare states as a combination of dressed states, Eq. (5.5), and thus find that each dipole operator can be written as a combination of six different dressed state transitions. Despite this, the separate photon correlations for both dipoles still exhibit perfect antibunching, as we see in Fig. 6.7. The frequencies at which the oscillations in the correlations occur are in fact the same as for the total radiated field, i.e., $\omega_-/2\pi$ and $\omega_+/2\pi$, for the slow and fast oscillations respectively.

6.2.3 Cross-correlations

The two remaining terms from Eq. 6.12 are, as mentioned, cross-correlations. For the auto-correlation we consider the likelihood of detecting an emission from one mode at a time τ after detecting an emission from the same mode. For the cross-correlation, we consider the two modes to be different. We first define the cross-correlation of an emission from the $\boldsymbol{d}_{eg}$ dipole a time τ after detecting an emission from the $\boldsymbol{d}_{fe}$ dipole:

$$g^{(2)}_{fe\to eg} = \frac{\langle \hat{\sigma}^+_{fe}(0)\hat{\sigma}^+_{eg}(\tau)\hat{\sigma}^-_{eg}(\tau)\hat{\sigma}^-_{fe}(0)\rangle_{ss}}{\langle \hat{\sigma}^+_{fe}\hat{\sigma}^-_{fe}\rangle_{ss}\langle \hat{\sigma}^+_{eg}\hat{\sigma}^-_{eg}\rangle_{ss}}, \tag{6.15}$$

and then the cross-correlation for the $\boldsymbol{d}_{fe}$ dipole conditioned on an emission from the $\boldsymbol{d}_{eg}$ dipole:

$$g^{(2)}_{eg\to fe} = \frac{\langle \hat{\sigma}^+_{eg}(0)\hat{\sigma}^+_{fe}(\tau)\hat{\sigma}^-_{fe}(\tau)\hat{\sigma}^-_{eg}(0)\rangle_{ss}}{\langle \hat{\sigma}^+_{fe}\hat{\sigma}^-_{fe}\rangle_{ss}\langle \hat{\sigma}^+_{eg}\hat{\sigma}^-_{eg}\rangle_{ss}}. \tag{6.16}$$

We begin, as always, with the simpler case of a weak drive. By investigating the cross-correlations we see that they behave exactly as we would expect for the cascaded decay. The photon correlation $g^{(2)}_{eg\to fe}(\tau)$, conditioned first on an emission from $\boldsymbol{d}_{eg}$ is clearly anti-correlated, as demonstrated in Fig. 6.8a. As we have established, the probability of getting a photon with frequency ω_{fe} directly after detecting one with frequency ω_{eg} is exactly zero. Swapping the operator order the cross-correlation, $g^{(2)}_{fe\to eg}(\tau)$, Fig. 6.8b, is strongly correlated. We expect for a decreasing drive strength that, much like in Fig. 6.4, $g^{(2)}(0)$ will increase.

Once again things are complicated once the dressed state transitions are introduced for stronger drive strengths. We have already encountered the features of the cross-correlations in Fig. 6.9, however, where we considered the photon correlations of the total radiated field. For the $eg \to fe$ cross-correlation, Fig. 6.9a, we see perfect initial anti-correlation, and the oscillations at frequency $|\omega_-|/2\pi$ are similar to a driven two-level atom. A stronger effective drive allows population to be shifted into the state $|f\rangle$ at a much faster rate, allowing for a transition from $|f\rangle$ to $|e\rangle$ to occur at a later time delay. The $fe \to eg$ cross-correlation, Fig. 6.9b, is strongly correlated, though nowhere near as correlated as for a weaker drive.

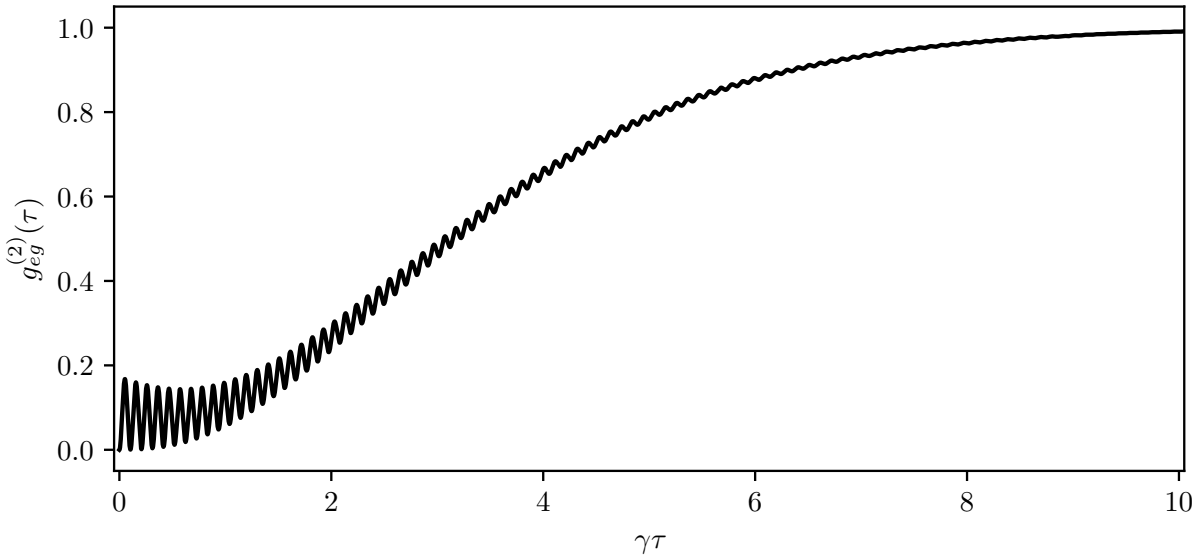

(a) Auto-correlation of $\hat{\sigma}^-_{eg}$.

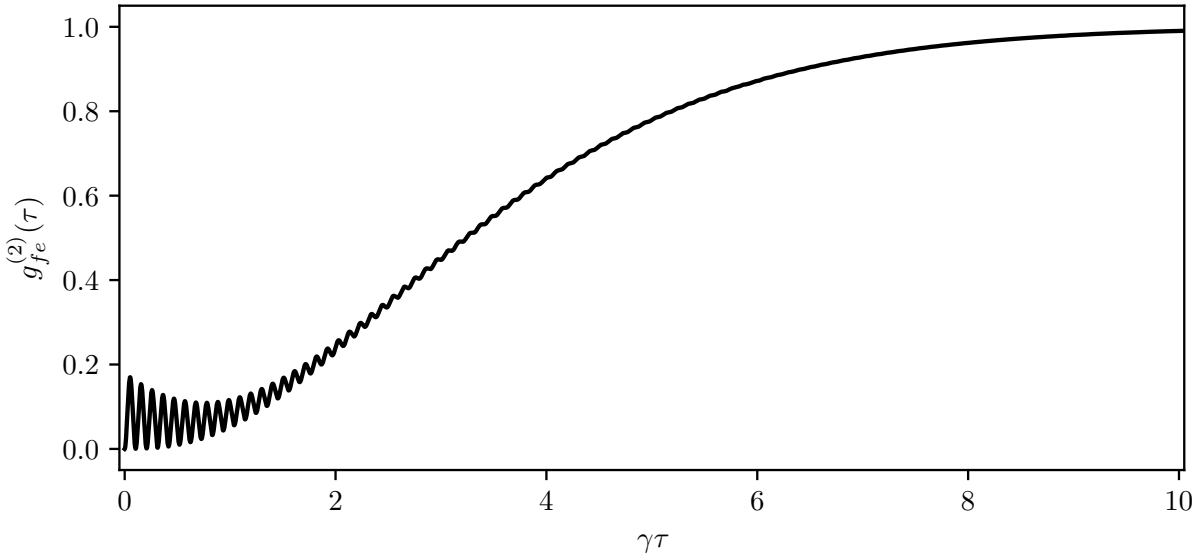

(b) Auto-correlation of $\hat{\sigma}^-_{fe}$.

Figure 6.6: Second-order correlations of the separate dipole operators. Parameters are $(\Omega/\gamma, \alpha/\gamma, \delta/\gamma, \xi) = (5.0, -120.0, 0.0, 1.0)$.

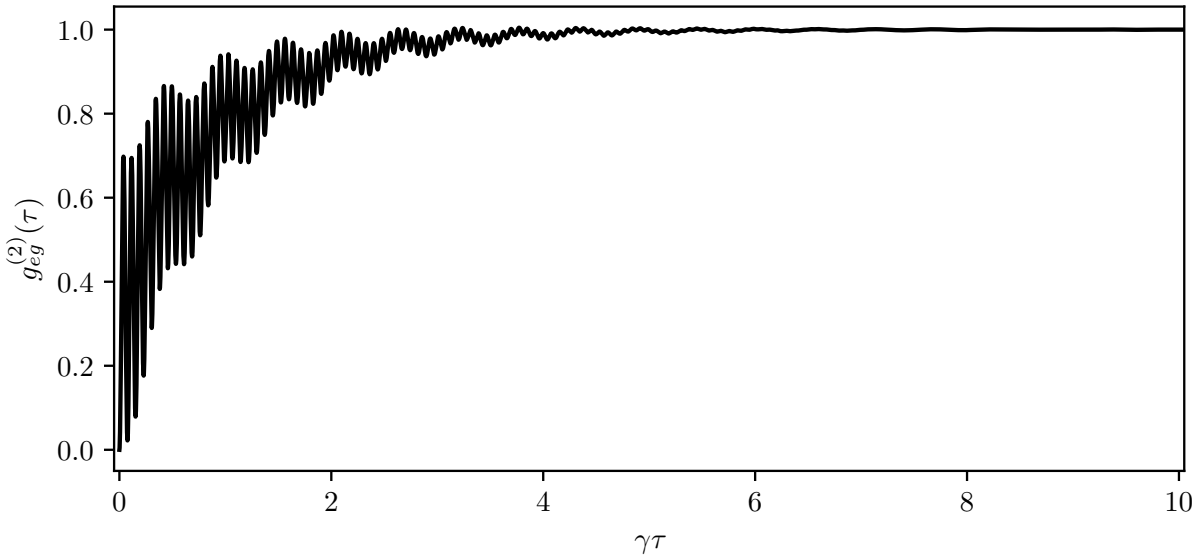

(a) Auto-correlation of $\hat{\sigma}^-_{eg}$.

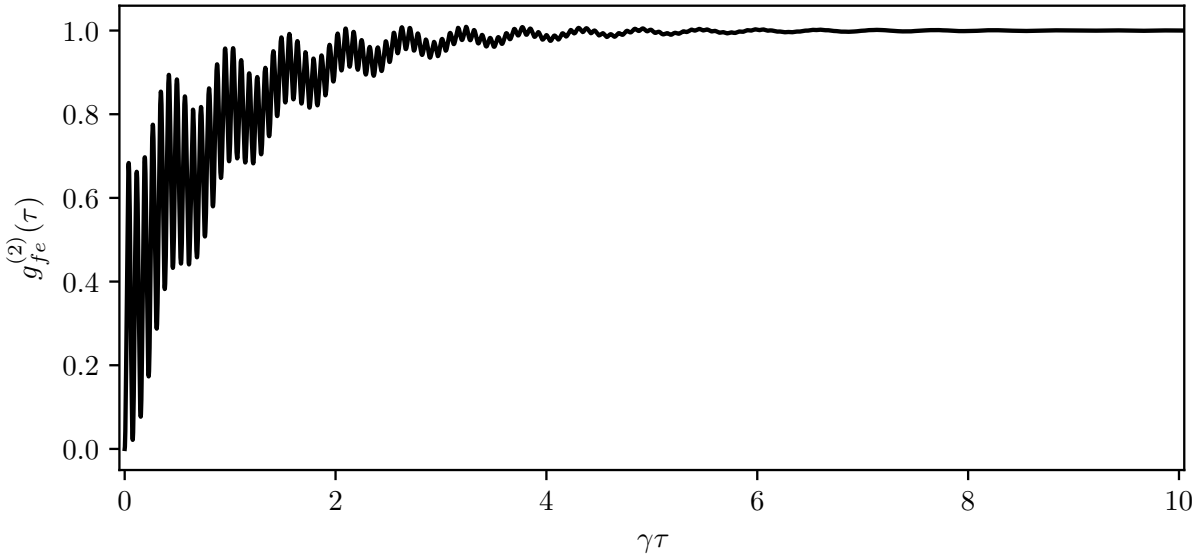

(b) Auto-correlation of $\hat{\sigma}^-_{fe}$.

Figure 6.7: Second-order correlations of the separate dipole operators. Parameters are $(\Omega/\gamma, \alpha/\gamma, \delta/\gamma, \xi) = (40.0, -120.0, 0.0, 1.0)$.

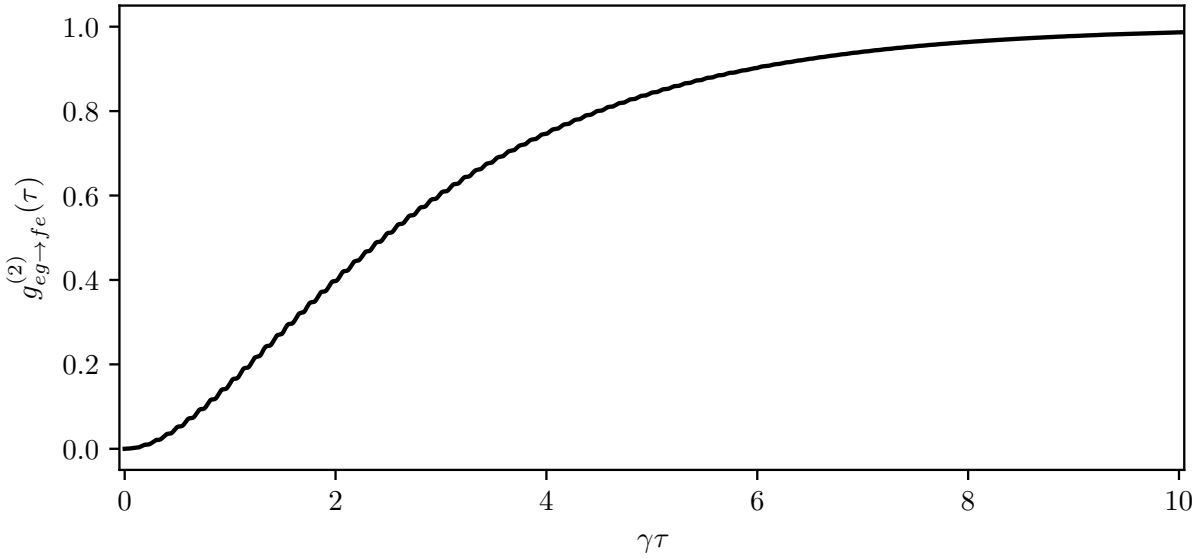

(a) Cross-correlation of $\hat{\sigma}^-_{eg}$ followed by $\hat{\sigma}^-_{fe}$.

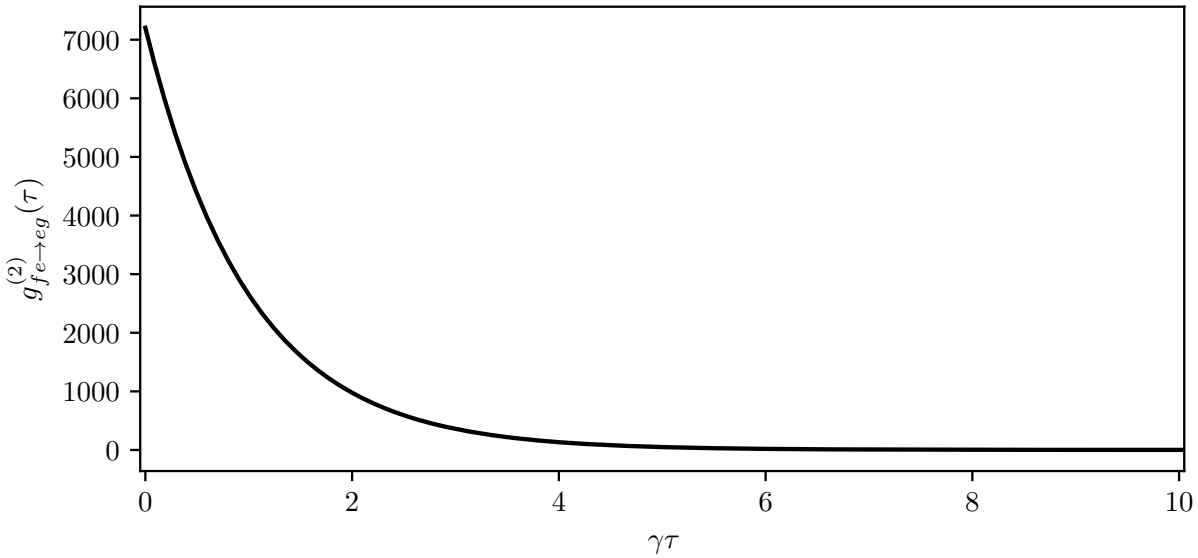

(b) Cross-correlation of $\hat{\sigma}^-_{fe}$ followed by $\hat{\sigma}^-_{eg}$.

Figure 6.8: Cross-correlations of the separate dipole operators. Parameters are $(\Omega/\gamma, \alpha/\gamma, \delta/\gamma, \xi) = (5.0, -120.0, 0.0, 1.0)$.

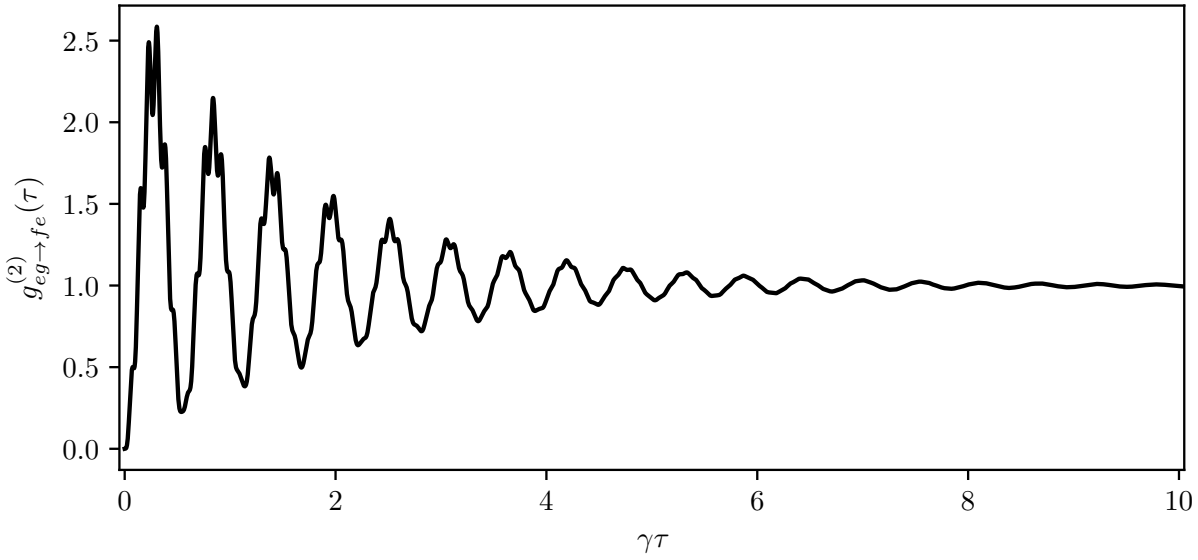

(a) Cross-correlation of $\hat{\sigma}^-_{eg}$ followed by $\hat{\sigma}^-_{fe}$.

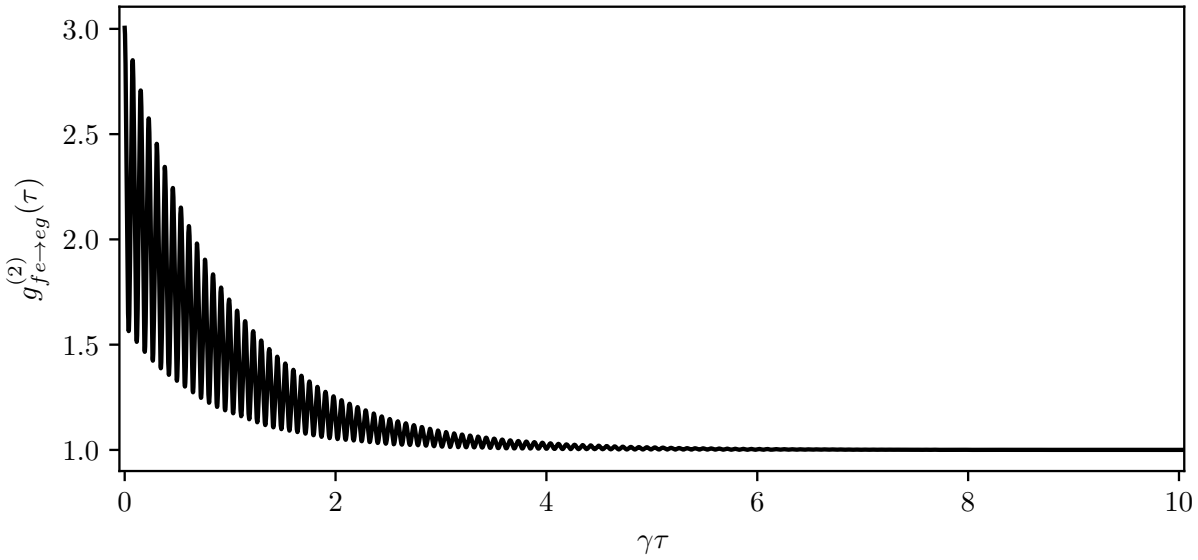

(b) Cross-correlation of $\hat{\sigma}^-_{fe}$ followed by $\hat{\sigma}^-_{eg}$.

Figure 6.9: Cross-correlations of the separate dipole operators. Parameters are $(\Omega/\gamma, \alpha/\gamma, \delta/\gamma, \xi) = (40.0, -120.0, 0.0, 1.0)$.

6.3 Lorentzian Filter Cavity

We now aim to investigate the photon correlations for specific transitions made in the cascade decay. We were able to do this in the limited case of a very weak drive by considering the separate dipole operators, $\hat{\sigma}_{eg}^{-}$ and $\hat{\sigma}_{fe}^{-}$. Once the drive strength increases and more transitions are made possible, however, we must take another approach.

In an experimental setting, in order to correlate the photons of a specific transition we would first need to filter the light. In this section we will adopt a simple method by coupling the fluorescence of the three-level atom into a *scanning interferometer* – a system known as a "cascaded system" [60]. We begin by describing the scanning interferometer as a lossy cavity, which has a Lorentzian shaped power spectrum. We then give a brief outline of a cascaded open system in the context of our system of interest. With the cavity acting as a Lorentzian filter we are able to focus our interest onto specific transitions.

With the background theory set, we then calculate the photon correlations of the cascade transitions, referencing back to the peaks of the incoherent fluorescence spectrum, and provide a numerical survey.

6.3.1 Filter Cavity

We model the scanning interferometer as a damped harmonic oscillator, with full Hamiltonian similar to Eq. (3.17), but with

$$\hat{H}_a = \hbar\Delta_a \hat{a}^\dagger \hat{a}, \tag{6.17}$$

where Δ_a is the detuning of the oscillator relative to ω_d, and $\hat{a}^\dagger$ ($\hat{a}$) are the creation (annihilation) operators. The derivation for the master equation of the damped harmonic oscillator follows the same procedure used to derive the master equation of the three-level atom in Sect. (3.1.3). Following through with the derivation we arrive at the *master equation for a damped harmonic oscillator*

$$\frac{\mathrm{d}}{\mathrm{d}t}\hat{\rho} = \frac{1}{i\hbar}[\hat{H}_a, \hat{\rho}] + \frac{\kappa_a}{2}\left(2\hat{a}\hat{\rho}\hat{a}^\dagger - \hat{a}^\dagger\hat{a}\hat{\rho} - \hat{\rho}\hat{a}^\dagger\hat{a}\right), \tag{6.18}$$

where we have neglected both the effect of a thermal environment and the frequency shifts, and

$$\kappa_a = 2\pi\varrho(\Delta_a)|g(\Delta_a)|^2, \tag{6.19}$$

is the cavity decay rate.

We can calculate the first-order correlation function, $\langle\hat{a}^\dagger(t)\hat{a}(t+\tau)\rangle$, for the cavity by first deriving the equation of motion for the operator expectation $\langle\hat{a}\rangle$ (Ref. [28], Sect. 1.5.3),

$$\frac{\mathrm{d}}{\mathrm{d}t}\langle\hat{a}\rangle = \mathrm{tr}\left[\left(\frac{\mathrm{d}}{\mathrm{d}t}\hat{\rho}\right)\hat{a}\right] = -\left(\frac{\kappa_a}{2} + i\Delta_a\right)\langle\hat{a}\rangle, \tag{6.20}$$

and then using the quantum regression procedure, whereby the equation of motion for the correla-

tion function is

$$\frac{\mathrm{d}}{\mathrm{d}t}\langle\hat{a}^\dagger(t)\hat{a}(t+\tau)\rangle = -\left(\frac{\kappa_a}{2}+i\Delta_a\right)\langle\hat{a}^\dagger(t)\hat{a}(t+\tau)\rangle, \tag{6.21}$$

which, in the steady state limit $t\to\infty$, has the solution

$$g^{(1)}(\tau) = e^{-(\kappa_a/2+i\Delta_a)\tau}. \tag{6.22}$$

Recalling the Wiener-Khintchine theorem, Eq. (5.24), the power spectrum of this cavity is the Fourier transform of the correlation function, i.e., a Lorentzian centred on Δ_a with full-width at half-maximum κ_a.

6.3.2 Cascaded Open System

We consider a composite system where we have a source subsystem, the atom with Hamiltonian Eq. (4.6), whose output is coupled to a target subsystem, the cavity filter with Hamiltonian Eq. (6.17), at a distance d, as illustrated in Fig. 6.10. The fluorescence of the atom is coupled through a partially transmitting mirror into a ring cavity. If the fluorescence is resonant with the cavity it will be able to pass through another partially transmitting mirror on the other side of the cavity, such that the ring cavity acts as a transmission filter; incident light that is off resonance is reflected rather than transmitted. Following the approach of Carmichael (Ref. [30], Sect. 19.2), the total Hamiltonian is $\hat{H} = \hat{H}_S + \hat{H}_R + \hat{H}_{SR}$ where

$$\hat{H}_S = \hat{H}_{\text{source}} + \hat{H}_{\text{target}}, \tag{6.23a}$$

$$\hat{H}_R = \sum_j \hbar\omega_j \hat{r}_j^\dagger \hat{r}_j, \tag{6.23b}$$

$$\hat{H}_{SR} = \hat{H}_{SR}^{\text{source}} + \hat{H}_{SR}^{\text{target}}, \tag{6.23c}$$

where $\hat{H}_{\text{source}} = \hat{H}_A$, $\hat{H}_{\text{target}} = \hat{H}_a$, and the reservoir interactions are

$$\hat{H}_{SR}^{\text{source}} = \hbar\sqrt{\gamma}\left[\hat{\Sigma}\hat{\mathcal{E}}^\dagger(0) + \text{H.c.}\right], \tag{6.24a}$$

$$\hat{H}_{SR}^{\text{target}} = \hbar\sqrt{\kappa_a}\left[\hat{a}\hat{\mathcal{E}}^\dagger(d) + \text{H.c.}\right], \tag{6.24b}$$

where we have expressed the electric field in photon flux units as

$$\hat{\mathcal{E}}(z) \equiv -i\sqrt{\frac{2\epsilon_0 Ac}{\hbar\frac{1}{2}(\omega_{eg}+\omega_{fe})}}\hat{\boldsymbol{e}}\cdot\hat{\boldsymbol{E}}^{(+)}(z,0). \tag{6.25}$$

The two subsystems are coupled to different field operators, $\hat{\mathcal{E}}(0)$ and $\hat{\mathcal{E}}(d)$, which are correlated, so it is not permissible to treat the reservoir interactions as independent. Instead we consider the *time-retarded density operator*

$$\hat{\chi}_{\text{ret}} \equiv \hat{U}_{\text{source}}(-d/c)\hat{\chi}\hat{U}_{\text{source}}^\dagger(-d/c), \tag{6.26}$$

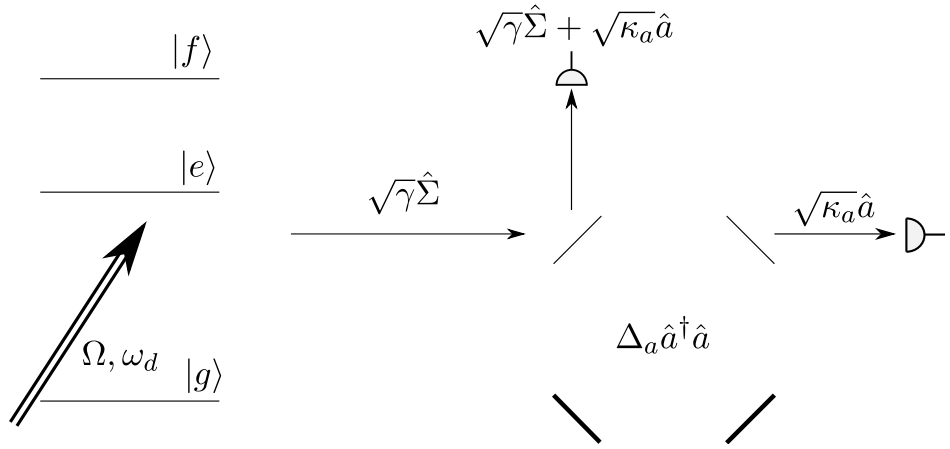

Figure 6.10: Schematic of the single-filter system, where the fluorescence is emitted into the ring cavity. It first encounters a mirror with very small transmission coefficient, mainly reflecting into the upper detector but with a small transmission. If the fluorescence is resonant with the cavity, at frequency Δ_a, it will build up over many round trips inside the cavity and be transmitted either through the first partially transmitting mirror, towards the upper detector, or out the side, to the right-most detector. For exact resonance, the field directed towards the upper detector is π out of phase with the incident field reflected from the input mirror, which results in destructive interference and no net output towards the upper detector.

where

$$\hat{U}_{\text{source}}(-d/c) \equiv e^{-\frac{i}{\hbar}(\hat{H}_{\text{source}}+\hat{H}_R+\hat{H}_{SR}^{\text{source}})(-d/c)}. \tag{6.27}$$

The Schrödinger equation for the density operator now becomes

$$\frac{\mathrm{d}}{\mathrm{d}t}\hat{\chi}_{\text{ret}} = \frac{1}{i\hbar}[\hat{H}_{\text{ret}}, \hat{\chi}_{\text{ret}}], \tag{6.28}$$

where the only difference between $\hat{H}_{\text{ret}}$ and Eq. (6.23) is that the interaction term is changed:

$$\hat{H}_{SR}^{\text{target}} \longrightarrow \hat{U}_{\text{source}}(d/c)\hat{H}_{SR}^{\text{target}}\hat{U}_{\text{source}}^\dagger(d/c). \tag{6.29}$$

Now the electric field of the reservoir freely propagates from the atom to the target cavity, so we find that the Hamiltonian becomes

$$\hat{H}_{\text{ret}} = \hat{H}_S^c + \hat{H}_R + \hat{H}_{SR}^c, \tag{6.30}$$

where

$$\hat{H}_S^c = \hat{H}_{\text{source}} + \hat{H}_{\text{target}} + \frac{i\hbar}{2}\sqrt{\gamma\kappa_a}\left(\hat{a}\hat{\Sigma}^\dagger - \hat{\Sigma}\hat{a}^\dagger\right), \tag{6.31}$$

and the source and target now couple to the reservoir at the same spatial location:

$$\hat{H}_{SR}^c = \hbar\left[\left(\sqrt{\gamma}\hat{\Sigma} + \sqrt{\kappa_a}\hat{a}\right)\hat{\mathcal{E}}^\dagger(0) + \text{H.c.}\right]. \tag{6.32}$$

We can now follow through with the familiar procedure to derive the master equation for the reduced density operator

$$\hat{\rho}_{\text{ret}}(t) \equiv \text{tr}\left[\hat{\chi}_{\text{ret}}(t)\right]. \tag{6.33}$$

Adding in the decay of the cavity, we finally obtain the *master equation for a three-level atom cascaded with a target scanning interferometer*:

$$\begin{aligned}\frac{\mathrm{d}}{\mathrm{d}t}\hat{\rho} = \frac{1}{i\hbar}[\hat{H}_c, \hat{\rho}] + \frac{1}{2}\left(2\hat{J}_c^a\hat{\rho}\hat{J}_c^{a\dagger} - \hat{J}_c^{a\dagger}\hat{J}_c^a\hat{\rho} - \hat{\rho}\hat{J}_c^{a\dagger}\hat{J}_c^a\right) \\ + \frac{\kappa_a}{2}\left(2\hat{a}\hat{\rho}\hat{a}^\dagger - \hat{a}^\dagger\hat{a}\hat{\rho} - \hat{\rho}\hat{a}^\dagger\hat{a}\right),\end{aligned} \tag{6.34}$$

with Hamiltonian

$$\hat{H}_c = \hat{H}_A + \hbar\Delta_a\hat{a}^\dagger\hat{a} + \frac{i\hbar}{2}\sqrt{\gamma\kappa_a}\left(\hat{a}\hat{\Sigma}^\dagger - \hat{\Sigma}\hat{a}^\dagger\right), \tag{6.35}$$

where $\hat{H}_A$ is the Hamiltonian for the driven atom, Eq. (4.6), and cascaded decay operator

$$\hat{J}_c^a = \sqrt{\gamma}\hat{\Sigma} + \sqrt{\kappa_a}\hat{a}. \tag{6.36}$$

6.3.3 Auto-correlation

As we have established, the second-order correlation function is related to the probability of detecting another photon at a time τ after a first detection. To clarify the situation, it can be useful to consider the system in terms of a quantum trajectory experiment. The evolution of the system is now governed by the Schrödinger equation with non-Hermitian Hamiltonian (Ref. [30], p. 491)

$$\hat{H} = \hat{H}_A + \hbar\Delta_a\hat{a}^\dagger\hat{a} - i\hbar\frac{\gamma}{2}\hat{\Sigma}^\dagger\hat{\Sigma} - i\hbar\kappa_a\hat{a}^\dagger\hat{a} - i\hbar\sqrt{\gamma\kappa_a}\hat{a}^\dagger\hat{\Sigma}, \tag{6.37}$$

where it is made clear in this Hamiltonian that the cascaded system is coupled in one direction only. With the current system set up we expect only two types of detections. If the fluorescence is resonant with the cavity and is not reflected at the first partially transmitting mirror, it enters the ring cavity and can leave out the other side, with a detection corresponding to the jump operator

$$\hat{J}_a = \sqrt{\kappa_a}\hat{a}; \tag{6.38}$$

otherwise it passes through the input mirror again to reach the same detector as the initially reflected fluorescence; thus, the second detection corresponds to a superposition of reflected and transmitted fluorescence, with jump operator Eq. (6.36).

We may now think of the second-order correlation in terms of a detector going "click". Specifically, given a detection from the transmission channel, what is the probability of another detection occurring after a time τ. We then work from the answer to this question and define the *second-order*

correlation for the filter cavity

$$g^{(2)}_{\text{Auto}}(\tau) = \frac{\langle \hat{a}^\dagger(0)\hat{a}^\dagger(\tau)\hat{a}(\tau)\hat{a}(0)\rangle_{ss}}{\langle \hat{a}^\dagger\hat{a}\rangle^2_{ss}}. \tag{6.39}$$

In Sect. 6.2.2, for a weak drive field, we saw that the separate dipole operators correspond to the transitions expected from the two steps of the cascade decay. Using the results of that section as a reference we aim to reproduce the photon correlations (Fig. 6.6) with the filter cavity cascaded system. In Fig. 6.11 we set the filter to be resonant with the ω_{eg} transition. Looking at the auto-correlation, it comes as no surprise that the light is anti-bunched. Moving the filter resonance to match the ω_{fe} transition (Fig. 6.12) we see that the emitted light is also anti-bunched There is, however, one important difference in these figures and those of the dipole operators, Fig. 6.6, and that is the lack of rapid oscillations. We have now come across the first unavoidable issue with the filter cavity.

In order for us to resolve the fast oscillations, the cavity linewidth κ_a must be roughly as large as the frequency of oscillations, which, for a low drive, is approximately the detuning from single-photon resonance, $\alpha/2 + \delta$. This means that at two-photon resonance $\kappa_a \approx |\alpha|/2$. If it is much smaller, the rapid oscillations will be averaged out – exactly what we see in Figs. 6.11 and 6.12. The filter has a Lorentzian shape, however, which has very long tails. If we were to make κ_a large enough to capture the oscillations, the cavity would contain some "contamination" of other frequencies, no longer acting as a sufficient filter. Even for a smaller bandwidth, however, we have seen that the filter can still resolve whether the emitted light is correlated or not.

We move on, now, to the strong driving regime where we are able to resolve the correlations of the dressed states transitions – something we were unable to do with the dipole operators in the previous section. It appears from the dressed state transitions shown in Fig. 5.1 that all but one of the transitions are anti-bunched, with the single bunched transition responsible for the ω_d peak in the fluorescence spectrum of Fig. 5.9. By setting the cavity resonant to the ω_d transition in Fig. 6.13, we see that the light is indeed bunched as expected – because the $|+\rangle$ to $|+\rangle$ and $|-\rangle$ to $|-\rangle$ transitions may be immediately followed by the same respective transition. Unlike the rapid oscillations for the weak drive, in this case the cavity is able to resolve the more prominent oscillations as the beat frequency is $|\omega_-| \approx 11.23 \ll |\alpha|/2$. Shifting the cavity resonance slightly to the left, we now focus on the $|-\rangle$ to $|0\rangle$ transition with frequency $\omega_d + \omega_-$. We see in Fig. 6.14 that, as we already stated, the light from this transition is also anti-bunched. We see even more pronounced antibunching when focusing on the ω_{eg} doublet in Fig. 6.15; we see in Fig. 5.1 that each individual transition, excluding ω_d, can only occur once in a cascade decay.

Figures 6.16, 6.17, and 6.18 all show the auto-correlation for the $|+\rangle$ to $|0\rangle$ transition for three different values of ξ. While the spectrum changes with each value, the auto-correlations indicate the emitted light from this transition is still antibunched. This is to be expected as the dressed states and their frequencies maintain the form shown in Fig. 5.1. We find, in fact, that the correlations for any each value of ξ remains qualitatively the same.

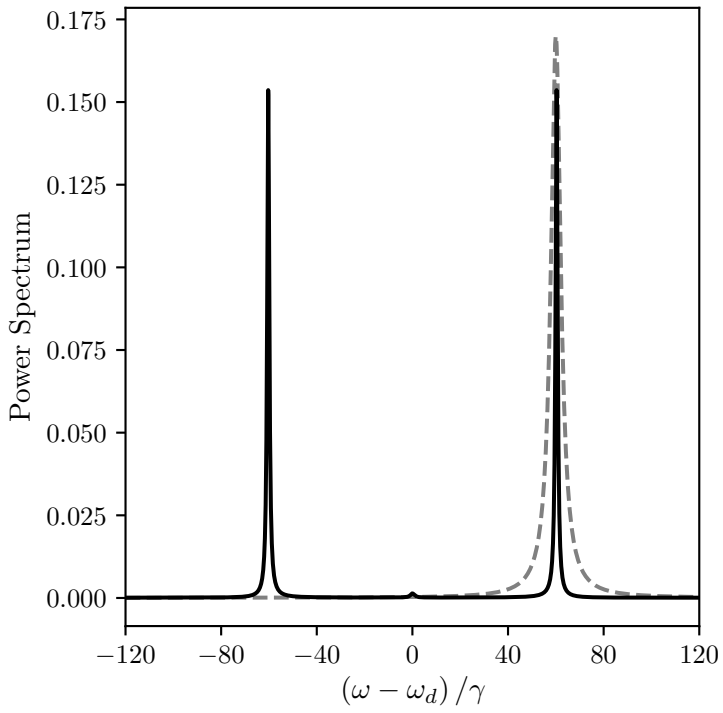

(a) Incoherent fluorescence spectrum (solid) with filter cavity (dashed).

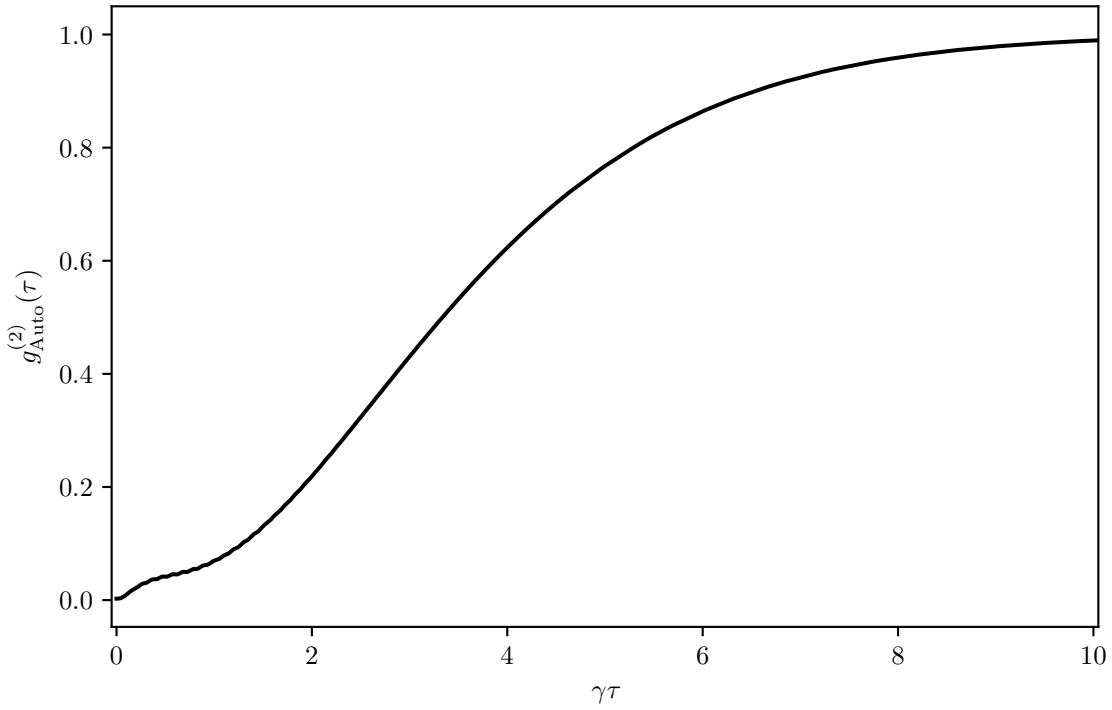

(b) Auto-correlation.

Figure 6.11: Filtered second-order auto-correlation for the ω_{eg} transition and a weak drive. Parameters are $(\Omega/\gamma, \alpha/\gamma, \delta/\gamma, \xi, \Delta_a/\gamma, \kappa_a/\gamma) = (40.0, -120.0, 0.0, 1.0, 60.0, 5.0)$.

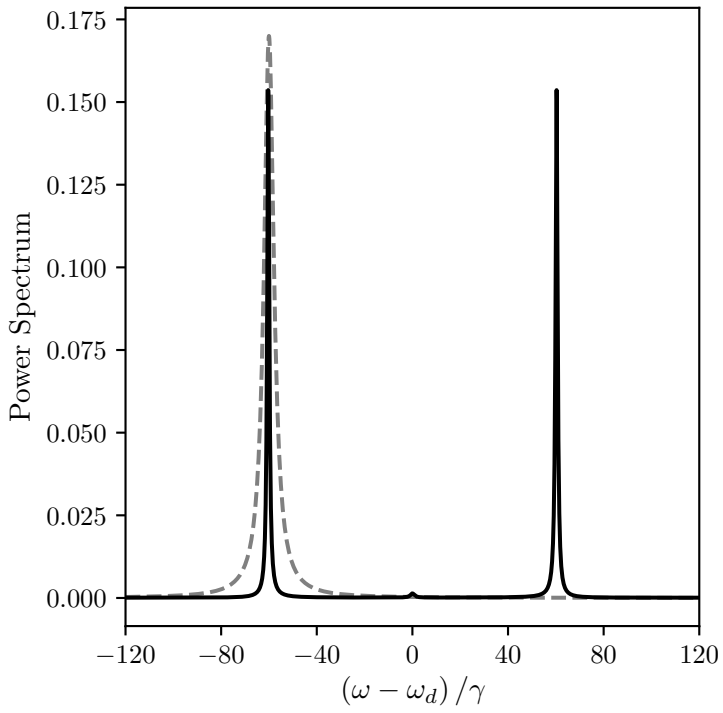

(a) Incoherent fluorescence spectrum (solid) with filter cavity (dashed).

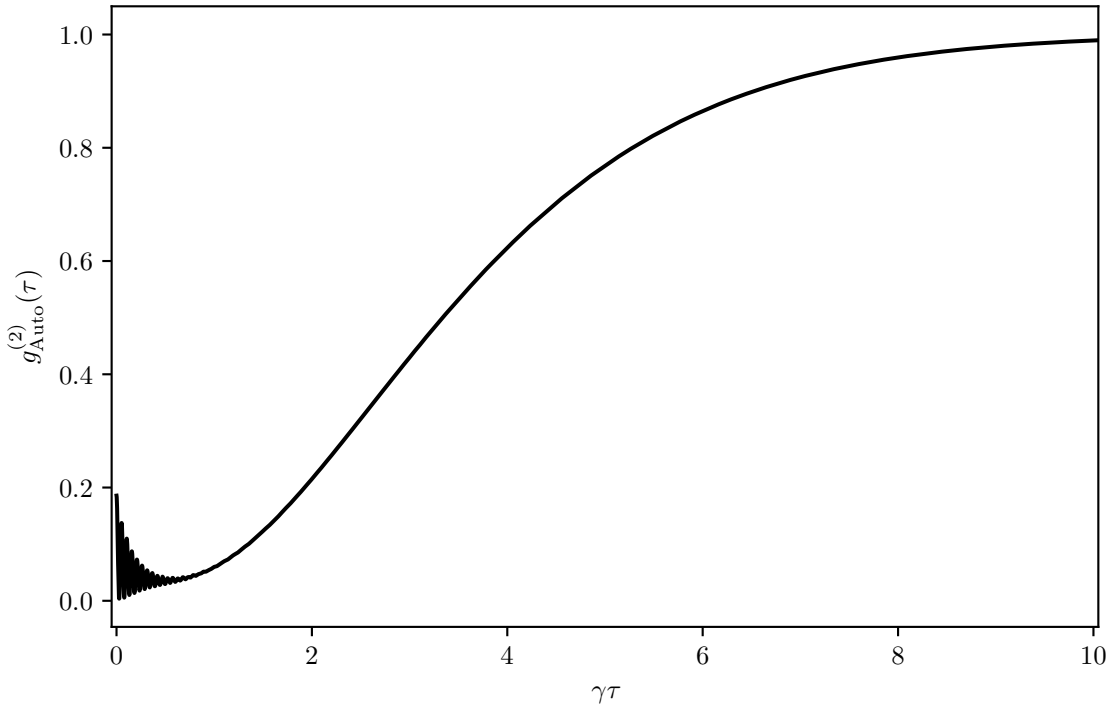

(b) Auto-correlation.

Figure 6.12: Filtered second-order auto-correlation for the ω_{fe} transition and a weak drive. Parameters are $(\Omega/\gamma, \alpha/\gamma, \delta/\gamma, \xi, \Delta_a/\gamma, \kappa_a/\gamma) = (40.0, -120.0, 0.0, 1.0, -60.0, 10.0)$.

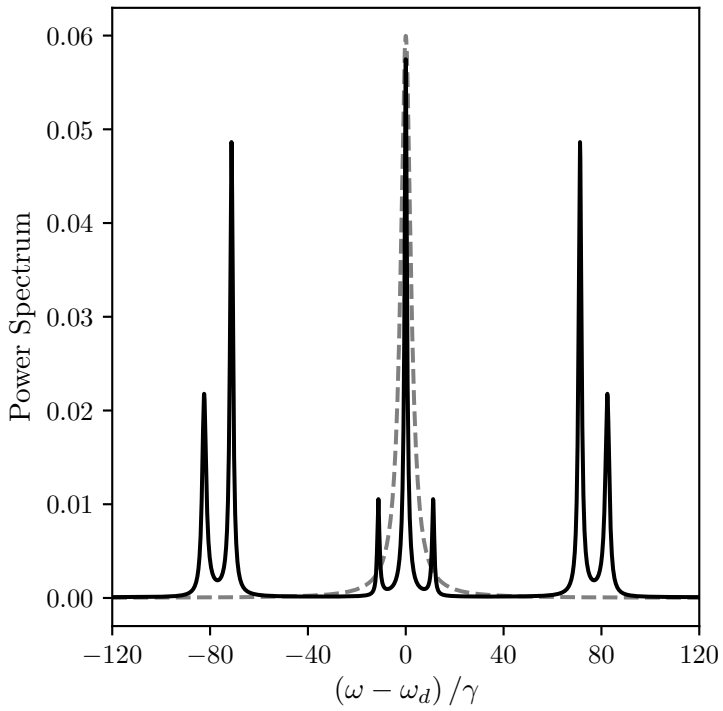

(a) Incoherent fluorescence spectrum (solid) with filter cavity (dashed).

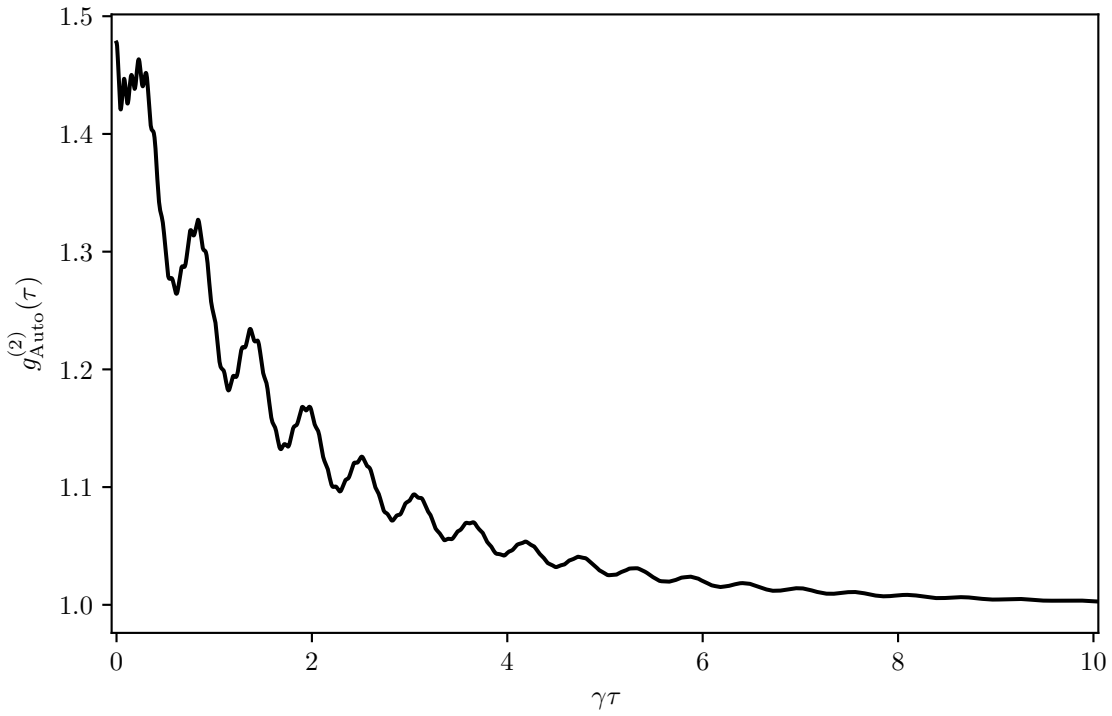

(b) Auto-correlation.

Figure 6.13: Filtered second-order auto-correlation for the centre peak of the central triplet. Parameters are $(\Omega/\gamma, \alpha/\gamma, \delta/\gamma, \xi, \Delta_a/\gamma, \kappa_a/\gamma) = (40.0, -120.0, 0.0, 1.0, 0.0, 5.0)$.

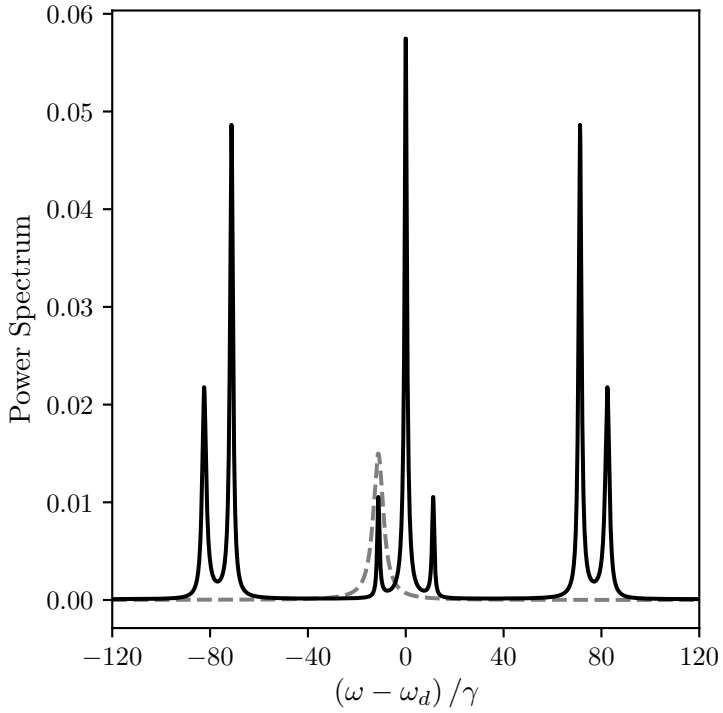

(a) Incoherent fluorescence spectrum (solid) with filter cavity (dashed).

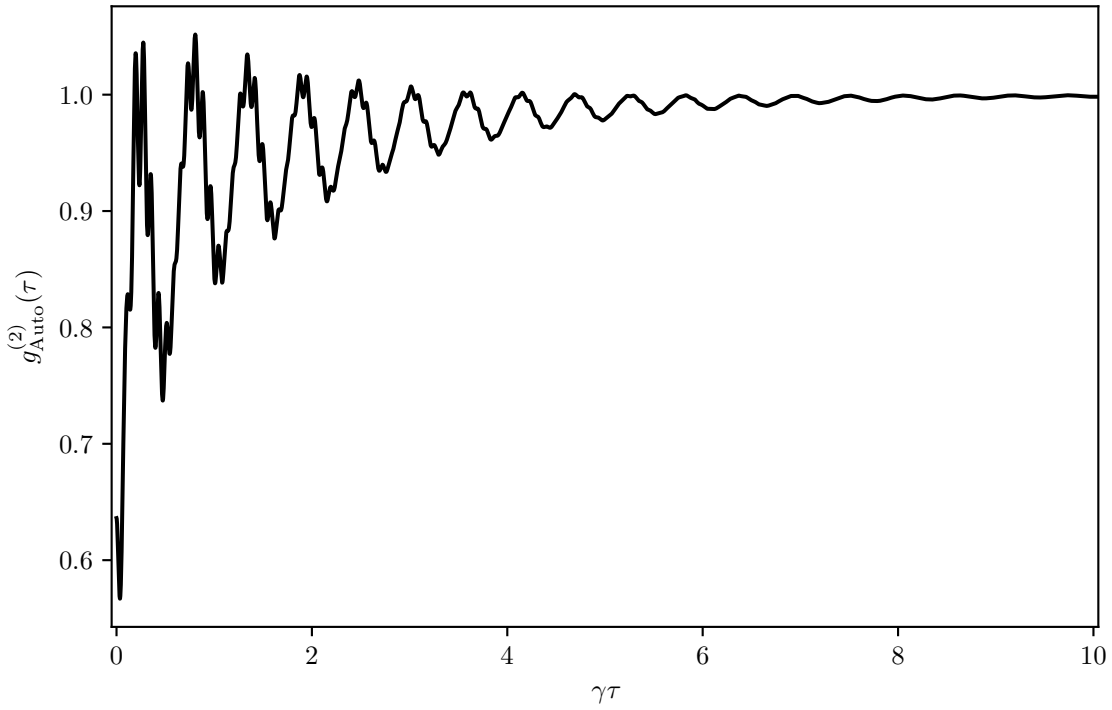

(b) Auto-correlation.

Figure 6.14: Filtered second-order auto-correlation for the left peak of the central triplet. Parameters are $(\Omega/\gamma, \alpha/\gamma, \delta/\gamma, \xi, \Delta_a/\gamma, \kappa_a/\gamma) = (40.0, -120.0, 0.0, 1.0, -11.23, 5.0)$.

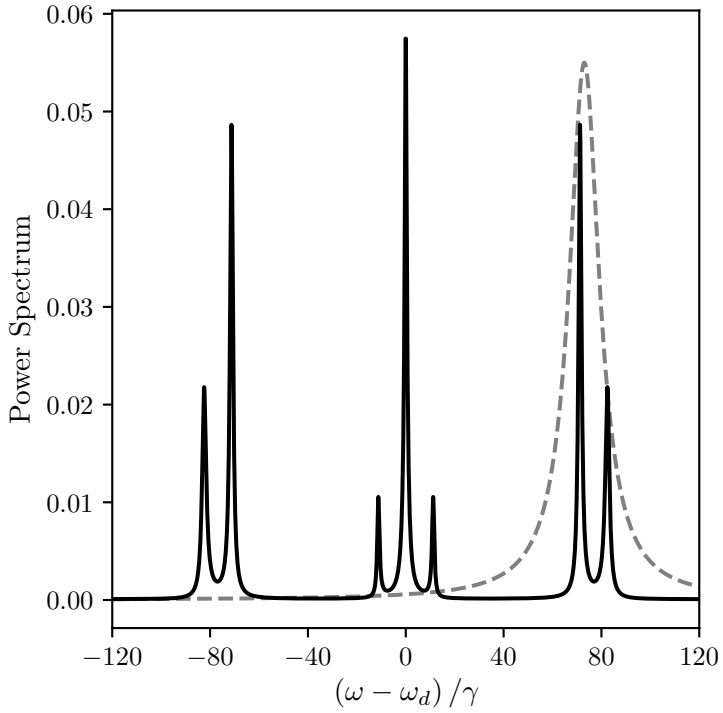

(a) Incoherent fluorescence spectrum (solid) with filter cavity (dashed).

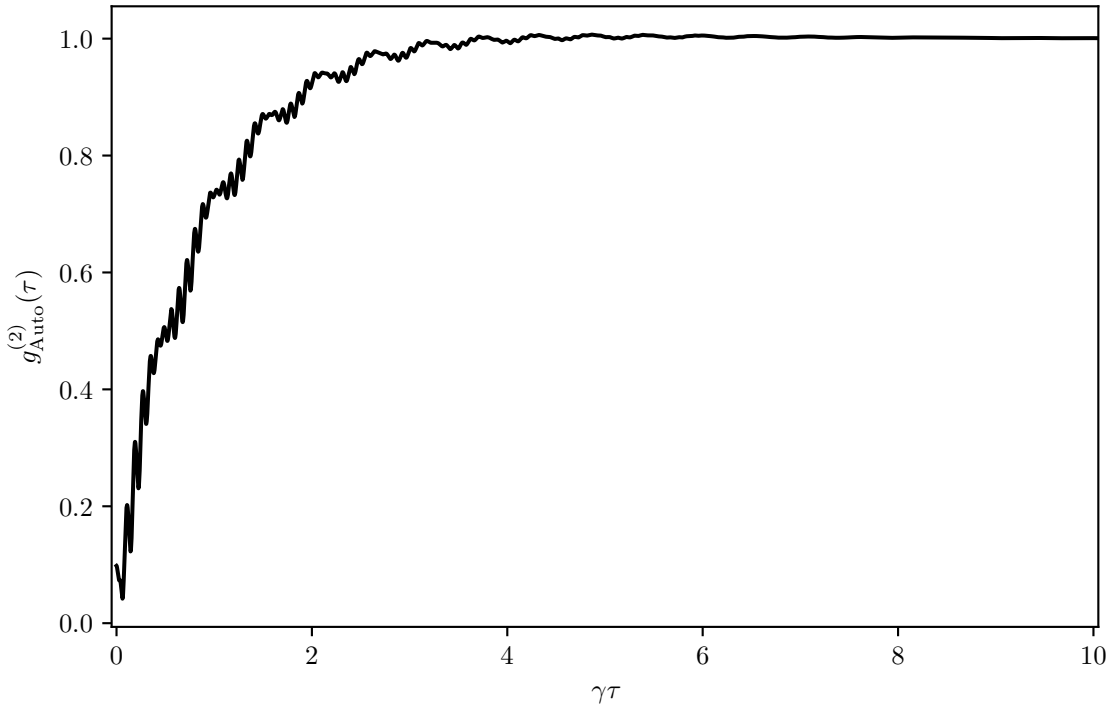

(b) Auto-correlation.

Figure 6.15: Filtered second-order auto-correlation for the ω_{eg} doublet. Parameters are $(\Omega/\gamma, \alpha/\gamma, \delta/\gamma, \xi, \Delta_a/\gamma, \kappa_a/\gamma) = (40.0, -120.0, 0.0, 1.0, 73.0, 15.0)$.

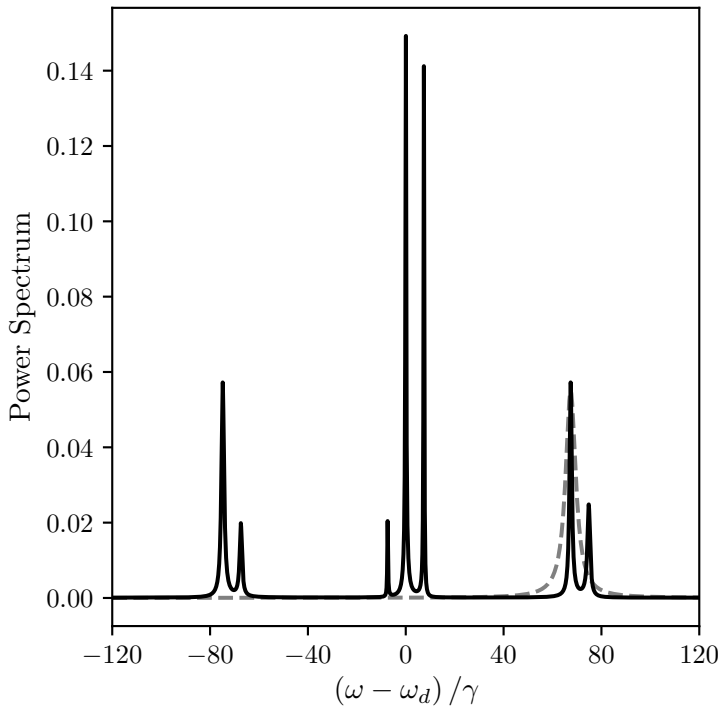

(a) Incoherent fluorescence spectrum (solid) with filter cavity (dashed).

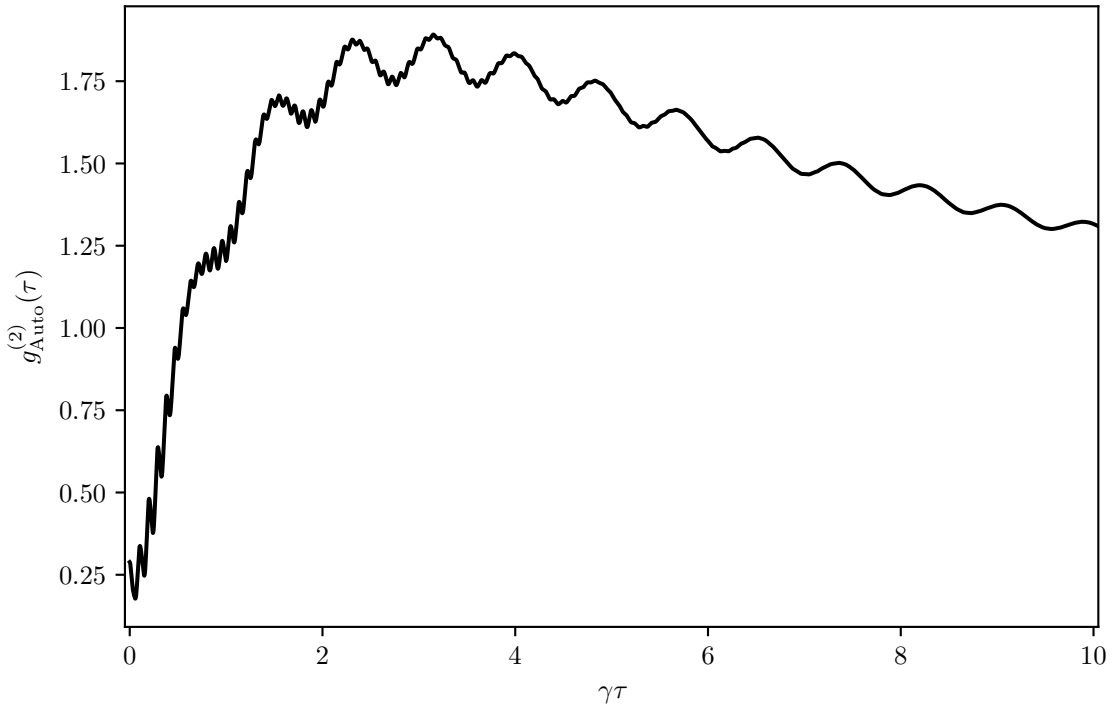

(b) Auto-correlation.

Figure 6.16: Filtered second-order auto-correlation for the $\omega_d+\omega_+$ transition, $\xi = 0.5$. Parameters are $(\Omega/\gamma, \alpha/\gamma, \delta/\gamma, \xi, \Delta_a/\gamma, \kappa_a/\gamma) = (40.0, -120.0, 0.0, 1.0, 67.42, 5.0)$.

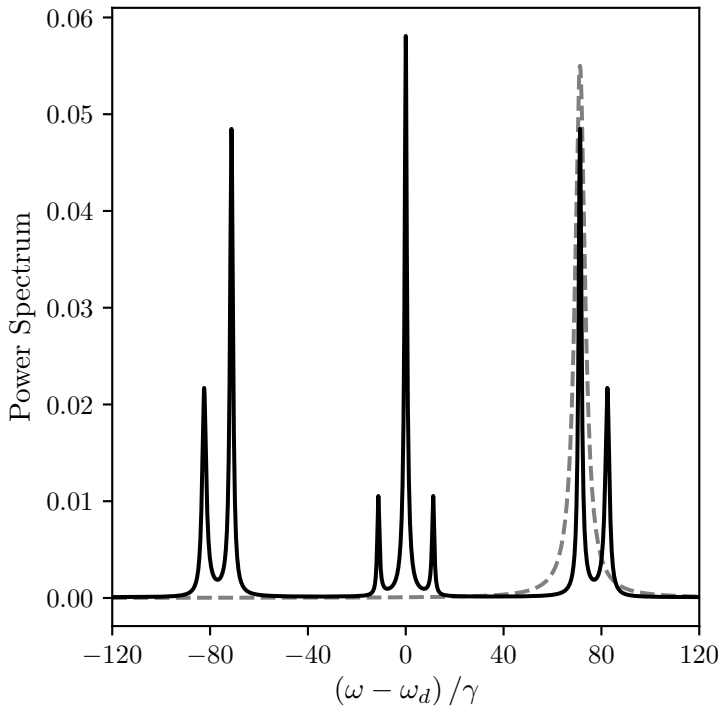

(a) Incoherent fluorescence spectrum (solid) with filter cavity (dashed).

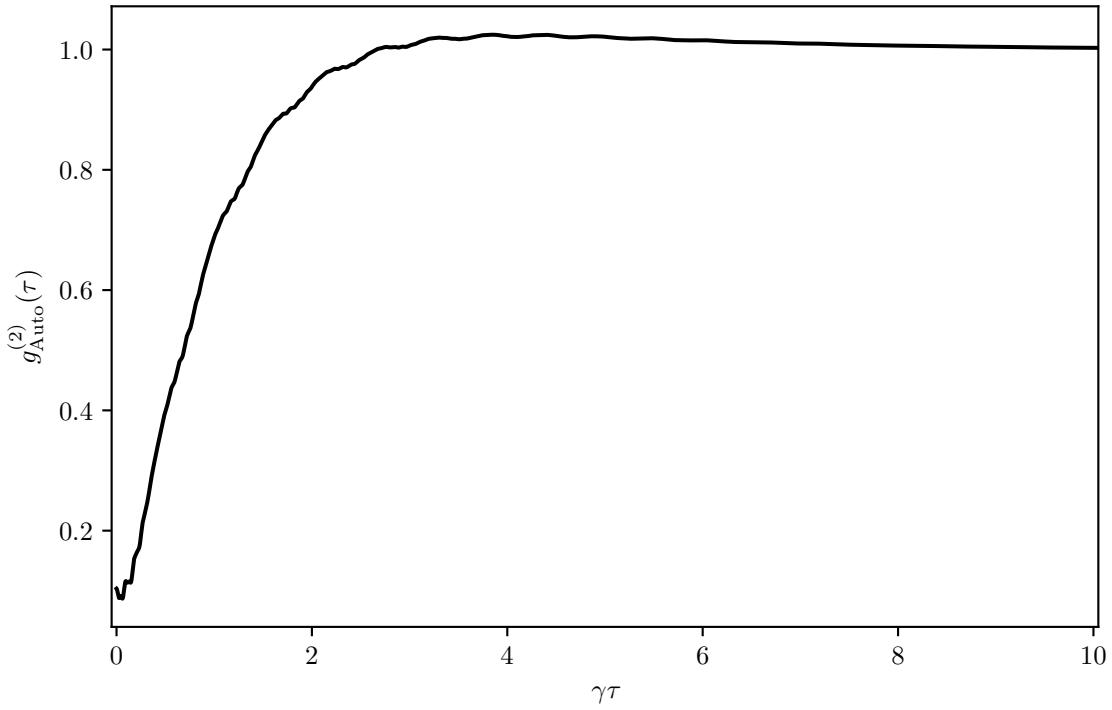

(b) Auto-correlation.

Figure 6.17: Filtered second-order auto-correlation for the $\omega_d+\omega_+$ transition, $\xi = 1.0$. Parameters are $(\Omega/\gamma, \alpha/\gamma, \delta/\gamma, \xi, \Delta_a/\gamma, \kappa_a/\gamma) = (40.0, -120.0, 0.0, 1.0, 76.9, 5.0)$.

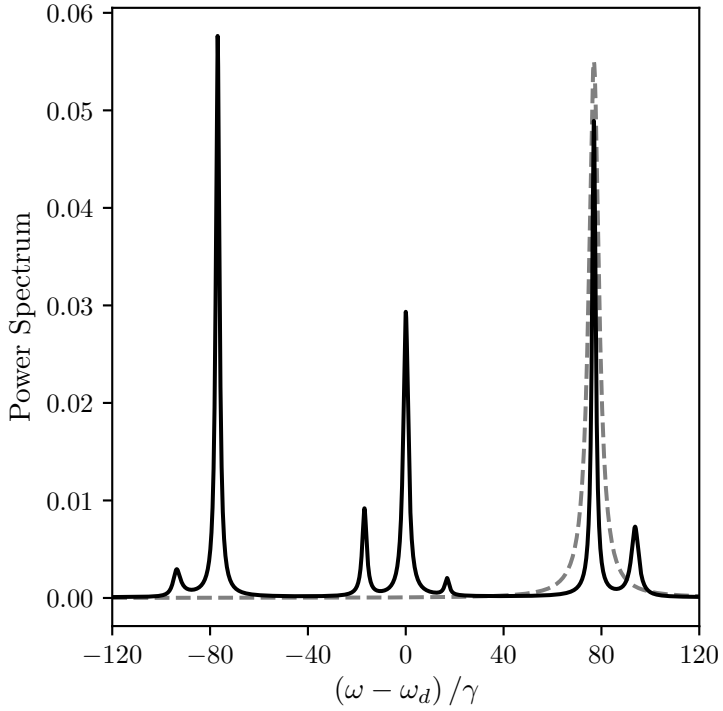

(a) Incoherent fluorescence spectrum (solid) with filter cavity (dashed).

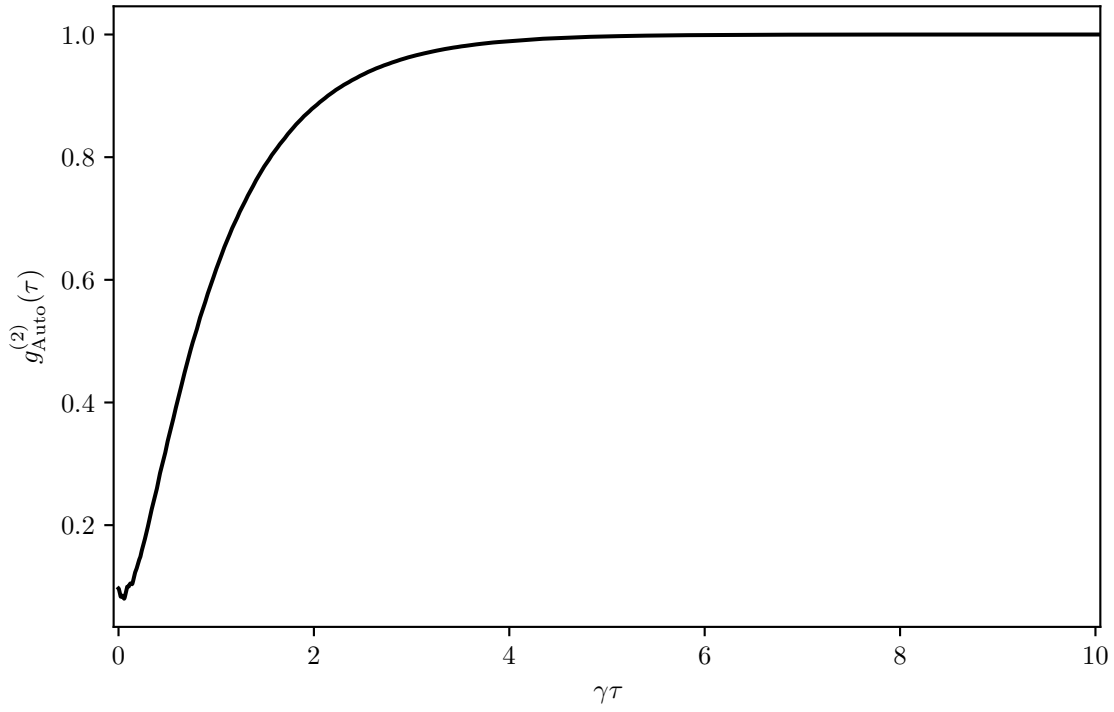

(b) Auto-correlation.

Figure 6.18: Filtered second-order auto-correlation for the $\omega_d+\omega_+$ transition, $\xi = 1.5$. Parameters are $(\Omega/\gamma, \alpha/\gamma, \delta/\gamma, \xi, \Delta_a/\gamma, \kappa_a/\gamma) = (40.0, -120.0, 0.0, 1.5, 76.9, 5.0)$.

6.3.4 Analytic expression for weak drive limit

The basis states for the cascaded system can be described as a tensor product of the atomic states and the Fock states of the cavity:

$$|\psi\rangle = |n\rangle \otimes |i\rangle = |n, i\rangle\,, \tag{6.40}$$

where $n = 0, 1, 2, \ldots$, and $i \in g, e, f$. In the weak drive limit, the system state is dominated by the ground state $|g, 0\rangle$, and, following the method of Carmichael (Ref. [30], Sect. 16.2), we may expand the state vector in the *two-quanta truncation*,

$$|\tilde{\psi}\rangle = |0, g\rangle + \tilde{\alpha}(t)\,|0, e\rangle + \tilde{\beta}(t)\,|0, f\rangle + \tilde{\gamma}(t)\,|1, g\rangle + \tilde{\delta}(t)\,|1, e\rangle + \tilde{\eta}(t)\,|2, g\rangle\,, \tag{6.41}$$

and solve the Schrödinger equation

$$\frac{\mathrm{d}}{\mathrm{d}t}\,|\tilde{\psi}\rangle = \frac{1}{i\hbar}\hat{H}\,|\tilde{\psi}\rangle\,, \tag{6.42}$$

with Hamiltonian Eq. (6.37). Thus, since quantum jumps are extremely rare when the drive field is weak, we assume the atom evolves freely with the Hamiltonian used in trajectory theory. From the state expansion, Eq. (6.41), we obtain the *equations of motion in the two-quanta truncation with weak driving*:

$$\dot{\tilde{\alpha}} = \left[-\frac{\gamma}{2} + i\left(\frac{\alpha}{2} + \delta\right)\right]\tilde{\alpha}(t) - i\frac{\Omega}{2}, \tag{6.43a}$$

$$\dot{\tilde{\beta}} = -i\xi\frac{\Omega}{2}\tilde{\alpha}(t) + \left(-\frac{\gamma}{2}\xi^2 + 2i\delta\right)\tilde{\beta}(t), \tag{6.43b}$$

$$\dot{\tilde{\gamma}} = -\sqrt{\gamma\kappa_a}\tilde{\alpha}(t) - (\kappa_a + i\Delta_a)\,\tilde{\gamma}(t), \tag{6.43c}$$

$$\dot{\tilde{\delta}} = -\sqrt{\gamma\kappa_a}\xi\tilde{\beta}(t) - i\frac{\Omega}{2}\tilde{\gamma}(t) + \left[-\left(\frac{\gamma}{2} + \kappa_a\right) + i\left(\frac{\alpha}{2} + \delta - \Delta_a\right)\right]\tilde{\delta}(t), \tag{6.43d}$$

$$\dot{\tilde{\eta}} = -\sqrt{2\gamma\kappa_a}\tilde{\delta}(t) - 2\,(\kappa_a + i\Delta_a)\,\tilde{\eta}(t). \tag{6.43e}$$

In each of these equations we retain terms to the dominant power of Ω only. Then, making the following substitutions:

$$y_e = -\frac{\gamma}{2} + i\left(\frac{\alpha}{2} + \delta\right), \tag{6.44a}$$

$$y_f = -\frac{\gamma}{2}\xi^2 + 2i\delta, \tag{6.44b}$$

$$N = \kappa_a + i\Delta_a, \tag{6.44c}$$

we solve for the steady state coefficients

$$\tilde{\alpha}_{ss} = i\frac{\Omega}{2}\frac{1}{y_e}, \tag{6.45a}$$

$$\tilde{\beta}_{ss} = -\xi\left(\frac{\Omega}{2}\right)^2\frac{1}{y_e y_f}, \tag{6.45b}$$

$$\tilde{\gamma}_{ss} = -i\sqrt{\gamma\kappa_a}\frac{\Omega}{2}\frac{1}{y_e N}, \tag{6.45c}$$

$$\tilde{\delta}_{ss} = \frac{1}{y_e y_f N}\frac{\sqrt{\gamma\kappa_a}}{y_e - N}\left(\frac{\Omega}{2}\right)^2\left(y_e - \xi^2 N\right), \tag{6.45d}$$

$$\tilde{\eta}_{ss} = -\frac{1}{\sqrt{2}y_e y_f N^2}\frac{\gamma\kappa_a}{y_e - N}\left(\frac{\Omega}{2}\right)^2\left(y_e - \xi^2 N\right). \tag{6.45e}$$

The second-order correlation, Eq. (6.39), is now recast in the form

$$g^{(2)}_{\text{Auto}}(\tau) = \frac{\langle\tilde{\psi}(\tau)|\hat{a}^\dagger\hat{a}|\tilde{\psi}(\tau)\rangle}{\langle\tilde{\psi}_{ss}|\hat{a}^\dagger\hat{a}|\tilde{\psi}_{ss}\rangle}, \tag{6.46}$$

where $|\tilde{\psi}\rangle_{ss}$ is the state vector in the steady state, and $|\tilde{\psi}(\tau)\rangle$ is the time-dependent solution to Eq. (6.43) with initial condition

$$\begin{aligned}|\tilde{\psi}(\tau=0)\rangle &= \frac{\hat{a}\,|\tilde{\psi}_{ss}\rangle}{\sqrt{\langle\tilde{\psi_{ss}}|\hat{a}^\dagger\hat{a}|\tilde{\psi}_{ss}\rangle}} \\ &= \frac{1}{\sqrt{\bar{n}_{ss}}}\left(\tilde{\gamma}_{ss}\,|0,g\rangle + \tilde{\delta}_{ss}\,|0,e\rangle + \sqrt{2}\tilde{\eta}_{ss}\,|1,g\rangle\right),\end{aligned} \tag{6.47}$$

where, to dominant orders of Ω, the steady state photon number is

$$\bar{n}_{ss} = |\tilde{\gamma}_{ss}|^2 + |\tilde{\delta}_{ss}|^2 + 2|\tilde{\eta}_{ss}|^2 \approx |\tilde{\gamma}_{ss}|^2 = \gamma\kappa_a\left(\frac{\Omega}{2}\right)^2|Ny_e|^{-2}. \tag{6.48}$$

Finally, adopting the single-quantum truncation

$$|\tilde{\psi}(\tau)\rangle = |0,g\rangle + \tilde{\alpha}(\tau)\,|0,e\rangle + \tilde{\gamma}(\tau)\,|1,g\rangle\,, \tag{6.49}$$

the second-order correlation simplifies as

$$g^{(2)}_{\text{Auto}}(\tau) = \frac{|\tilde{\gamma}(\tau)|^2}{|\tilde{\gamma}_{ss}|^2}, \tag{6.50}$$

with

$$\tilde{\gamma}(\tau) = -i\frac{\Omega}{2}\frac{\sqrt{\gamma\kappa_a}}{y_e N} - \frac{\sqrt{\gamma\kappa_a}}{y_e + N}C_1 e^{y_e\tau} + C_2 e^{-N\tau}, \tag{6.51}$$

where

$$C_1 = \frac{\tilde{\delta}_{ss}}{|\tilde{\gamma}_{ss}|} - \tilde{\alpha}_{ss}, \tag{6.52a}$$

$$C_2 = \frac{\sqrt{2}\tilde{\eta}_{ss}}{|\tilde{\gamma}_{ss}|} + \frac{\sqrt{\gamma\kappa_a}}{N}\tilde{\alpha}_{ss} + \frac{\sqrt{\gamma\kappa_a}}{y_e + N}C_1 \tag{6.52b}$$

are the integration constants obtained by solving for $\tilde{\alpha}(t)$ and $\tilde{\gamma}(t)$. Substituting Eqs. (6.48) and (6.51) into Eq. (6.50), we finally obtain an analytic expression for the *filtered second-order correlation in the weak-driving limit*:

$$g^{(2)}_{\text{Auto}}(\tau) = \left| 1 + \frac{N}{\tilde{\alpha}_{ss}\left(y_e + N\right)} C_1 e^{y_e \tau} - \frac{N}{\sqrt{\gamma\kappa_a}\tilde{\alpha}_{ss}} C_2 e^{-N\tau} \right|^2 . \tag{6.53}$$

From this equation we are able to confirm many of the observations made thus far. First, as expected, by taking κ_a to infinity we recover the unfiltered correlation which oscillates at a frequency $-(\alpha/2 - \delta)$.

6.4 Filtered Cross-Correlations

In this section we take the cascaded filtering system one step further by introducing a *second* filtering cavity. We can then tune the two cavities to different transitions allowing us to *cross-correlate* the photons emitted from each.

6.4.1 Two-filter composite system

For the single-cavity system we coupled the entirety of the fluorescence into the cavity. With the two-filter system we couple, on average, half of the fluorescence into each cavity. This can be done by introducing a partially transmitting mirror which splits the fluorescence, or, as illustrated in Fig. 6.19, by splitting the fluorescence into two opposite decay channels.

Adding in the Hamiltonian components for the second filter, cavity b, the Hamiltonian for this new composite system has a similar form to Eq. (6.35),

$$\hat{H}_c = \hat{H}_A + \hbar\Delta_a \hat{a}^\dagger \hat{a} + \hbar\Delta_b \hat{b}^\dagger \hat{b} + \frac{i\hbar}{2}\sqrt{\frac{\gamma\kappa_a}{2}}\left(\hat{a}\hat{\Sigma}^\dagger - \hat{\Sigma}\hat{a}^\dagger\right) + \frac{i\hbar}{2}\sqrt{\frac{\gamma\kappa_b}{2}}\left(\hat{b}\hat{\Sigma}^\dagger - \hat{\Sigma}\hat{b}^\dagger\right), \tag{6.54}$$

with a similar master equation to Eq. (6.34),

$$\begin{aligned}\frac{\mathrm{d}}{\mathrm{d}t}\hat{\rho} = \frac{1}{i\hbar}[\hat{H}_c, \hat{\rho}] &+ \frac{1}{2}\left(2\hat{J}^a_c\hat{\rho}\hat{J}^{a\dagger}_c - \hat{J}^{a\dagger}_c\hat{J}^a_c\hat{\rho} - \hat{\rho}\hat{J}^{a\dagger}_c\hat{J}^a_c\right) + \frac{\kappa_a}{2}\left(2\hat{a}\hat{\rho}\hat{a}^\dagger - \hat{a}^\dagger\hat{a}\hat{\rho} - \hat{\rho}\hat{a}^\dagger\hat{a}\right) \\ &+ \frac{1}{2}\left(2\hat{J}^b_c\hat{\rho}\hat{J}^{b\dagger}_c - \hat{J}^{b\dagger}_c\hat{J}^b_c\hat{\rho} - \hat{\rho}\hat{J}^{b\dagger}_c\hat{J}^b_c\right) + \frac{\kappa_b}{2}\left(2\hat{b}\hat{\rho}\hat{b}^\dagger - \hat{b}^\dagger\hat{b}\hat{\rho} - \hat{\rho}\hat{b}^\dagger\hat{b}\right),\end{aligned} \tag{6.55}$$

and cascade decay operators

$$\hat{J}^a_c = \sqrt{\frac{\gamma}{2}}\hat{\Sigma} + \sqrt{\kappa_a}\hat{a}, \tag{6.56a}$$

$$\hat{J}^b_c = \sqrt{\frac{\gamma}{2}}\hat{\Sigma} + \sqrt{\kappa_b}\hat{b}. \tag{6.56b}$$

Unsurprisingly, the non-Hermitian Hamiltonian governing the free evolution of the two-filter system

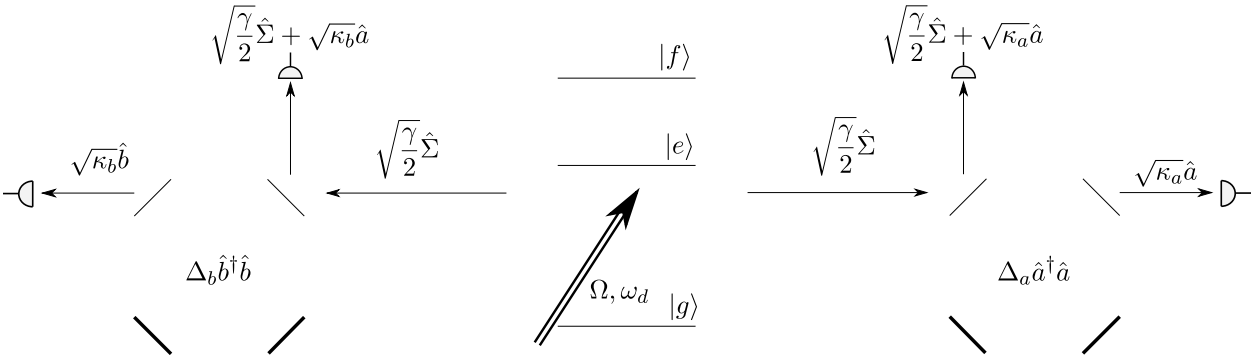

Figure 6.19: This system is almost identical to the single-filter system, Fig. 6.10, but with a second cavity to the left. Here the resonance is emitted into each cavity at a rate $\gamma/2$.

also has a similar form to Eq. (6.37),

$$\hat{H} = \hat{H}_A + \hbar\Delta_a\hat{a}^\dagger\hat{a} + \hbar\Delta_b\hat{b}^\dagger\hat{b} - i\hbar\frac{\gamma}{2}\hat{\Sigma}^\dagger\hat{\Sigma} - i\hbar\kappa_a\hat{a}^\dagger\hat{a} - i\hbar\kappa_b\hat{b}^\dagger\hat{b} - i\hbar\sqrt{\frac{\gamma\kappa_a}{2}}\hat{\Sigma}\hat{a}^\dagger - i\hbar\sqrt{\frac{\gamma\kappa_b}{2}}\hat{\Sigma}\hat{b}^\dagger, \tag{6.57}$$

with jump operators Eqs. (6.38) and (6.56), and in addition

$$\hat{J}_b = \sqrt{\kappa_b}\hat{b}. \tag{6.58}$$

6.4.2 Cross-correlations

In order to determine the cross-correlation of the transitions, we set a condition on the detectors, just as we did in section 6.2.3. When the cavities are resonant with different transition, we aim to correlate the light from cavity a with the light from cavity b. We therefore aim to calculate the probability of detecting a transmission from cavity b at a time τ after detecting a transmission from cavity a. We thus define the *filtered second-order cross-correlation* for the two-filter system:

$$g^{(2)}(\tau) = \frac{\langle\hat{a}^\dagger)(0)\hat{b}^\dagger(\tau)\hat{b}(\tau)\hat{a}(0)\rangle_{ss}}{\langle\hat{a}^\dagger\hat{a}\rangle_{ss}\langle\hat{b}^\dagger\hat{b}\rangle_{ss}}. \tag{6.59}$$

When we considered the separate dipole operators we saw, in Fig. 6.8, perfect examples of correlated and uncorrelated light when the drive field was weak. Setting one filter resonant with the $|f\rangle$ to $|e\rangle$ and the other on the $|e\rangle$ to $|g\rangle$ transition we see similar results – as we would expect. When conditioned on an $|e\rangle$ to $|g\rangle$ emission, we find that the photon detections are mostly anti-correlated, as demonstrated in Fig. 6.20. The correlation is not, however, as "neat" as for the dipole operators. Due to the cavities having a finite bandwidth, there will inevitably be a delay in their response, which is the cause of the large initial value and sudden drop. If we were to increase

the bandwidth of cavity b we would see this response time decrease, causing the initial peak to decay even faster. When we "swap" the cavities around, with the correlation now condition on an $|f\rangle$ to $|g\rangle$ emission, we see, in Fig. 6.21, that the emissions are strongly correlated. While these results come as no surprise, we can now be confident that the filtered-cross correlations give us reasonable results.

We now increase the drive strength so that we can investigate the correlations of the dressed state transitions. Focusing now on the single-photon doublets, we would still expect to see a photon from the ω_{eg} doublet after a photon from the ω_{fe} doublet is detected. From the dressed state picture, Fig. 5.1, we see that the two transitions that contribute to the ω_{fe} doublet, $|0\rangle$ to $|+\rangle$ and $|-\rangle$ to $|+\rangle$, may be immediately followed by either a $|+\rangle$ to $|0\rangle$ or $|+\rangle$ to $|-\rangle$ transition. We see, in Fig. 6.22, that this is precisely what occurs, as there is a very strong correlation between the two. Swapping the filters around, however, does not give us the strong anti-correlation we saw for a weak drive. Figure 6.23 shows the cross-correlation oscillating at a frequency $\omega_-/2\pi$, the same frequency we have seen appear previously. Just as with the previous cases, the drive field is now strong enough to constantly excite the atom into the state $|f\rangle$. The individual transitions in the doublets, however, are strongly anti-correlated, as shown in Fig. 6.24 . The two transitions these peaks results from both start from the dressed state $|+\rangle$ and therefore cannot occur immediately after the other.

We have already seen, in Fig. 6.13, that the central peak is strongly self-correlated, due to the relatively high number of possible dressed state transitions of frequency ω_d. While the central peak may have multiple possible transitions, its two nearest side-peaks only have one possible transition each; from the dressed state ladder, we see one of these transitions directly follows the other. The cascaded decay of $|0\rangle$ to $|-\rangle$ followed by $|-\rangle$ to $|0\rangle$ suggests a strong cross-correlation, provided a $|0\rangle$ to $|-\rangle$ transition is detected first. Tuning the two cavities onto these transitions we see that this is also the case, as shown in Fig. 6.25.

As with all the two-filter correlations, Fig. 6.25 has an initial artefact that arises due to the response time of the cavity. The issues that came from employing a single Lorentzian filter in the previous section are also present here. There is a limit as to how close the two transition frequencies we investigate can be as we need a linewidth large enough to resolve the peak, but not so large as to include both frequencies in the same filter.

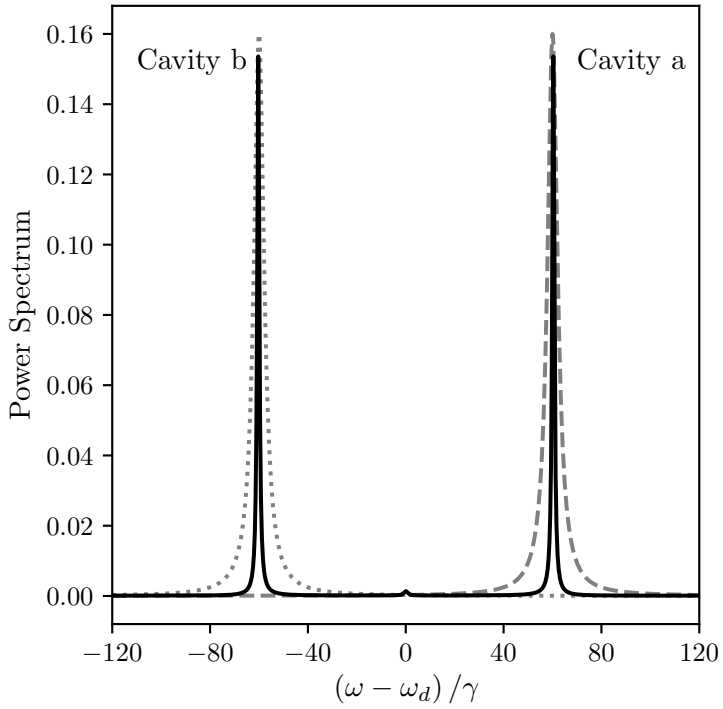

(a) Incoherent fluorescence spectrum (solid) with filter cavities a (dashed) and b (dotted).

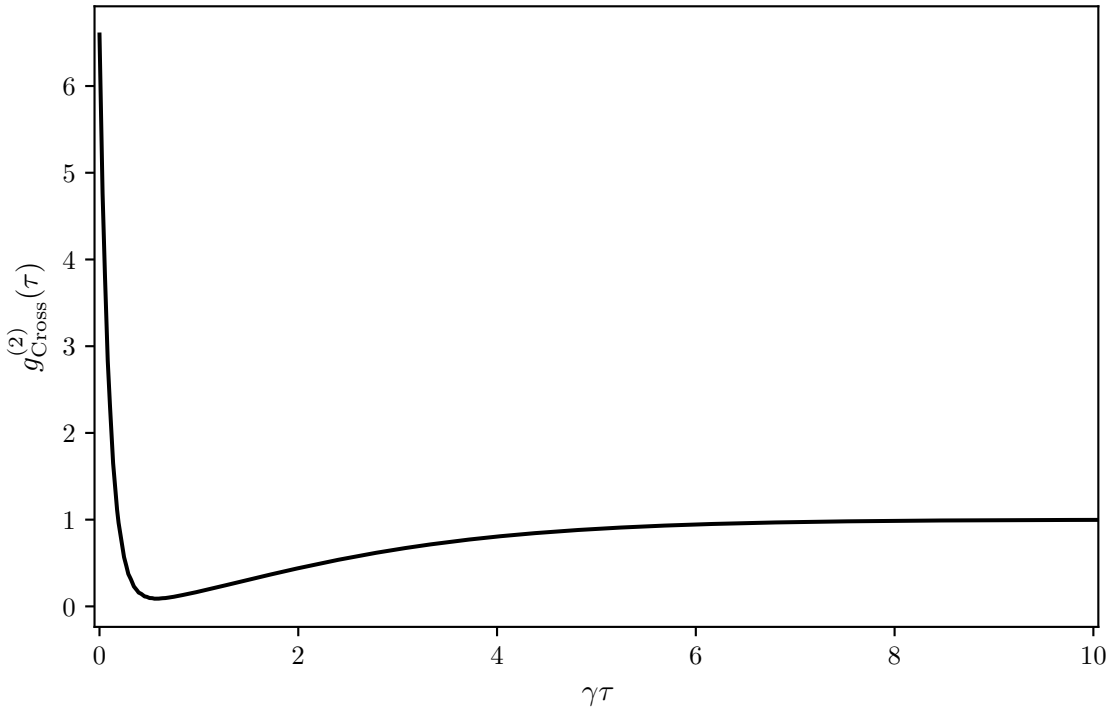

(b) Cross-correlation.

Figure 6.20: Filtered second-order cross-correlation for a weak drive: ω_{eg} conditioned on ω_{fe}. Parameters are $(\Omega/\gamma, \alpha/\gamma, \delta/\gamma, \xi, \Delta_a/\gamma, \kappa_a/\gamma, \Delta_b/\gamma, \kappa_b/\gamma) = (5.0, -120.0, 0.0, 1.0, 60.0, 5.0, -60.0, 5.0)$.

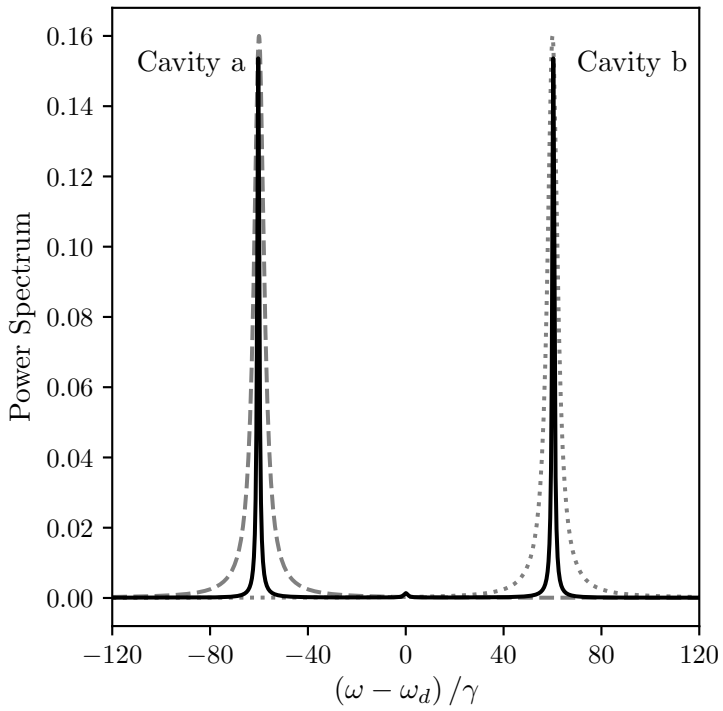

(a) Incoherent fluorescence spectrum (solid) with filter cavities a (dashed) and b (dotted).

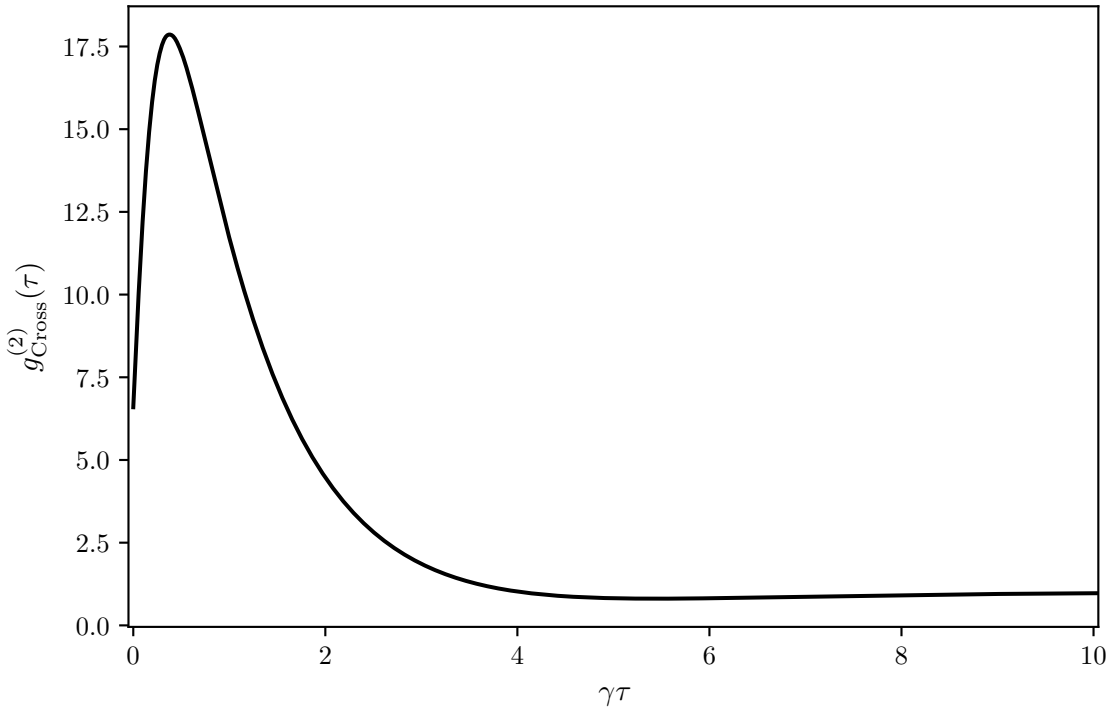

(b) Cross-correlation.

Figure 6.21: Filtered second-order cross-correlation for a weak drive: ω_{fe} conditioned on ω_{eg}. Parameters are $(\Omega/\gamma, \alpha/\gamma, \delta/\gamma, \xi, \Delta_a/\gamma, \kappa_a/\gamma, \Delta_b/\gamma, \kappa_b/\gamma) = (5.0, -120.0, 0.0, 1.0, -60.0, 5.0, 60.0, 5.0)$.

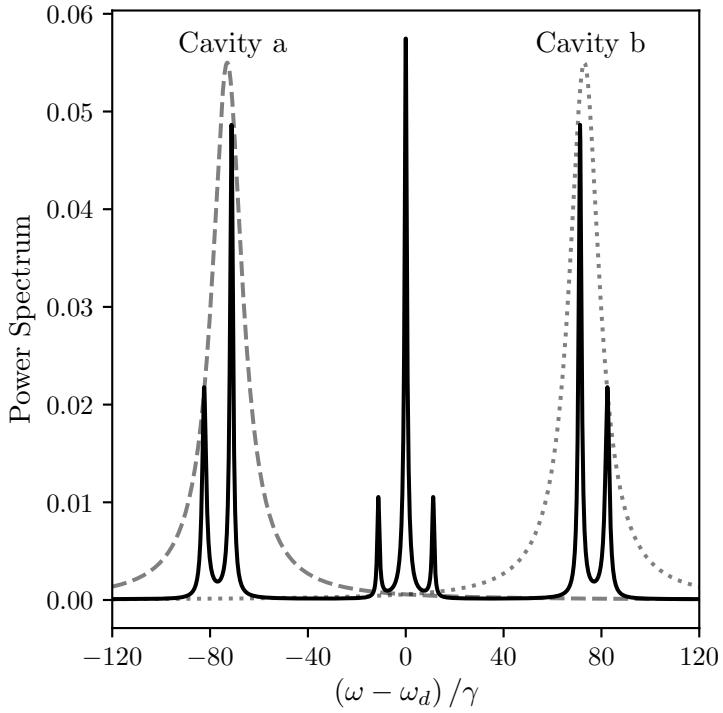

(a) Incoherent fluorescence spectrum (solid) with filter cavities a (dashed) and b (dotted).

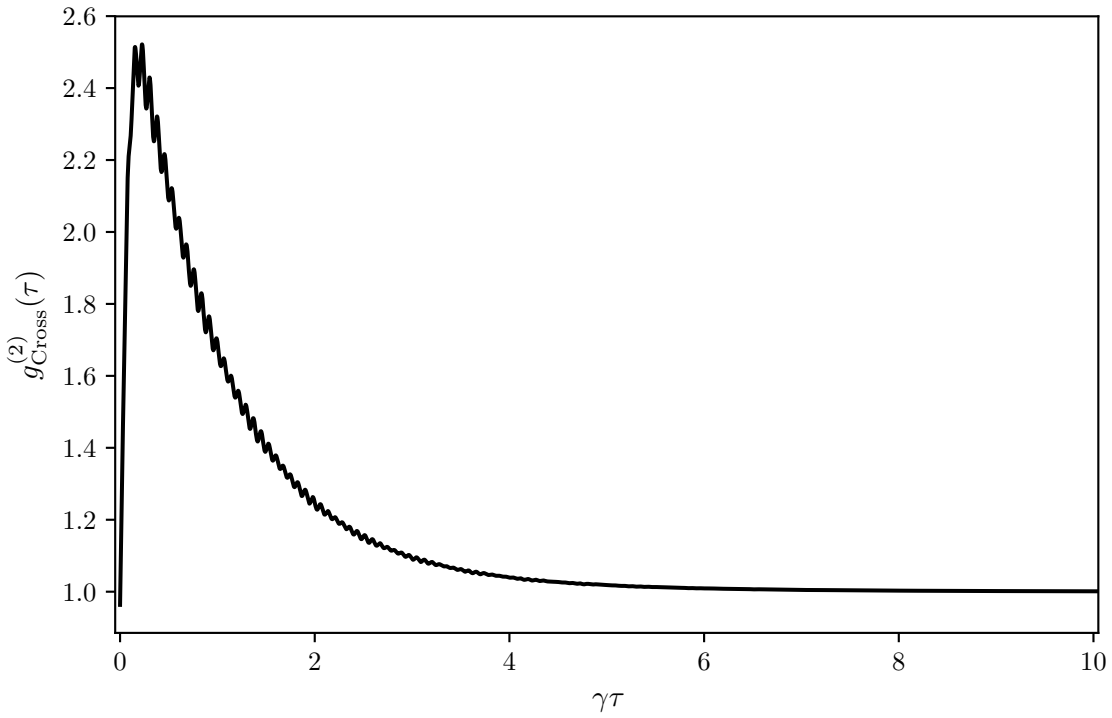

(b) Cross-correlation.

Figure 6.22: Filtered second-order cross-correlation for emission on the ω_{eg} doublet conditioned on emission on the ω_{fe} doublet. Parameters are $(\Omega/\gamma, \alpha/\gamma, \delta/\gamma, \xi, \Delta_a/\gamma, \kappa_a/\gamma, \Delta_b/\gamma, \kappa_b/\gamma) = (40.0, -120.0, 0.0, 1.0, -73.0, 15.0, 73.0, 15.0)$.

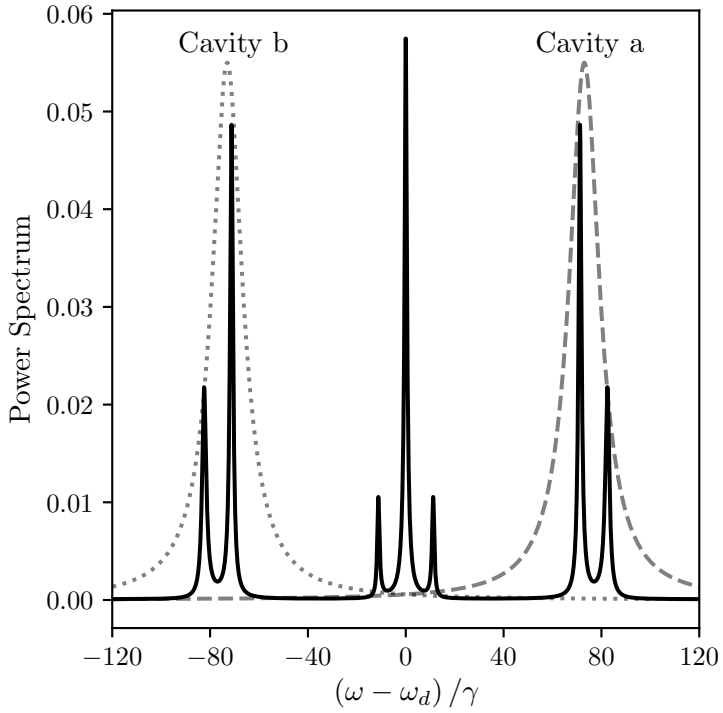

(a) Incoherent fluorescence spectrum (solid) with filter cavities a (dashed) and b (dotted).

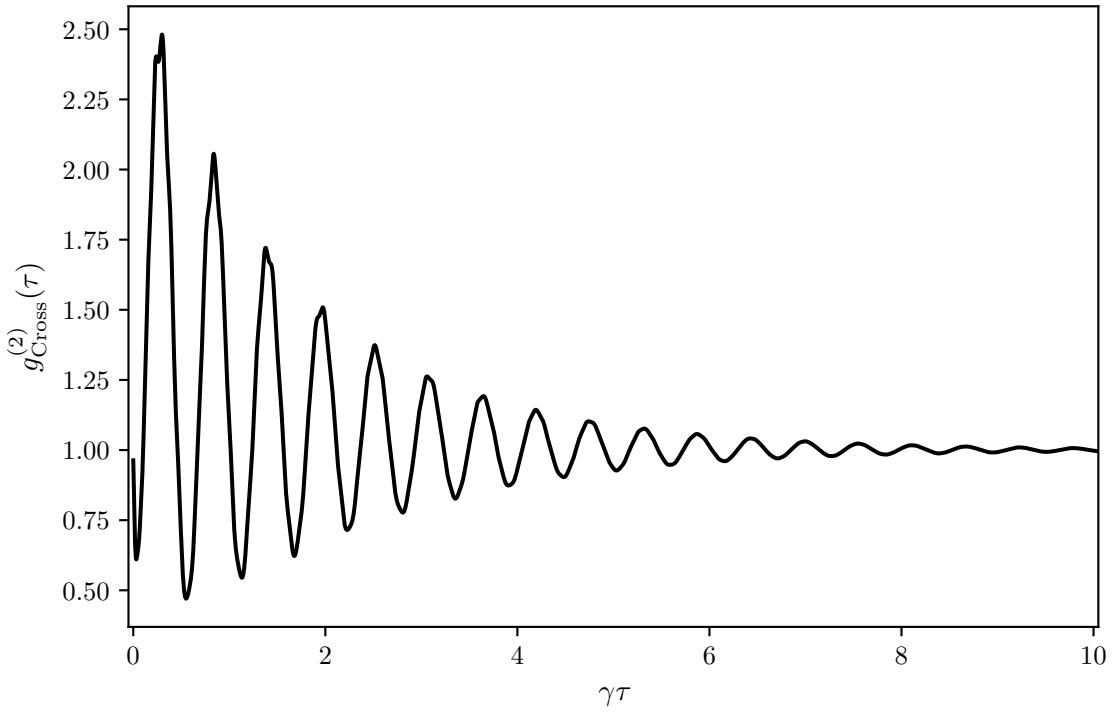

(b) Cross-correlation.

Figure 6.23: Filtered second-order cross-correlation for emission on the ω_{fe} doublet conditioned on emission on the ω_{eg} doublet. Parameters are $(\Omega/\gamma, \alpha/\gamma, \delta/\gamma, \xi, \Delta_a/\gamma, \kappa_a/\gamma, \Delta_b/\gamma, \kappa_b/\gamma) = (40.0, -120.0, 0.0, 1.0, 73.0, 15.0, -73.0, 15.0)$.

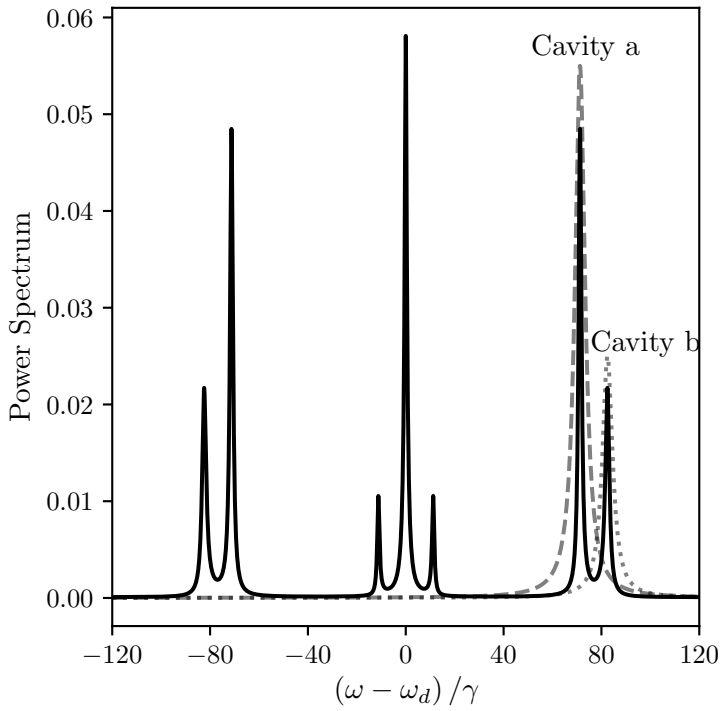

(a) Incoherent fluorescence spectrum (solid) with filter cavities a (dashed) and b (dotted).

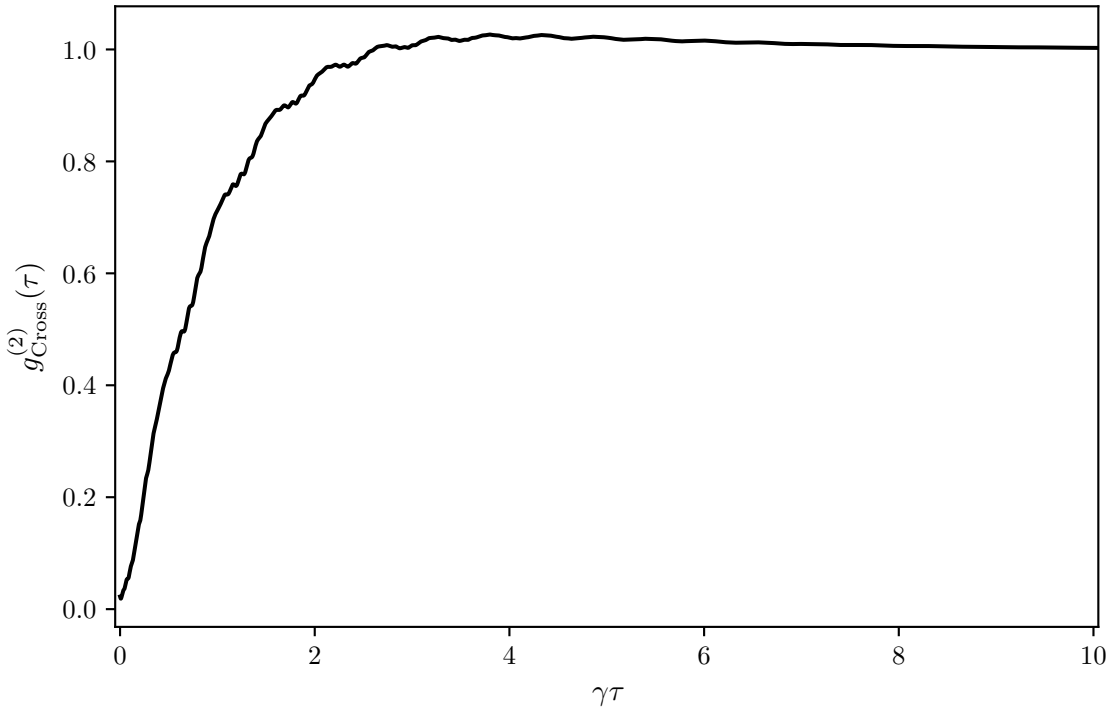

(b) Cross-correlation.

Figure 6.24: Filtered second-order cross-correlation for $\omega_d + (\omega_+ - \omega_-)$ conditioned on $\omega_d + \omega_+$. Parameters are $(\Omega/\gamma, \alpha/\gamma, \delta/\gamma, \xi, \Delta_a/\gamma, \kappa_a/\gamma, \Delta_b/\gamma, \kappa_b/\gamma) = (40.0, -120.0, 0.0, 1.0, 71.23, 5.0, 82.46, 5.0)$.

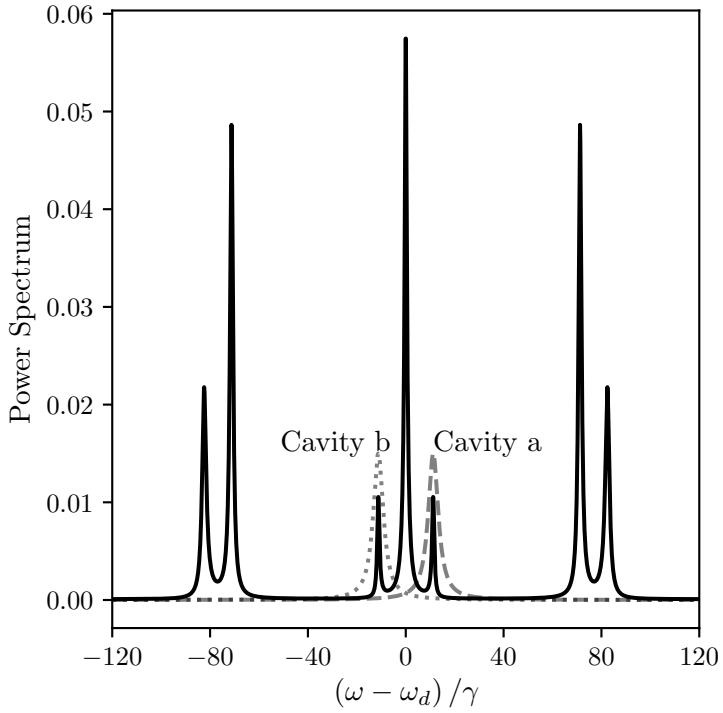

(a) Incoherent fluorescence spectrum (solid) with filter cavities a (dashed) and b (dotted).

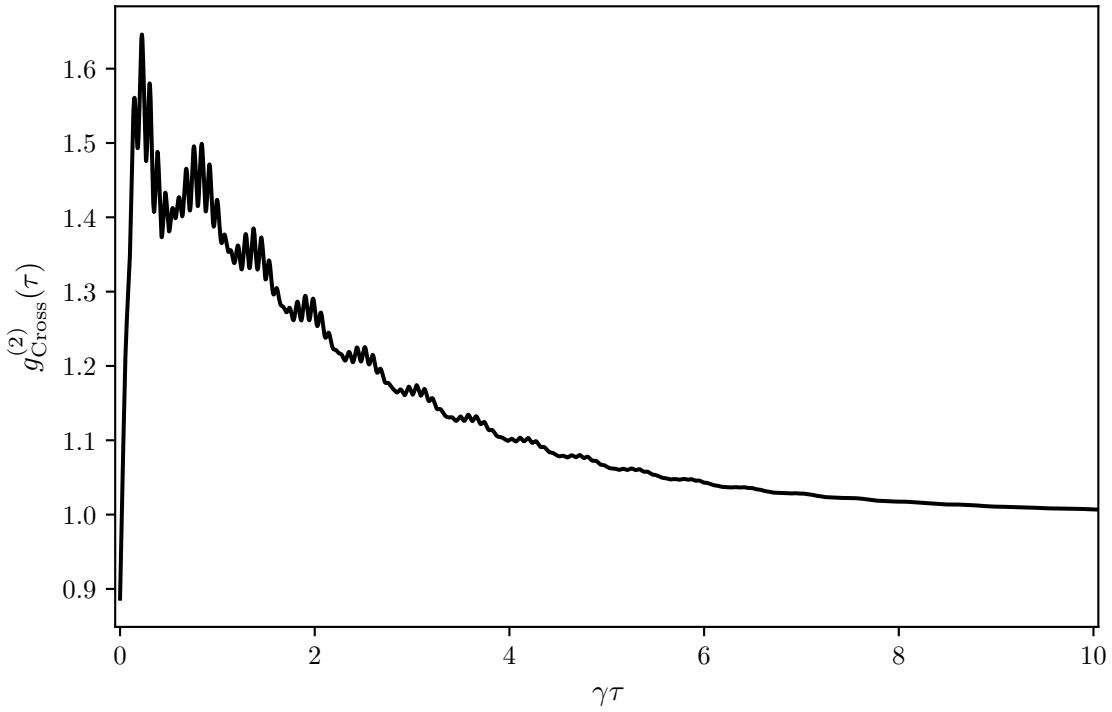

(b) Cross-correlation.

Figure 6.25: Filtered second-order cross-correlation for $\omega_d - \omega_+$ conditioned on $\omega_d + \omega_+$. Parameters are $(\Omega/\gamma, \alpha/\gamma, \delta/\gamma, \xi, \Delta_a/\gamma, \kappa_a/\gamma, \Delta_b/\gamma, \kappa_b/\gamma) = (40.0, -120.0, 0.0, 1.0, 11.23, 5.0, -11.23, 5.0)$.

7 Conclusion

Let us begin with a summary of the topics covered in this thesis. At first, we studied the interaction of a three-level atom with a quantised radiation field, adopting the dipole and rotating wave approximations. We then treated the system as an open system, allowing for an energy loss mechanism – spontaneous emission. We approached the open system with two different techniques, namely the Lindblad master equation and quantum trajectory theory.

We began the numerical results with a survey of the steady states of the atom. We derived a time-independent expression of the driven atom in a frame rotating at the drive frequency. This allowed us to introduce two very important parameters: the drive detuning from two-photon resonance, and the anharmonicity of the two dipoles. We briefly adopted a model where the intermediate level of the atom was adiabatically eliminated from the driving process, but remained for the decay. With this model we were able to derive analytic expressions for the steady state density operator.

Following this we derived expressions for the dressed states and their respective frequencies for the case of two-photon resonance. For a weak drive field the dressed states resembled the bare states, with only two transitions for the cascaded decay. When the drive strength increased, however, the number of possible transitions increased to twelve, with seven distinct transition frequencies. We saw this effect when we computed the incoherent fluorescence spectrum of the atom, where, for an increasing drive strength, the two single-photon transition peaks split into a doublet, and a Mollow-like triplet centred on the drive frequency emerged.

In the final chapter we investigated the photon-photon correlations of the fluorescence by computing the second-order correlation function. To start with we looked at the correlation of the total dipole operator and found that, for a weak drive, the emitted photons were super bunched; due to the cascaded decay, after detecting the first photon from the $|f\rangle$ to $|e\rangle$ transition, we expect, approximately within an atomic lifetime, to detect another from the $|e\rangle$ to $|g\rangle$ transition. If the drive is very weak the time between detection pairs increases, pushing the initial correlation value higher as it becomes clearer that the photons are bunched. For a higher drive, however, the photons are slightly antibunched and the correlations oscillate at the dressed frequency ω_-.

We split the total dipole operator into its two separate components, one for each dipole, and computed the auto- and cross-correlations. For a weak drive, the dipole operators directly correspond to the two single-photon transitions. We see this in the auto-correlation as the light is perfectly anitbunched, and the cross-correlations show a strong correlation for detecting a photon from the $|e\rangle$ to $|g\rangle$ transition directly after detecting one from the $|f\rangle$ to $|e\rangle$ transition. We know, however, that we can compose the bare states as a combination of dressed states, where for a strong drive, these dressed states split far from eachother. Thus the separate dipole operators are a combination of several different dressed state transitions.

In order to correlate individual dressed transitions, we approached the system as a cascaded open system, where we coupled the fluorescence into a filter cavity; the cavity acted as a tunable Lorentzian filter with a finite linewidth. We found that the photons corresponding to the central peak of the spectrum, centred on the drive frequency, were bunched. This was to be expected as our dressed state picture predicted two pairs of cascade emissions, all resulting in a frequency ω_d. The other transitions, however, were all antibunched.

Finally, we added a second filter cavity so we could cross-correlate photons from different transitions, further confirming our understanding of decay via dressed state transitions. There was a strong correlation between the single-photon peaks, even when the peaks split into respective doublets.

The fluorescence spectrum of the driven atom that we calculated closely match those of Gasparinetti et al. (Ref. [12]) as we see the emergence of a central triplet and two doublets that are Stark shifted from the single-photon transition. Our results for the second-order correlations, however, only qualitatively match. The bunching of the ω_d transition and the antibunching of the other transitions were evident, however our results show oscillations in the correlations whereas Ref. [12] does not. Our method of filtering the fluorescence goes beyond the secular approximation used for their results. It is also important to note that experimentally, the fluorescence of their artificial atom was digitally filtered, which we would expect to give different results to our cascaded system.

While we have conducted a numerical survey over various different parameters, the parameter space is very large. There is still room to explore the effect that driving off two-photon resonance has on the correlations. One other avenue for future extension is in determining another method of frequency filtering. The Lorentzian filter proved to be sufficient in our computations, however, a Lorentzian has long reaching tails. A more precise theoretical filter, such as a bandpass filter, would be a fine addition to the quantum optics computational toolbox.

A Simulation Code

Most of the code use to generate the results was written in Fortran 90. The code can be found at the Github repository: https://github.com/jnga773/Two_Photon_Resonance_Ladder_System.

The simulation code is based on the Lindblad master equation, solving for the density operator $\hat{\rho}(t)$ using the Runge-Kutta 4^{th} technique. For the power spectrum results we numerically solve the differential equation and the quantum regression theorem, Eq. (3.37), to solve for the first-order correlation function. The power spectrum is then calculated using a Fast Fourier Transform (FFT) technique.

The second-order correlation function was calculated using two methods: solving the Lindblad master equation as before, and using quantum trajectory theory to simulate the detectors of a photon counting experiment.

Bibliography

1. Brown, R. H. & Twiss, R. Q. "A test of a new type of stellar interferometer on Sirius". *Nature* **178,** 1046 (1956) (cit. on p. 1).
2. Brown, R. H., Twiss, R. Q., *et al.* "Correlation between photons in two coherent beams of light". *Nature* **177,** 27 (1956) (cit. on pp. 1, 56).
3. Brown, R. H. & Twiss, R. Q. "Interferometry of the intensity fluctuations in light-I. Basic theory: the correlation between photons in coherent beams of radiation". *Proc. R. Soc. A* **242,** 300 (1957) (cit. on p. 1).
4. Brown, R. H. & Twiss, R. "Interferometry of the intensity fluctuations in light. II. An experimental test of the theory for partially coherent light". *Proc. R. Soc. A* **243,** 291–319 (1958) (cit. on p. 1).
5. Glauber, R. J. "Photon Correlations". *Phys. Rev. Lett.* **10,** 84 (1963) (cit. on p. 1).
6. Glauber, R. J. "The Quantum Theory of Optical Coherence". *Phys. Rev.* **130,** 2529 (1963) (cit. on pp. 1, 21).
7. Carmichael, H. J. & Walls, D. F. "A quantum-mechanical master equation treatment of the dynamical Stark effect". *J. Phys. B* **9,** 1199 (1976) (cit. on pp. 1, 57).
8. Walls, D. "Evidence for the quantum nature of light". *Nature* **280,** 451 (1979) (cit. on pp. 1, 57).
9. Kimble, H. J., Dagenais, M. & Mandel, L. "Photon Antibunching in Resonance Fluorescence". *Phys. Rev. Lett.* **39,** 691 (1977) (cit. on pp. 1, 57).
10. Kimble, H. J. "The quantum internet". *Nature* **453,** 1023 (2008) (cit. on p. 1).
11. Devoret, M. H. & Schoelkopf, R. J. "Superconducting circuits for quantum information: an outlook". *Science* **339,** 1169 (2013) (cit. on pp. 1, 27).
12. Gasparinetti, S. *et al.* "Two-Photon Resonance Fluorescence of a Ladder-Type Atomic System". *arXiv e-prints,* arXiv:1901.00414 (2019) (cit. on pp. 1, 27–29, 50, 94).
13. Gasparinetti, S. *et al.* "Correlations and Entanglement of Microwave Photons Emitted in a Cascade Decay". *Phys. Rev. Lett.* **119,** 140504 (2017) (cit. on pp. 1, 10, 27, 29).
14. Koshino, K. *et al.* "Observation of the Three-State Dressed States in Circuit Quantum Electrodynamics". *Phys. Rev. Lett.* **110,** 263601 (2013) (cit. on p. 1).
15. Mollow, B. "Power Spectrum of Light Scattered by Two-Level Systems". *Phys. Rev.* **188,** 1969 (1969) (cit. on pp. 1, 46).

16. Aspect, A., Roger, G., Reynaud, S., Dalibard, J. & Cohen-Tannoudji, C. "Time Correlations between the Two Sidebands of the Resonance Fluorescence Triplet". *Phys. Rev. Lett.* **45,** 617–620 (8 1980) (cit. on p. 1).

17. Alexanian, M. & Bose, S. K. "Two-photon resonance fluorescence". *Phys. Rev. A* **74,** 063418 (6 2006) (cit. on p. 1).

18. Zhu, S.-Y., Narducci, L. M. & Scully, M. O. "Quantum-mechanical interference effects in the spontaneous-emission spectrum of a driven atom". *Phys. Rev. A* **52,** 4791 (1995) (cit. on p. 1).

19. Pegg, D. T., Loudon, R. & Knight, P. L. "Correlations in light emitted by three-level atoms". *Phys. Rev. A* **33,** 4085 (1986) (cit. on p. 1).

20. Shamailov, S., Parkins, A., Collett, M. & Carmichael, H. "Multi-photon blockade and dressing of the dressed states". *Opt. Commun.* **283,** 766 (2010) (cit. on p. 1).

21. Carreño, J. C. L., Del Valle, E. & Laussy, F. P. "Frequency-resolved Monte Carlo". *Sci. Rep.* **8,** 6975 (2018) (cit. on p. 1).

22. Peng, Z.-a., Yang, G.-q., Wu, Q.-l. & Li, G.-x. "Filtered strong quantum correlation of resonance fluorescence from a two-atom radiating system with interatomic coherence". *Phys. Rev. A* **99,** 033819 (3 2019) (cit. on p. 1).

23. Walls, D. & Milburn, G. *Quantum Optics* 2nd ed. (Springer Berlin Heidelberg, 2008) (cit. on pp. 5, 8, 21, 42, 44, 57).

24. Scully, M. & Zubairy, M. *Quantum Optics* (Cambridge University Press, 1997) (cit. on pp. 9, 42).

25. Glauber, R. J. "Coherent and incoherent states of the radiation field". *Phys. Rev.* **131,** 2766 (1963) (cit. on p. 10).

26. Sakurai, J. & Napolitano, J. *Modern Quantum Mechanics* 2nd ed. (Pearson Education Inc., 2017) (cit. on p. 12).

27. Puri, R. *Mathematical Methods of Quantum Optics* (Springer, Berlin, Heidelberg, 2001) (cit. on pp. 13, 35).

28. Carmichael, H. J. *Statistical Methods in Quantum Optics 1: Master Equations and Fokker-Planck Equations* (Springer Berlin Heidelberg, 2013) (cit. on pp. 15, 22, 43, 44, 68).

29. Alsing, P. & Carmichael, H. J. "Spontaneous dressed-state polarization of a coupled atom and cavity mode". *Quantum Optics: Journal of the European Optical Society Part B* **3,** 13 (1991) (cit. on p. 22).

30. Carmichael, H. J. *Statistical Methods in Quantum Optics 2: Non-Classical Fields* (Springer Berlin Heidelberg, 2007) (cit. on pp. 22, 69, 71, 81).

31. Carmichael, H. J. in *Strong Light-Matter Coupling: From Atoms to Solid-State Systems* (ed Kwek Leong-chuan Auffeves Alexia, G. D.) 99–154 (World Scientific Publishing Company, 2013) (cit. on p. 25).

32. Kümmerer, B. & Maassen, H. "An ergodic theorem for quantum counting processes". *J. Phys. A* **36,** 2155 (2003) (cit. on p. 25).

33. Cresser, J. D. "Ergodicity of Quantum Trajectory Detection Records". in *Directions in Quantum Optics* (eds Carmichael, H. J., Glauber, R. J. & Scully, M. O.) (Springer Berlin Heidelberg, Berlin, Heidelberg, 2001), 358 (cit. on p. 25).

34. Schoelkopf, R. & Girvin, S. "Wiring up quantum systems". *Nature* **451,** 664 (2008) (cit. on p. 27).

35. Josephson, B. "Possible new effects in superconductive tunnelling". *Phys. Lett.* **1,** 251 (1962) (cit. on p. 27).

36. Josephson, B. D. "The discovery of tunnelling supercurrents". *Rev. Mod. Phys.* **46,** 251 (1974) (cit. on p. 27).

37. Nakamura, Y., Pashkin, Y. A. & Tsai, J. "Coherent control of macroscopic quantum states in a single-Cooper-pair box". *Nature* **398,** 786 (1999) (cit. on p. 27).

38. Friedman, J. R., Patel, V., Chen, W., Tolpygo, S. & Lukens, J. E. "Quantum superposition of distinct macroscopic states". *Nature* **406,** 43 (2000) (cit. on p. 27).

39. Martinis, J. M., Nam, S., Aumentado, J. & Urbina, C. "Rabi Oscillations in a Large Josephson-Junction Qubit". *Phys. Rev. Lett.* **89,** 117901 (2002) (cit. on p. 27).

40. Wallraff, A. *et al.* "Strong coupling of a single photon to a superconducting qubit using circuit quantum electrodynamics". *Nature* **431,** 162 (2004) (cit. on p. 27).

41. Vion, D. *et al.* "Manipulating the Quantum State of an Electrical Circuit". *Science* **296,** 886 (2002) (cit. on p. 27).

42. Makhlin, Y., Schön, G. & Shnirman, A. "Quantum-state engineering with Josephson-junction devices". *Rev. Mod. Phys.* **73,** 357 (2001) (cit. on p. 27).

43. Fan, B., Milburn, G. J. & Stace, T. M. in *Superconducting Devices in Quantum Optics* (eds Hadfield, R. H. & Johansson, G.) 139–162 (Springer International Publishing, Cham, 2016) (cit. on p. 27).

44. Pechal, M. *et al.* "Superconducting Switch for Fast On-Chip Routing of Quantum Microwave Fields". *Phys. Rev. Applied* **6,** 024009 (2016) (cit. on pp. 27, 28).

45. Koch, J. *et al.* "Charge-insensitive qubit design derived from the Cooper pair box". *Phys. Rev. A* **76,** 042319 (2007) (cit. on p. 27).

46. Pashkin, Y. A., Astafiev, O., Yamamoto, T., Nakamura, Y. & Tsai, J. S. "Josephson charge qubits: a brief review". *Quantum Information Processing* **8,** 55 (2009) (cit. on p. 27).

47. Bishop, L. S. *et al.* "Nonlinear response of the vacuum Rabi resonance". *Nature Physics* **5,** 105 (2009) (cit. on p. 28).

48. Sinatra, A, Castelli, F, Lugiato, L., Grangier, P & Poizat, J. "Effective two-level model versus three-level model". *Quantum and Semiclassical Optics: Journal of the European Optical Society Part B* **7,** 405 (1995) (cit. on p. 33).

49. Wu, Y. & Yang, X. "Effective two-level model for a three-level atom in the Ξ configuration". *Phys. Rev. A* **56,** 2443 (1997) (cit. on p. 33).

50. Autler, S. H. & Townes, C. H. "Stark Effect in Rapidly Varying Fields". *Phys. Rev.* **100,** 703 (1955) (cit. on p. 34).

51. Schuster, D. I. *et al.* "ac Stark Shift and Dephasing of a Superconducting Qubit Strongly Coupled to a Cavity Field". *Phys. Rev. Lett.* **94,** 123602 (2005) (cit. on p. 34).

52. Wei, C., Suter, D., Windsor, A. S. M. & Manson, N. B. "ac Stark effect in a doubly driven three-level atom". *Phys. Rev. A* **58,** 2310 (1998) (cit. on p. 34).

53. Mandel, L. & Wolf, E. *Optical Coherence and Quantum Optics* (Cambridge University Press, 1995) (cit. on p. 39).

54. Brooker, G. *Modern Classical Optics* (OUP Oxford, 2003) (cit. on pp. 42, 55).

55. Hertel, I. & Schulz, C. *Atoms, Molecules and Optical Physics 2: Molecules and Photons - Spectroscopy and Collisions* (Springer Berlin Heidelberg, 2014) (cit. on pp. 42, 44).

56. Louisell, W. *Quantum Statistical Properties of Radiation* (Wiley, 1990) (cit. on p. 44).

57. Barnett, S. M. & Radmore, P. M. *Methods in Theoretical Quantum Optics* (Clarendon Press, 1997) (cit. on p. 45).

58. Bounouar, S. *et al.* "Path-Controlled Time Reordering of Paired Photons in a Dressed Three-Level Cascade". *Phys. Rev. Lett.* **118,** 233601 (2017) (cit. on p. 50).

59. Holm, D. A. & Sargent, M. "Theory of two-photon resonance fluorescence". *Opt. Lett.* **10,** 405–407 (1985) (cit. on p. 51).

60. Carmichael, H. J. "Quantum trajectory theory for cascaded open systems". *Phys. Rev. Lett.* **70,** 2273 (1993) (cit. on pp. 55, 68).

61. Loudon, R. *The Quantum Theory of Light* 1st ed., 448 (OUP Oxford, 1973) (cit. on p. 56).

62. Loudon, R. "Non-classical effects in the statistical properties of light". *Rep. Prog. Phys.* **43,** 913 (1980) (cit. on p. 57).

63. Paul, H. "Photon antibunching". *Rev. Mod. Phys.* **54,** 1061 (1982) (cit. on p. 57).